
GAZİ ÜNİVERSİTESİ
Gazi
1926

INVESTIGATION OF OXYGEN FORMATION FROM WATER AT COBALT-OXO CENTER BY MULTI CONFIGURATIONAL QUANTUM CHEMICAL METHODS

A THESIS SUBMITTED TO
THE GRADUATE SCHOOL OF NATURAL AND APPLIED SCIENCES
OF
GAZİ UNIVERSITY

BY

Osama QANDEEL

A THESIS SUBMITTED TO
THE GRADUATE SCHOOL OF NATURAL AND APPLIED SCIENCES
OF GAZİ UNIVERSITY

IN PARTIAL FULFILLMENT OF THE REQUIREMENTS
FOR
THE DEGREE OF MASTER OF SCIENCE
IN
CHEMISTRY

April 2022

ETHICAL STATEMENT

I hereby declare that in this thesis study I prepared in accordance with thesis writing rules of Gazi University Graduate School of Natural and Applied Sciences;

- All data, information and documents presented in this thesis have been obtained within the scope of academic rules and ethical conduct,
- All information, documents, assessments and results have been presented in accordance with scientific ethical conduct and moral rules,
- All material used in this thesis that are not original to this work have been fully cited and referenced,
- No change has been made in the data used,
- The work presented in this thesis is original,

or else, I admit all loss of rights to be incurred against me.

Osama QANDEEL

20/04/2022

INVESTIGATION OF OXYGEN FORMATION FROM WATER AT COBALT-OXO CENTER BY MULTI CONFIGURATIONAL QUANTUM CHEMICAL METHODS

(M. Sc. Thesis)

Osama QANDEEL

GAZİ UNIVERSITY

GRADUATE SCHOOL OF NATURAL AND APPLIED SCIENCES

April 2022

ABSTRACT

In the quest for commercialization of water splitting for energy related purposes, Water Oxidation Reaction (WOR) has gained significant attention. Understanding the mechanism of the WOR can help to design novel effective catalysts. Cobalt oxides were one of the first discovered heterogenous catalysts for WOR. Among water oxidation catalysts (WOCs), cobalt based mononuclear catalysts have been in center of interest due to their electronic features and to their abundance. The Co-O center in the catalyst is considered as the center of the reaction. Therefore, modelling it correctly is important for understanding the mechanism. In this study, the Co-O center was characterized by five different cobalt based mononuclear complexes. The common feature of all Co-O centers is that it exhibited three unpaired electrons in their ground quartet state. Neither oxo nor oxyl notion alone could describe it completely but rather a mix of them as Co-oxo/oxyl can give a better picture of the system. In this study, this interesting electronic fingerprint was shown to be a key feature in O-O bond formation. After studying the Co-oxo/oxyl center in different molecules, a more detailed study of the O-O bond formation step was performed. The O-O bond formation has the highest energy barrier between reaction steps and is very important for WOR. Using CASSCF methods the approaching of H2O fragment to the Co-O center was scanned. Herein, we suggest an alternative to the conventional single step nucleophilic attack mechanism of O-O bond formation. Interestingly, before the electron transfer is achieved, the approach of nucleophile (H2O moiety) to the electrophile region (Co-O Center) disturbs the orbitals and electrons, and forms a new state, then an O-O bond is formed.

Science Code : 20119

Key Words : DFT, CASSCF, WOC, Catalyst, Cobalt, Cobalt oxo

Page Number : 93

Supervisor : Prof. Dr. Yavuz DEDE

KOBALT-OKSO MERKEZİNDE SUDAN OKSİJEN ELDESİNİN ÇOK KONFİGÜRASYONLU KUANTUM KİMYASAL METOTLARLA İNCELENMESİ

(Yüksek Lisans Tezi)

Osama QANDEEL

GAZİ ÜNİVERSİTESİ
FEN BİLİMLERİ ENSTİTÜSÜ

Nisan 2022

ÖZET

Enerji üretmek için suyun ayrıştırılmasının ticarileştirilmesi arayışında, suyun yükseltgenme tepkimesi çok dikkat çekmektedir. WOR mekanizmasını anlamak, yeni ve etkili katalizörler tasarlamamıza yardımcı olabilir. Kobalt oksitler, WOR için ilk keşfedilen heterojen katalizörlerden biridir. Suyun Yükseltgenme Katalizörleri arasında, kobalt bazlı mononükleer katalizörler, elektronik özellikleri ve yeryüzündeki bolluğu nedeniyle ilgi odağı olmuştur. Katalizördeki Co-O merkezi, reaksiyon merkezi olarak kabul edilir. Bu nedenle, bu merkezi doğru bir şekilde modellemek, mekanizmayı anlamak için önemlidir. Bu çalışmada, Co-O merkezini beş farklı kobalt bazlı mononükleer kompleksi ile karakterize edilmiştir. Co-O merkezinin hepsinde ortak özelliği, temel halin kuartet olması ve üç eşleşmemiş elektrona sahip olmasıdır. okso veya oksil kavramı tek başına Co-O merkezini tanımlamak için yeterli değildir, ancak Co-okso/oksil olarak tanımlanırsa sistem için daha iyi bir resim oluşturur. Bu çalışmada, bu ilginç elektronik parmak izinin O-O bağ oluşumunda önemli bir özellik olduğu gösterildi. Farklı moleküllerdeki Co-okso/oksil merkezi çalıştıktan sonra, O-O bağ oluşum adımının daha ayrıntılı bir incelemesi sürdürüldü. O-O bağ oluşumu, reaksiyon adımları arasında en yüksek enerji bariyerine sahiptir ve WOR için oldukça önemlidir. CASSCF yöntemlerini kullanarak H2O'nun Co-O merkezine yaklaşmasını incelendi. Bu çalışmada, O–O bağ oluşumunun geleneksel tek adımlı nükleofilik saldırı mekanizmasına bir alternatif önerdik. Şöyleki, elektron transferi gerçekleşmeden önce, nükleofilin (H2O) elektrofilik bölgeye (Co-O) yaklaşması elektronları ve orbitalleri deforme ederek yeni bir hal oluşturur, sonra O-O bağı oluşur.

Bilim Kodu : 20119

Anahtar Kelimeler : DFT, CASSCF, WOC, Catalyst, Cobalt, Cobalt oxo

Sayfa Adedi : 93

Danışman : Prof. Dr. Yavuz DEDE

TEŞEKKÜR

Tez çalışmalarımda, değerli bilgileriyle beni yönlendiren, yardımını ve desteği esirgemeyen danışman hocam Prof. Dr. Yavuz DEDE'ye şükran ve minnetlerimi sunarım. Tez çalışmalarımdaki katkılarından dolayı Muhammed BÜYÜKTEMİZ'e ve Dilara Berna YILDIZ'a teşekkürlerimi sunarım

Deneysel çalışmaları tezime ilham kaynağı teşkil eden Doç. Dr. Ferdi KARADAŞ'a teşekkürlerimi sunarım.

Tez çalışmalarımda Bilgisayar altyapısını kullandığım TÜBİTAK TRUBA'ya teşekkür ederim. Eğitimim boyunca bana burs sağlayan YTB başkanlığına teşekkür ederim

Desteklerini esirgemeyen aileme teşekkür ederim.

CONTENTS

Page

Page

Page

Page

LIST OF TABLES

Table **Page**

LIST OF FIGURES

Figure **Page**

LIST OF SCHEMES

Scheme **Page**

NOMENCLATURE

The abbreviations used in this study are presented below along with their explanations.

Abbreviation	Descriptions
PSI	Photosystem I
PSII	Photosystem II
OEC	Oxygen evolving complex
PCET	Proton Coupled Electron Transfer
WOR	Water Oxidation Reaction
WOC	Water Oxidation Catalyst
LUMO	Lowest Unoccupied Molecular Orbital
HOMO	Highest Occupied Molecular Orbital
SOMO	Singly Occupied Molecular Orbital
EER	Enhanced Exchange Reactivity
JT	Jahn–Teller
DFT	Density Functional Theory
CASSCF	Complete Active Space Self Consistent field

1. INTRODUCTION

Water is one of the most abundant and vital substances around us. One important biological process that includes water is photosynthesis. Photosynthesis is a key part in the plant's energy cycle, it is used by plants to convert energy from sunlight to storable and usable forms. The energy stored in chemical form is later being used in several processes that keep the plants alive. The utilization of solar energy by photosynthesis every day on earth allowed life to flourish and survive for millions of years.

Within photosynthesis, there are two main systems. the Photosystem I and II (PSI and PSII). The PSII is responsible for absorbing sunlight and splitting water. The products of the splitting are oxygen molecules, electrons, and protons. Oxygen is released into the air while the electrons and protons are provided to PSI. After that, PSI absorbs sunlight too and converts it into energy molecules for the cell (Allakhverdiev, 2011; Fromme and Grotjohann, 2011; Govindjee and Krogmann, 2005). The importance of this process is not limited to plants only but also for other creatures who depend on them in the food chain. Thus, the absorption of solar energy is vital to many forms of life on earth.

In our modern world, the use of energy in its different forms is one of the important characteristics of human civilization. The energy demand has hugely increased after the industrial revolution and still increasing until our day. And as the world is shifting away from fossil fuels, new renewable sources must be developed that are clean, sustainable, and efficient. Researchers have been exploring ways to imitate nature and benefit from solar energy to fulfill the different needs of our civilization.

Solar energy is promising and have significant potential due to the amount of sunlight that hits earth surface, the solar radiation at earth surface is estimated on average to be around 173 000 billion kWh every hour, while worldwide electricity consumption in 2019 was 23 845 billion kWh (U.S. Energy Information Administration). Therefore, the amount of sunlight reaching earth's surface in one hour is more than 7 times the annual electricity consumption in the world. Subsequently, if an effective method was developed to harvest it, it will solve one of our biggest issues for today. For their potential, solar energy technologies,

in general, are getting attention, and they are projected to have an increasing share in the international energy market (Skoczkowski, Bielecki, and Wojtyńska, 2019).

On the other hand, the most popular method to generate electricity from solar energy which is solar cells comes with a set of challenges that decrease their practicality. One of them is the energy storage problem. Current solar panel systems cannot alone provide sufficient and effective electricity to the grid. This is because the sun is not available throughout the day and solar energy varies in its intensity over the year. This requires electricity to be stored on a large scale to sustain continuous supply to the grid.

However, electricity storage on a big scale enough for the whole grid is quite challenging and requires enormous effort to deal with it. But while big scale energy storage as electricity is not feasible by batteries or classical small scale storage methods, new alternatives is suggested to overcome this problem.

The energy may be stored as chemical energy which can be converted to electricity or other energy forms in a feasible way. One of the proposed systems to do so is the artificial photosynthesis in which energy collected by solar farms is used to split water and produce hydrogen and oxygen gases. The hydrogen gas can be stored and transported in order to be used again as energy or for other industrial purposes (Lewis, 2007).

The artificial Photosystems are designed to elucidate PSII system to form O_2 gas from water. But, unlike the PSII system, the product of reduction part of the reaction is H_2 gas. While in the Photosystem, the product of reduction part of PSII is electrons and protons that are used to synthesis energy molecules within the plant.

Water split reaction consists of oxidation and reduction half-reactions. The reduction half-reaction is a considerably easy reaction that exhibits no major barriers compared to the other half. The oxidation part has a potential of 1.23 V against NHE. This make the reaction unfavorable thermodynamically and requires high amount of energy (Najafpour and Govindjee, 2011).

We can talk about two kinds of barriers of concern here, the thermodynamic barrier and the kinetic barrier. The thermodynamic barrier cannot be avoided because it arises from the

difference between reactants and products, which is not affected by the reaction pathway and kinetics. The kinetic barrier on the other side depends on the reaction pathway. Pathway dependent kinetic energy barrier can be lowered using different kinds of catalysts. Therefore, the goal of any catalyst developed will be to lower the reaction barrier to its minimum.

Despite the big interest in WOR especially in the last decades, our knowledge about the detailed mechanism of the reaction, intermediates, and transition states involved is still humble and a matter of debate. The main reason for that is the difficulty of isolating the short-lived intermediates experimentally. In such cases, while experiments cannot provide all the details, theoretical methods play a crucial role. The data that is accessible by different computational chemistry methods can help to understand the mechanism of the reaction.

Many catalysts for WOR have been introduced and studied in the literature, regardless of the absence of a clear understanding of WOR mechanism. In order to design better catalysts based on rational design principles, a clearer understanding of the mechanism is needed (Hemmerling, Mathur, and Linic, 2021; Najafpour, Moghaddam, Allakhverdiev, and Govindjee, 2012).

Third row transition metals are known for their capabilities and usefulness as catalysts in variety of chemical reactions. Specifically, under the scope of WOR, Ir and Ru based catalysts have shown interesting features and performance (Li et al., 2019; Matheu et al., 2019). In spite of this, to keep the catalyst practically usable in the real world, it must be based on relatively abundant first row metals. Cobalt based catalysts have been getting attention as potential WOR catalysts which are relatively abundant, cheap, and with interesting electronic features. In this study, we wanted to elucidate the electronic structure of cobalt-based systems and to study the pathway of the most important step in the reaction.

The WOR catalysts in general could be classified into two groups, the multi metal center catalysts, and mono-nuclear ones. In both cases, the reaction is thought to be initiated by forming an M–O center or centers by a series of Proton Coupled Electron Transfers. The M–O center later acts as the center of the reaction and a series of events will follow to release O_2.

Between reaction steps, the O–O bond formation consists the highest energy barrier (Shaffer, Xie, and Concepcion, 2017). The bond is formed by attacking or interaction within the M–O center of the catalyst with a nucleophile moiety such as H_2O. The oxygen of H_2O interacts with the oxygen of the M–O forming the O–O bond. So, to get a better insight into the formation of the O–O bond, the M–O structure should be studied and characterized in detail. The structure and nature of the M–O center are thought to be informative of which transition states and intermediates will evolve during the reaction and which reaction path will be followed (Turhan et al., 2018).

For early transition metals, many M–O complexes have been identified (Andris et al., 2019; Bernasconi et al., 2017a; B. Wang et al., 2017), and their role in many reactions has been studied. Such as, Iron in Cytochromes P450 enzymes (Meunier and Bernadou, 2002). Another example of an M–O complex is the Mn-Ca clusters found in the OEC of the PSII system (Najafpour et al., 2012).

The M–O center contains a high count of *d* electrons from the metal, which plays an important role in the reaction. The involvement of metal and *d* electrons in degenerate states raises the complexity of the system and puts more restrictions on which methods can be used. Accuracy and cost of computational chemistry methods highly vary, thus the selection of the method must be optimized to use the highest accuracy possible with the most economical method affordable in terms of computational resources.

The systems studied in this thesis contain a Co center with several ligands, each system has high count of electrons with different spin states and the calculations involve electron transfer events. Thus, intending to correctly describe the systems, it becomes more and more important to use methods that include multiple configurations into the calculations. In such situations, the computational cost will be higher and the results will be more accurate and reliable.

In this context, it is much more feasible from a computational point of view to perform calculations with DFT methods, due to their low computational costs. DFT is a single configurational method based on electron density (Hohenberg and Kohn, 1964). DFT is used widely in computational chemistry with reasonable accuracy for ground state calculations and calculations where a single electronic configuration is dominant, which does not include

bond formation-breaking events. Therefore, using DFT may bring on some obstacles when dealing with our systems.

In order to describe the electronic structure more accurately, the followed approach was to perform a Complete Active Space Self Consistence Field (CASSCF) calculation followed by perturbative treatment. Using CASSCF, it is feasible to examine big systems and focus more on the orbitals where electron transfer is taking place. However, compared to single determinant approaches CASSCF has more tight limitations on the size of studied molecules as it is a highly expensive method in terms of CPU processing, disk, and memory requirements.

The work in this study is organized as follows, (i) In the first part, a set of cobalt-centered molecules (Figure 1.1.) have been studied with both DFT and CASSCF methods aiming to properly describe the Co–O center. (ii) In the second part, one model system was picked (L2) and the H_2O attack toward the Co–O center and O–O bond formation was studied in detail. The small size of the model system allowed us to perform the calculations at a higher level of theory compared to the first part. The path from the approaching H_2O until the bond is formed was scanned by CASSCF methods.

The five molecules of interest are shown in Figure 1.1.

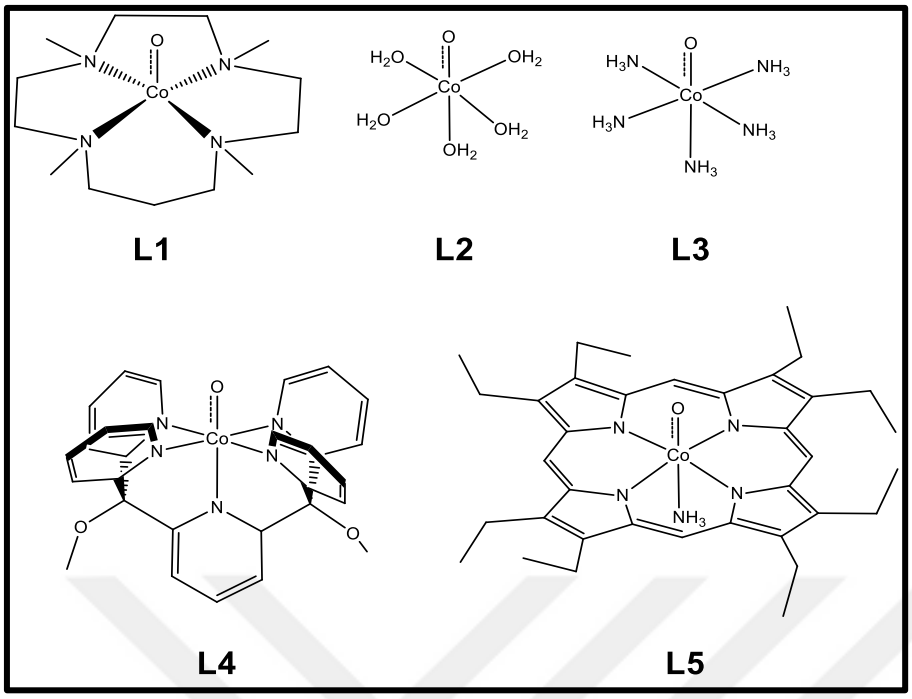

Figure 1.1. Molecules of interest

L1 is a non-heme cobalt complex synthesized by Wang et al., in 2017. It was shown to be capable to act as oxidant in C–H bond activation, intermetal oxygen atom transfer, and olefin epoxidation reactions (B. Wang et al., 2017).

L2 is a hypothetical model system to model a cobalt oxide heterogeneous catalyst. Between metal oxides, cobalt oxides have been known for decades to be capable of oxidizing water molecules.

L3 is a hypothetical system close to L2 with different ligands.

L4 is the first example of stable homogenous mono-Cobalt WOC. It was first synthesized by Berlinguette et al., in 2011 (Wasylenko, Ganesamoorthy, Borau-Garcia, and Berlinguette, 2011).

L5 is an example of a porphine cobalt complex. Cobalt porphyrins have been suggested to be catalysts for water oxidation (Nakazono, Rene Parent, and Sakai, 2013). L5 (2,3,7,8,12,13,17,18-Octaethyl-21H, 23H-porphine cobalt) in particular has low oxidation potential and high stability (Kadish, 1986).

2. THEORETICAL FOUNDATION

2.1. Water Oxidation Reaction (WOR)

Splitting water is a redox reaction. In the oxidation half, protons, electrons, and molecular oxygen are formed. The oxidation half is known as WOR and has a high overpotential barrier of 1.23 V vs NHE at 0.0 pH.

$$2H_2O_{(l)} \rightarrow O_{2(g)} + 4H^+_{(aq)} + 4e^- \quad E^0 = 1.23V \tag{2.1}$$

Versus normal hydrogen electrode (NHE) at pH = 0.0

On the contrary, the reduction half is more feasible with an overpotential of 0.0 V against NHE at pH 0.0. (Which is the definition of the normal hydrogen electrode cell itself)

$$4H^+_{(aq)} + 4e^- \rightarrow 2H_{2(g)} \quad E^0 = 0.0V \tag{2.2}$$

Versus normal hydrogen electrode (NHE) at pH = 0.0

The outcome of the reduction half can be different in different systems; the nature's photosystem produces hydrocarbons to be used in the cell, while the goal of most artificial systems is to produce H_2 (Matheu et al., 2019; Najafpour et al., 2012). The reduction half will not be in our interest in the scope of this study, and we will be focused more on the part of oxidation.

Regardless of the long-time effort spent on WOR, the exact mechanisms and nature of intermediates, both in nature and in artificial systems, is still a matter of debate (Dau et al., 2010). This uncertainty can be attributed to, the short-lived intermediates that are difficult to isolate and the complexity of the electron transfer processes.

However, many researchers have come to compile a general picture of what is happening. The general proposed mechanism for WOR is shown in Scheme 2.1 independent of the specific metal center involved.

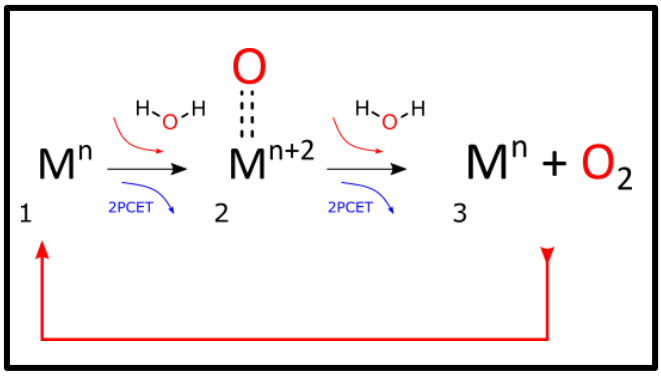

Scheme 2.1. General mechanism for WOR

The reaction is initiated by a proton coupled electron transfer (PCET) step followed by another PCET to achieve the M–O intermediate. The reaction can then advance in one of two pathways depending on geometry and electronic structures. But in either pathway and as a result of another 2 PCET steps it will yield molecular oxygen as a product and the metal center will return back to its initial state. In this study, we will be investigating the reaction path from M–O to O–O bond formation.

The two main pathways from the intermediate M–O to O_2 are water nucleophilic attack (WNA or Acid-Base) or Interaction of two metal centers (I2M or radical coupling) and are shown in more detail in Scheme 2.2 below.

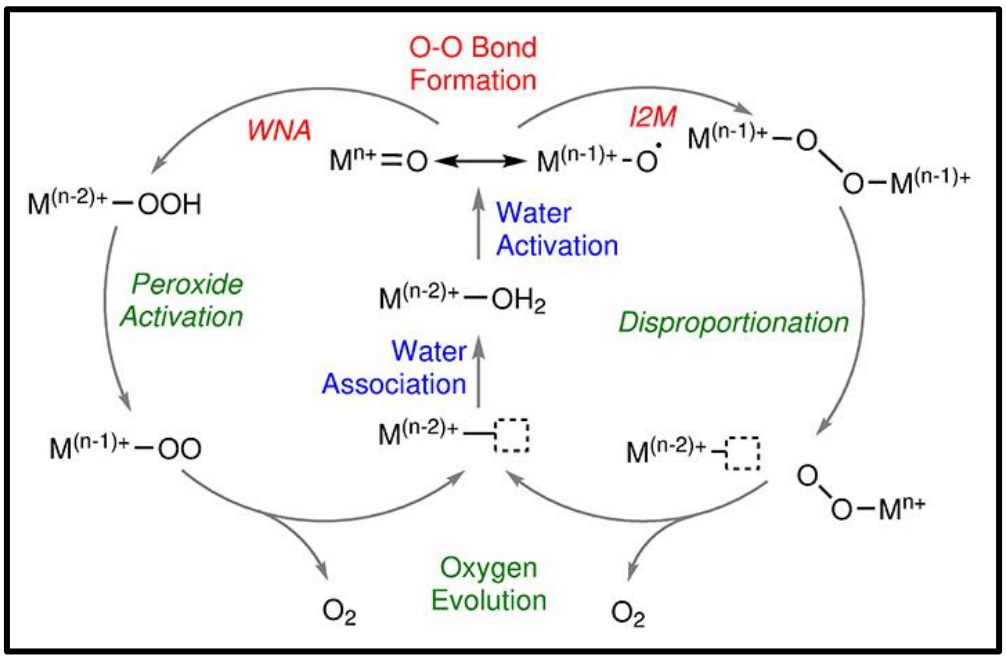

Scheme 2.2. Schematic overview of water oxidation mechanisms

M represents any redox active transition metal, n is the highest formal oxidation state reached by the metal center during catalysis (Schilling and Luber, 2018).

In the radical coupling mechanism, two M–O centers interact to make the O–O bond and release the O_2. For such a pathway to be chosen the two centers must show radical character localized on the O atom. Another important factor is the geometrical configuration. The geometry of the complexes must allow for the two oxygens to face each other and interact (Scheme 2.3) (Fan, Zhan, and Ahlquist, 2016).

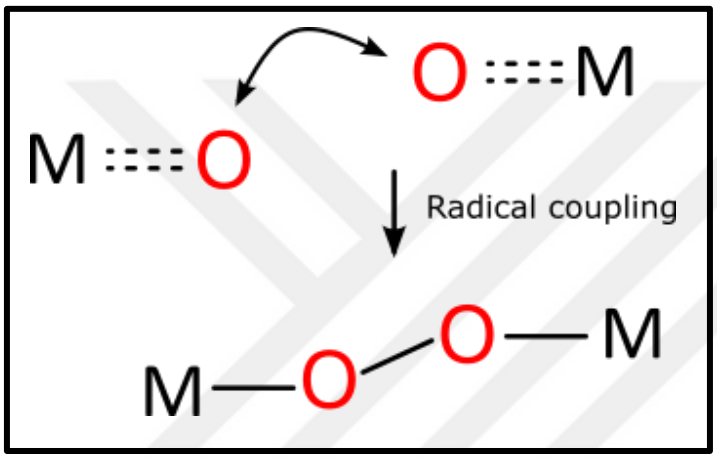

Scheme 2.3. Radical coupling mechanism

Although it may be expected that an interaction between two radical centers must be without barriers. The restricting geometrical requirements makes a smaller number of complexes meet the criteria. Hence, radical coupling is not achievable by every catalyst. *Fan et al.* have studied this issue on Ru based catalysts, they found that steric effects and ability to have face-to-face position between two M–O centers has significant effect on reaction pathway. Therefore, the expected barrierless pathway may exhibit some barriers if the geometry is not in face-to-face position. It is also stated that a significant spin density on the oxo is necessary for the reaction to be possible (Fan et al., 2016).

On the other side, the nucleophilic attack is more flexible in terms of geometry. In general, a nucleophilic attack happens when a nucleophile moiety attacks an electrophile moiety. In WOR, the nucleophilic moiety can be OH_2 with a lone pair on the oxygen atom giving it that nucleophilic character. Then it attacks the electrophilic center of M–O in the catalyst.

2.2. Water Nucleophilic Attack

In this study, we examine the Water Nucleophilic Attack (WNA) on Co–O center in more detail. The nucleophilic reactions are observed in various chemical reactions, one of the most famous ones are the S_N1 and S_N2 mechanisms in organic chemistry. Although the mechanism is quite different from WNA, the main idea is similar; a nucleophile moiety interacts with an electrophile to transfer its electrons. This can be done in more than one step or one step depending on the reacting molecules. In the WNA case, the electrophilic part is a coordination compound of a metal bound to a terminal oxygen. The electrons of the lone pair on the H_2O make it the nucleophilic part of the reaction

In the literature, the classical water nucleophilic attack is mainly described as a single-step reaction (Schilling and Luber, 2018). To form an O–O bond in a single step WNA, two electrons are transferred from the lone pair of H_2O to the LUMO orbital of the terminal O (Turhan et al., 2018).

Bernasconi et al. have addressed a notable matter related to the WNA pathway. They have shown that investigating the pathway PES by scan instead of investigating only the intermediates and TS structures may reveal a multistep WNA mechanism different than typical single step WNA (Bernasconi, Kazaryan, Belanzoni, and Baerends, 2017). They have studied an Fe complex by applying the thermodynamic integration scheme where the O–O bond formation was scanned in a Fe(IV)=O complex. The bond length was constrained to a constant length in every step and the length was decreased in intervals to perform the scan. By this method, a step-wise mechanism for the WNA was revealed, where H2O is oxidized first by the transition metal complex, in a second step the O−O bond formation takes place between the two radicaloid species, followed by deprotonation to form the hydroperoxide moiety (Scheme 2.4).

Thus, two steps of single electron transfer events result in the O–O bond formation, but unlike conventional WNA mechanisms, this mechanism results in Hydrogen peroxide formed instead of O_2.

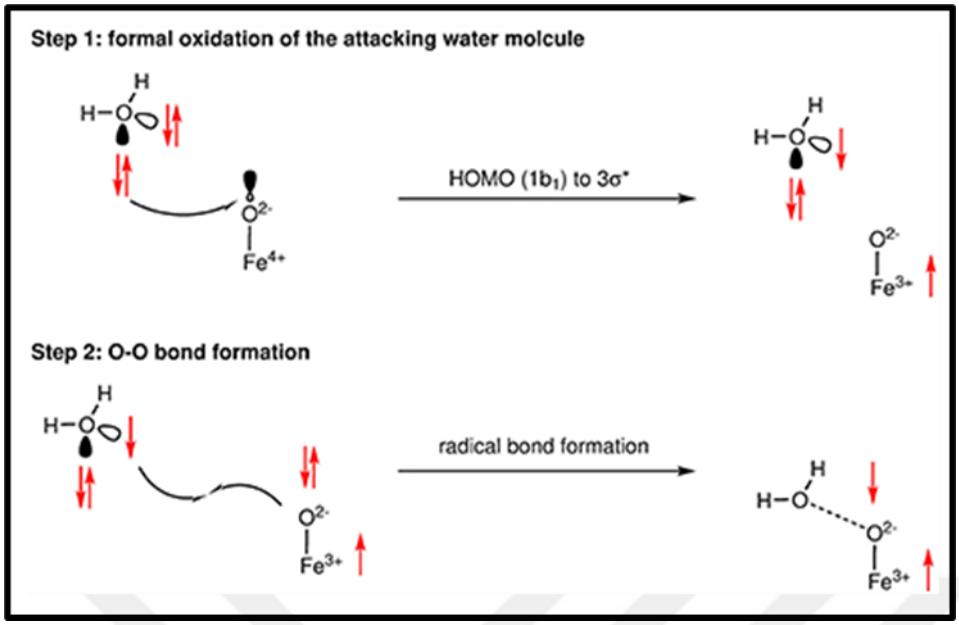

Scheme 2.4. Two step WNA mechanism (Bernasconi et al., 2017b)

A similar electron transfer mechanism was studied by Funes-Ardoiz and coworkers (Funes-Ardoiz, Garrido-Barros, Llobet, and Maseras, 2017) for a set of copper catalysts, The studied path resulted in a single electron transfer-water nucleophilic attack (SET-WNA).

From the mentioned studies above, it can be anticipated that the chosen approach of study may have effect on the results. in cases where a scan was performed over PES of WNA it revealed unusual mechanisms. Specially with limited data available from experiments, it is important to explore all the possible pathways of the reaction in order to clarify the most feasible mechanism with minimal error.

2.3. Metal Oxo

Metal-Oxo complexes have been suggested to be reactive intermediates in various oxidative transformations including WOR. The metal–oxo and its electronic structure have an important effect on the evolving reaction and its pathway. Various M–O complexes have been identified for early transition metals with bond orders reaching up to three for V, Mn, as well as Fe complexes featuring a double metal oxygen bond (oxo). The increasing count of d electrons that occupy antibonding orbitals (Figure 2.1) results in weakened bond order, which is reflected in difficulty of obtaining metal oxo complexes for late transition metals such as Co, Ni, and Cr.

Nevertheless, it is still possible to form a single weak bond with oxygen, in some cases a little modified coordination symmetry or high spin state configuration helps stabilize the bond and the complex (Andris et al., 2019; Kim et al., 2016; Larson, Battistella, Ray, Lehnert, and Nam, 2020). Also, lack of stable metal oxo complexes does not mean that they are not involved in the reaction, yet, metal oxo species as transient intermediates may be crucial to some mechanisms (Chen, Aschaffenburg, and Cuk, 2017).

Ligand field theory predicts that early transition metals with low d electron count can facilitate strong oxo bonds while it makes it harder to achieve high oxidation states. Nevertheless, as discussed above, WOR reaction demands serial PCET steps that exhaust the M center toward the O_2 release. Moreover, this contributes to the fast decay of the catalyst, especially for first row metals, which are less stable than their second and third row counterparts. The difficulties associated with first row complexes make it increasingly hard to design a stable, efficient, and cheap catalyst with high turnover frequency TOF. However, if such a catalyst has been designed it is anticipated that it will have superior features.

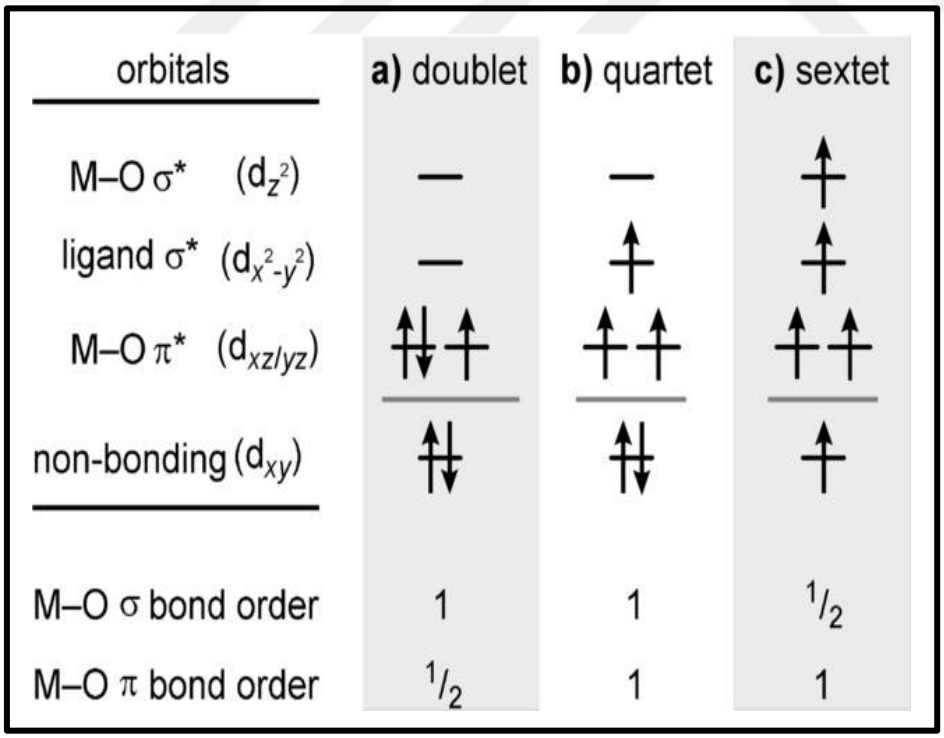

Figure 2.1. Electronic configuration of tetragonal d5 metal-oxo complexes in a) doublet, b) quartet, and c) sextet states, (Andris et al., 2019)

2.4. Oxo Wall

Many oxo complexes exist for early transition metals, this arises from that early transition metals can form stable oxo bonds with the terminal oxygen ligand (Larson et al., 2020). But going right in the periodic table, metals have more d electron count and with more d electrons in the M–O center, the antibonding orbitals are being filled and hence the total bond order is decreased. Consequently, a metal–oxo complex cannot be formed after the 8th group.

This phenomenon in literature is named Oxo Wall. In accordance with that, for late transition metals, there are no examples of such complexes with bond order greater than or equal to two.

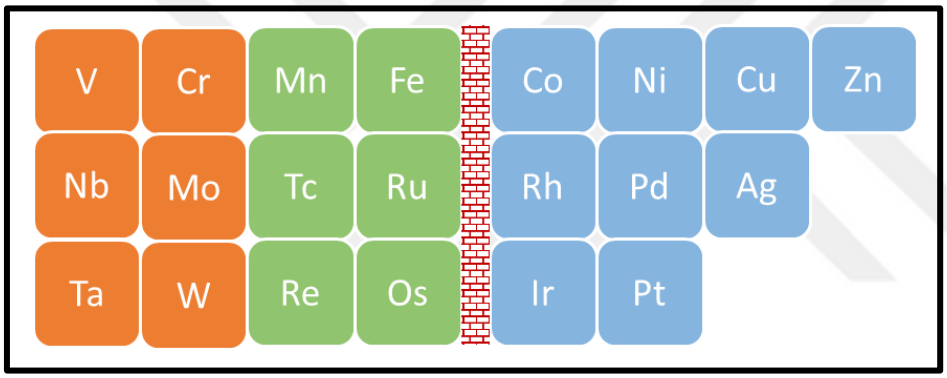

Figure 2.2. Oxo wall

On the other hand, the term oxo wall does not prohibit the existence of a double bond between the late transition metal and oxygen if the symmetry or spin state is changed and this has been a subject of little debate in the literature (Andris et al., 2019; Larson et al., 2020; B. Wang et al., 2017). Also, worth mentioning that the inability to form a stable bond and stable intermediate does not necessarily mean that the catalytic activity is low or the reaction will not occur, in contrast very short life-time of the intermediate may make the reaction more feasible and lower the reaction barrier.

Our studied Co centered molecules lay just on the edge of the oxo wall, which may attribute some interesting electronic features to it.

2.5. Water Oxidation Catalysts

Water Oxidation Catalysts (WOC) that catalysis WOR needs to be robust and efficient in order to be practically usable. The catalyst complex needs to be able to achieve high oxidation states enabling four PCET steps. The OEC of PSII system (which features a Mn_4CaO_5 cluster) carries out the WOR very effectively. With high TOF and yield, but the complex gets exhausted in a short time and requires the reconstruction of the Mn_4Ca cluster every 10-15 mins due to the damage caused by reacting with generated O_2, which is done by a sophisticated biological process (Matheu et al., 2019). Thus, the quest for an effective and stable artificial WOC is faced with several challenges.

The artificial counterparts of nature's system first emerged in the 1900s when the ability of cobalt oxides nanoparticles (CoO_x) to oxidize water molecules have been observed (Coehn and Gläser, 1902). This happened before the foundations of coordination chemistry have been set yet. Later, with the growth of our understanding of catalysts and coordination chemistry new catalysts were proposed, designed, and tested. Starting from the 1980s the number of new catalysts was growing rapidly (Hemmerling et al., 2021; Li et al., 2019; Matheu et al., 2019).

The very first examples of WOCs were mostly based on Ru and Ir like heavy metals with multiple metallic centers. By that time, it was thought that the mechanism depends crucially on several centers and interactions between them (similar to OEC) (Matheu et al., 2019), however, later, some single metallic centered catalysts have been identified. The identification of such systems opened a new era in the understanding of WOR and possible reaction pathways, nonetheless, it stayed in the region of rare and heavy earth metals.

Soon the rapidly developing research suggested many examples of first row metals as catalytic centers, the electronic structure of metals such as Mn and Fe helps in terms that it could achieve high oxidation states and vary the formal charge of metal centers and at the same time the complex stays stable. Both Mn in PSII and Fe in many catalysts developed later can have formal oxidation states starting from M^{2+} to M^{4+} or M^{5+} (Scheme 2.5) thus, facilitating the reaction to occur. In addition, the ability of those metals to initial state of the cycle without being exhausted is very important in order to have a high turnover capacity and overall effectiveness.

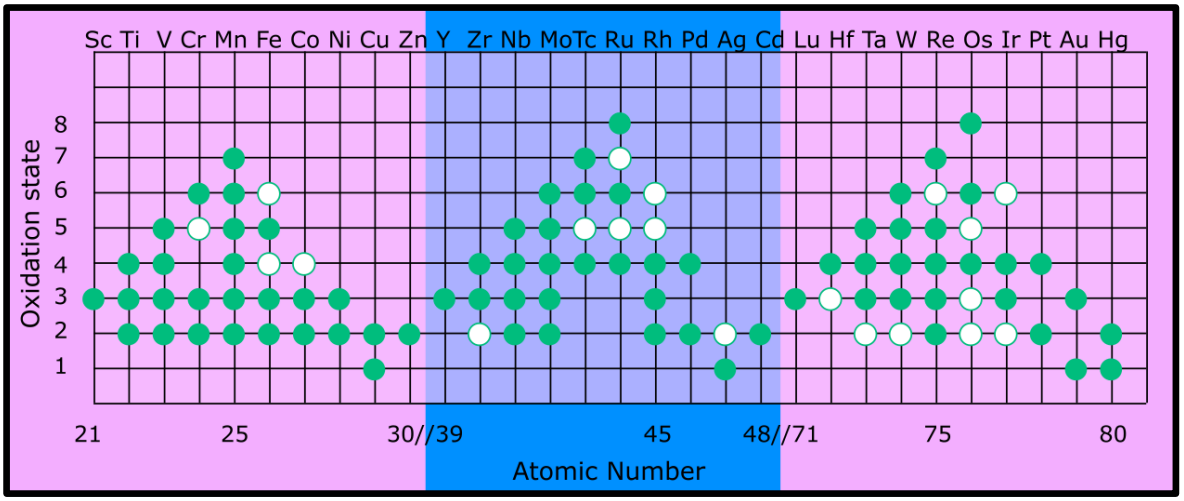

Scheme 2.5. Some of the oxidation states found in compounds of the transition-metal elements

The more common oxidation states are represented by solid circles, and the less common ones are represented by open circles (Oxtoby et al., 2007).

2.6. Cobalt Based WOCs

Although many homogenous cobalt catalysts have been added to the literature, in some of the cases, it turned out that the role of cobalt complexes is only as a pre-catalyst complex (Safdari et al., 2018), later decompose and precipitate toward the formation of (CoO_x) real heterogeneous catalysts. This reality while emphasizing the activity of Co for WOR, highlights poor stability of some Co complexes (Daniel et al., 2017; Ullman et al., 2014; J. W. Wang, Sahoo, and Lu, 2016). However, Wan and coworkers have provided an evidence on molecular level for the OER reactivity on a porphyrin cobalt complex, the decomposition of Co catalysts to cobalt oxides may be dependent on the involved substrate effects and solution environment (X. Wang, Cai, Wang, and Wan, 2019).

In 2011, Berlinguette and coworkers introduced the first example of a stable homogenous example of mononuclear Co based catalyst (Wasylenko et al., 2011). And from then on, many other complexes have been studied increasingly over the years. The abundance of Co in earth combined with its interesting electronic features gave it the potential to be a desired and efficient water oxidation catalyst.

Another interesting complex was studied by Nam and coworkers (B. Wang et al., 2017). The non-heme cobalt complex studied both experimentally and theoretically, showed a Co–O bond length of ~1.62 Å approaching the oxo double bond but not exactly breaking the oxo wall. It was noted that the ground state of the complex is the quartet state with three singly occupied orbitals. In accordance with what is expected theoretically from a d^5 metal center. As discussed above and shown in (Figure 2.1). The quartet state allows for the formation of a bond with a higher bond order compared to doublet or quartet spin states in a d^5 metal center, therefore, it is responsible for a more stable complex and lower energy. The complex had a quartet ground state with two of the three SOMO's were delocalized over the bond thus, it was a better explanation to show them over the bond and not localized over Co or O. (Scheme 2.6) this means that it is better to describe the bond as a combination of oxo and oxyl nature since any one of them alone will be misleading.

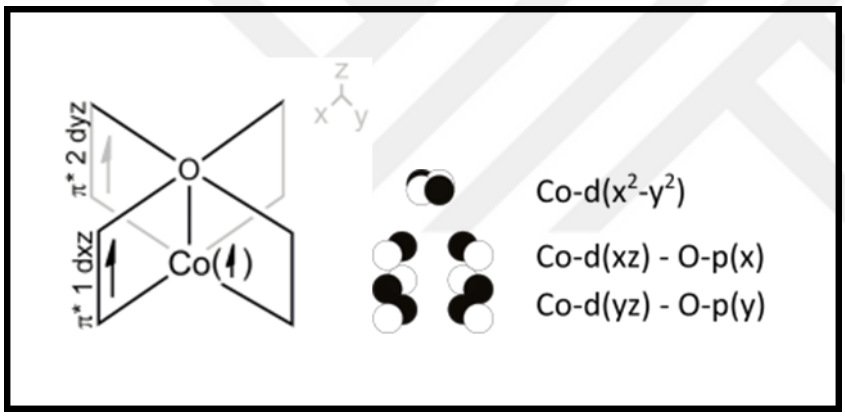

Scheme 2.6. Schematic representation of the 3 SOMO's of the quartet state in Co complex

In 2018, Karadas and coworkers studied a new cobalt-based catalyst, $Co_3(BO_3)_2$ under neutral conditions and has confirmed its stability and activity toward WOR (Turhan et al., 2018). It was shown experimentally that borate ligands resulted in enhanced activity and stability of the complex. Dede and coworkers investigated the $Co_3(BO_3)_2$ catalysts and used CASSCF method to analyze the complex (Turhan et al., 2018). It was shown that adding BO_3 ligands lowered the energy of the LUMO $d(z^2)$ compared to the complex without BO_3. The low energy of the LUMO was associated with more facile O–O bond formation.

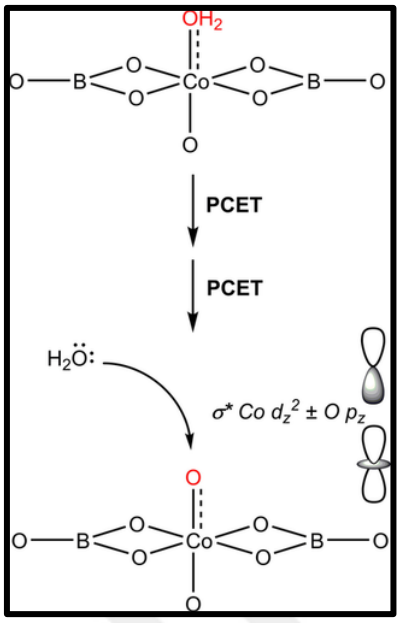

Figure 2.3. Schematic representation of WNA toward LUMO of Co–O center (Turhan et al., 2018)

Another interesting work by Sason Shaik and coworkersinvestigated the enhanced reactivity of Co compared to other metals involved in hangman corrole complexes in WOR (Lai et al., 2012).

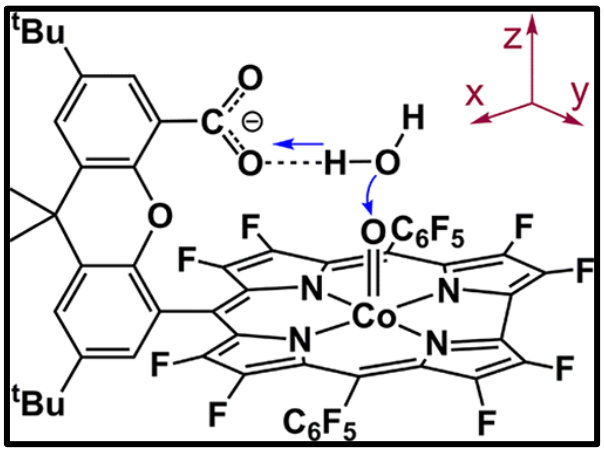

Figure 2.4. Co based hangman corrole complex example studied (Lai et al., 2012)

The study showed that the unique character of cobalt electronic structure is responsible for high potential of Co. This emphasized that Co may be the best metal to use in water oxidation. The activity of Co was explained in terms of Exchange Enhanced Reactivity (EER). EER suggests that the path allowing for the most exchange-enhanced in electrons would be the most feasible.

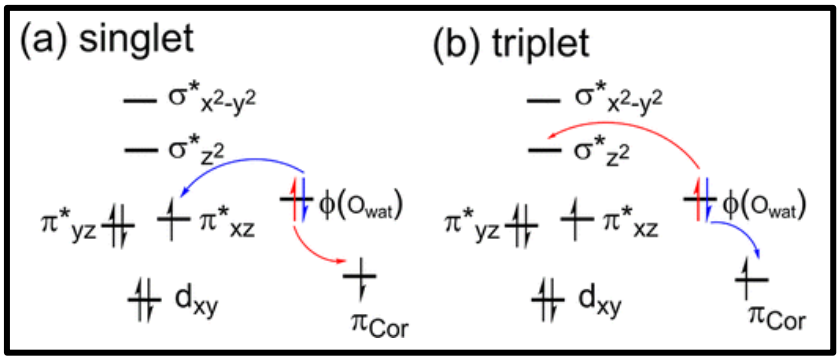

Figure 2.5. The two possible pathways of water attack to a Co based hangman corrole complex (Lai et al., 2012)

EER can tell us about two things, firstly, about the most favored spin state, and secondly, about which orbitals are involved. From those two points, we can draw a picture of how the geometrical path would be and why some metals work better than others.

Importance of biradicaloid oxene species [Co(II)–(·O·)]2+ was previously mentioned by Baik and Berlinguette and their coworkers as the responsible species for the activity of the intermediate spin state based on DFT calculations for **L4** complex, but neither how it is formed nor the existence of the same effect on the other spin states were mentioned (Crandell, Ghosh, Berlinguette, and Baik, 2015).

In that essence, if the formation of an oxene species was shown to be favorable, it could be explained by EER. Because a biradicaloid character obviously needs more single electrons and a higher spin state, therefore, it would allow for more exchange in electrons through the reaction.

3. METHODS

3.1. Schrödinger Equation

The basis of quantum chemistry methods is solving or trying to guess the best solution to the equation that describes the motion of electrons, the Schrödinger equation.

The simplest form of the Schrödinger equation is shown below in Equation 3.1, and it consists of the Hamiltonian operator ($\widehat{H}$) applied to a desired eigenfunction (wave function (Ψ) in this case) which is equal to the eigenvalue (Energy in this case E) multiplied by the eigenfunction.

$$\widehat{H}\Psi = E\Psi \tag{3.1}$$

The Hamiltonian operator has many parts that can be classified into two sets, the potential and kinetic energy operators as follows in Equation 3.2.

$$\widehat{H} = T_e + T_n + V_{ee} + V_{en} + V_{nn} \tag{3.2}$$

Where,
T_e: Kinetic energy of an electron
T_n: Kinetic energy of a nuclei
V_{ee}: Potential energy between two electrons
V_{en}: Potential energy between a nucleus and an electron
V_{nn}: Potential energy between two nuclei's

The kinetic energy terms of the Hamiltonian operator can be relatively easy to be dealt with compared to potential energy terms. Due to the reality that we lack a proper way to describe the interactions within Many–Particle Systems, an analytical solution including the potential energy term V_{ee} is out of our reach.

The Hamiltonian can be simplified knowing that nuclei with its protons and neutrons is much heavier than electrons, so the movement of the electrons is multifold greater than that of the

nuclei. Thus, the kinetic energy T_n term can be neglected and assumed to be zero. Also, the potential energy term V_{nn} can be assumed to be a constant number and added to the calculation. This approximation of fixed nuclei is called the Born-Oppenheimer approximation.

The Hamiltonian with Born Oppenheimer approximation is as follow in Equation 3.3.

$$\widehat{H}_{BO} = T_e + V_{ee} + V_{en} \tag{3.3}$$

Until this, if there were no more than one electron in the system the V_{ee} term would not exist and the equation at all would be solvable analytically. However, with two electrons or more existing in the system, the equation gets beyond our ability and understanding to solve it analytically.

Theoretical chemists through decades have developed several methods to get away with the V_{ee} term. Even if the exact solution could not be defined, with some good approximation and sufficient amount of computation a numerical solution can be obtained. The generated solution varies with accuracy depending on the method chosen and the system studied. Having said that, the desired accuracy of a solution is very different from a method to another and what works for some problems might not work well for other problems, so it is all about what is wanted to be known about the problem (Cramer; Jensen, 2007; Lewars, 2011).

3.2. Hartree–Fock Method

The most basic approximation to be made is to treat the interaction between atoms as averaged quantity and not take into account the explicit interactions between electrons. Thus, the equation can be solved more easily keeping in mind that also Born-Oppenheimer approximation is considered too. The operator is reduced as following in Equation 3.4.

$$\widehat{H}_{HF} = T_e + V_{en} \tag{3.4}$$

With only a term for kinetic energy of the electrons and a term for potential energy between particles. This means that the wavefunction is approximated by a single slater determinant. While this approximation results in energy always above the exact energy, due to that it does

not take into account the coulomb correlation. The difference between HF energy and exact energy is called the electronic correlation. Post-HF methods aim is to describe the electronic correlation energy accurately, giving a result closer to exact energy.

Yet, because the equation would be solved iteratively, we have to guess the wave function in the Schrödinger equation and obtain the corresponding E. Then we take the obtained result and refine the wave function guess accordingly. The process goes like this in many steps aiming to minimize E until desired accuracy is achieved.

This approach implements the use of the variational principle. The variational principle states that the energy (E) corresponding to ground state wavefunction in Equation 3.1 is the lowest value possible for the wavefunction among all possible wavefunctions. Accordingly, we can start the process by a trivial wavefunction, and independent of the starting wavefunction guess the energy would continue to be lower until it approaches the exact energy.

This was one of the two methods to solve numerically the Schrödinger equation, however, there is another way to solve it using the perturbation theory.

In perturbation theory, the first Hamiltonian $\widehat{H}^0$ is considered as the starting function. The first Hamiltonian will not include the electron-electron interaction term. After the first Hamiltonian ($\widehat{H}^0$), additional terms can be calculated and added to correct for electron correlation as shown in Equation 3.5. - 3.7.

$$\widehat{H} = \widehat{H}^0 + \widehat{H}^1 + \widehat{H}^2 + \widehat{H}^3 + \cdots + \widehat{H}^n \tag{3.5}$$

The energy and wavefunction also can be written as a series with increasing order

$$\psi = \psi^0 + \psi^1 + \psi^2 + \psi^3 + \cdots + \psi^n \tag{3.6}$$

$$E = E^0 + E^1 + E^2 + E^3 + \cdots + E^n \tag{3.7}$$

First step to solve the problem with perturbation theory, is to calculate the zero-order terms.

$$\widehat{H}^0 = T_e + V_{en} \ , \ \widehat{H}^0\Psi^0 = E^0\Psi^0 \tag{3.8}$$

With every degree added to the equation, the electronic correlation energy is calculated in a higher order.

$$\widehat{H}^n = V_{ee}^n \tag{3.9}$$

Thus, both the accuracy and computation demand are increased. The computation demand scales highly with increasing terms involved. So usually, only the second or third perturbation orders are sufficient for general purposes.

Either the variational or the perturbation principles can be used to solve the Schrödinger equation numerically (Cramer; Jensen, 2007; Lewars, 2011).

3.3. Basis Sets

In Hartree-Fock or other post-Hartree-Fock methods, basis sets are used to construct a wavefunction. A basis set is a set of functions used to describe atomic orbitals. By making a linear combination of basis functions molecular orbitals and the whole wavefunction can be constructed, as in Equation 3.10.

$$\psi_i = \sum_j c_{ij}\varphi_j \tag{3.10}$$

Where φ_j is a basis function that is used to build the wavefunction. And ψ_i is the wavefunction resulted of a linear combination of atomic orbitals (basis functions). The choice of basis set is a critical factor in determining both the accuracy of results and the cost of calculation.

Generally, there are two types of orbitals (One-electron functions) that are used to form a basis set; The Gaussian Type Orbitals (GTO's) and Slater Type Orbitals (STO's). An STO can describe the electron's wavefunction more accurately than GTO. however, an STO is generally more computationally demanding compared to GTO. But it turned out that

combining both types is the best practice. So, several GTOs are used to resemble an STO which is used to construct the wavefunction (Jensen, 2007; Lewars, 2011).

3.4. Configuration Interaction

The Configuration Interaction (CI) is a post-Hartree-Fock method based on the variational principle to solve the Schrödinger equation, within the Born-Oppenheimer approximation, for multi-electronic systems. It is regarded as the gold standard in quantum chemistry, and it can be used to validate other methods.

The trial wave function is written as a linear combination of determinants. Every configuration is represented as a Slater determinant made up of spin orbitals. The configuration interaction is constructed as a combination of these determinants. CI is calculated requiring that the energy is a minimum

$$\Psi_{\mathrm{CI}} = \sum_{\mathrm{k}} c_k \psi_k \tag{3.11}$$

Usually, it has a much higher cost compared to other methods and because of that, it is more suitable for small-sized systems. And for bigger systems, the computation cost grows exponentially (Jensen, 2007).

3.5. Density Functional Theory

Another way to deal with electron-electron interaction is to take the effect of electrons over an electron as density functional. Using the density functional theory method is advantageous; firstly, it gives more reliable results compared to HF. Secondly, it does that at a cheaper cost compared to other post HF methods. Also, the scalability of the method is more linear than full CI and other methods. The benefits of DFT made it popular to use for different chemical or solid-state problems among chemists and physicists as well.

DFT works very well with organic molecules and closed shell systems. However, when approaching the region of problems involving transition metals, excited states, or near-degeneracies DFT may fail to give very good and reliable results. So even if it is relatively

easy to obtain results from DFT, it may not provide accurate results at some certain problems (Hohenberg and Kohn, 1964; Kohn and Sham, 1965).

3.6. Complete Active Space SCF

CASSCF simply is applying the full CI approach over a specific part of the electronic space called the Active Space, assuming that these active space orbitals are the most significant for the specific problem being studied. Thus, instead of performing the nearly impossible full CI calculation on all of the orbital space, the focus can be over a small part of orbitals which believed to be more important, while the other spaces are treated in a single reference method. So the computational demand of the system is dependent mostly on the size of the active space (which is denoted as (e, N) where e refers to the number of electrons and N to number of orbitals), and the cost of a calculation will grow exponentially in a manner similar to the scaling of a CI calculation. Thus, there are computational limits on the size of the active space that can be in the reach of CASSCF. In addition to that, the increasing size of the system increases computational cost even if active space size stays constant. The computational cost scales in order of O^5 (O represents the system size) with system size in case of same active space size (Kreplin, Knowles, and Werner, 2019, 2020).

3.7. Perturbative Treatment

To add a subsequent correction step for the electron correlation energy after the CASSCF, a perturbative method can be used. One method can be used is NEVPT2 (n–electron valence state perturbation theory). NEVPT2 is analogous to applying Møller–Plesset perturbation theory to HF wavefunction, where NEVPT2 is applied to CASSCF wavefunction.

In this theory, the first order term of energy correction is expanded over a set of suitably chosen multireference functions which correctly take into consideration the two–electron interactions. This approach has been integrated and used by many quantum chemistry software's. It is advantageous due to its size consistency and efficiency properties (C. Angeli, Cimiraglia, Evangelisti, Leininger, and Malrieu, 2001; Celestino Angeli, Cimiraglia, and Malrieu, 2002; Celestino Angeli, Pastore, and Cimiraglia, 2006).

3.8. Computational Details

In the first part of this study, For L1, L2, L3, L4, and L5 geometry optimization was done using unrestricted M06L (Zhao and Truhlar, 2006), B3LYP (Becke, 1998) (Stephens, Devlin, Chabalowski, and Frisch, 2002), and ωB97x (Chai and Head-Gordon, 2008) density functionals, in combination with Los Alamos National Laboratory effective core potentials basis set of double zeta quality (LANL2DZ) (Hay and Wadt, 1998) and also Triple-zeta basis set (cc-Pvtz) (Balabanov and Peterson, 2005) was used. Vibrational frequency calculations on the stationary points were done to assure that they were correct minima. Optimization and frequency were performed with Gaussian 09 (Frisch et al., 2009). All possible spin states for molecules of interest were studied. Further single point energies were calculated on optimized geometries at (UM06L/cc-pVQZ, UB3LYP/cc-pVQZ, wB97XD/cc-pVQZ) level of theory. Relative energies calculated by the different functionals and basis sets were summarized and discussed in the text.

Complete active space self-consistent field (CASSCF) calculations were performed with MOLPRO 2020.2 software (Werner, Knowles, Knizia, Manby, and Schütz, 2012; H. J. Werner et al., 2020; Hans Joachim Werner et al., 2020) using LANL2DZ basis set (Hay and Wadt, 1998), the selected active space consists of eleven electrons in eleven orbitals CAS (11,11) which were five Co d-orbitals, three oxygen p-orbitals, and three virtual Co d-orbitals. Relative energies for different spin states for all molecules are summarized and discussed in the text. Orbital plots were rendered by Chemcraft software (Ga and Da, 2020) with Map points per angstrom of 7.65, map size of 1.75, and contour value of 0.062.

In the second part of this study, geometry optimization was done using CASSCF method in combination with def2-TZVP (Weigend and Ahlrichs, 2005) basis set. Vibrational frequency calculations on the stationary points were done to assure that they were correct minima. Optimization and frequency were calculated with MOLPRO 2020.2 software (Werner et al., 2012; H. J. Werner et al., 2020; Hans Joachim Werner et al., 2020). All possible spin states for molecules of interest were studied. Ground energy states were discussed in the text.

In the Complete Active Space Self-Consistent Field (CASSCF) calculations, the selected active space for L2 consists of thirteen electrons in twelve orbitals CAS (13,12) which were five Co d-orbitals, three oxygen p-orbitals, one O_w p-orbital, and three virtual orbitals.

Relative energies for different spin states for all molecules are studied. Orbital plots were rendered by Chemcraft software (Ga and Da, 2020) with map points per angstrom of 7.65, map size of 1.75, and contour value of 0.062.

4. RESULTS AND CONCLUSION

4.1. Cobalt–Oxo Center

To understand the reaction mechanism, we need to analyze the electronic structure of the metal center involved. Based on chemical intuition, if we compare Co in C_{4v} symmetry complexes to other first row metal complexes we see that it stands just on the edge of the oxo wall. This means that a change in spin state or other factors may have a big effect on the order and the strength of the Co–O bond.

The five molecules of interest were investigated using two methods of computational quantum chemistry, DFT and CASSCF. Firstly, a geometry optimization was performed on the complexes by DFT methods at various levels of theory, and a CASSCF calculation was done over the DFT geometries.

The DFT calculations concluded in Table 4.1 below showed different ground spin states for every molecule. For example, at the UB3LYP/LANL2DZ level of theory, the ground state for L1 was a quartet, sextet for L2, and doublet for L3, L4, and L5.

This was quite an interesting result due to the similarity of the Co center and its ligands in the five molecules of interest. However, the inconsistency may be attributed to functional or basis set related issues. To overcome those limitations, we tried the calculation again with different basis sets (LANL2DZ, cc-pVTZ, and cc-pVQZ) (Hay and Wadt, 1998; Weigend and Ahlrichs, 2005) and with various functionals (UB3LYP, UM06L, and UωB97xD) (Becke, 1998; Chai and Head-Gordon, 2008; Zhao and Truhlar, 2006). Using different functionals the result has not changed significantly, the same ground states still were observed at UM06L/LANL2DZ level of theory where the quartet was the ground state in L1 and L2, and doublet in L3, L4, and L5.

Nonetheless, the calculation with larger basis sets (Filatov, Reckien, Peyerimhoff, and Shaik, 2000) with the same functionals yielded a ground state of a quartet in molecules L1 – L4 with previously ground state doublet having slightly higher energy in L3 and L4. In the L5 case even if the ground state was doublet, the quartet was a near degenerate state with a little

energy difference. This result was confirmed later by calculating single point energies with an even larger basis set (cc-pVQZ) over the optimized geometries and there was no major shift in the results.

Importantly, the result of CASSCF single point calculations over DFT optimized geometries (CAS(11,11)/LANL2DZ//UB3LYP/LANL2DZ) showed a ground state of quartet type in all the molecules. This result may be indicating to the advantages of CASSCF over DFT, and its reliability in giving consistent results with even a small basis set. But on the other hand, it comes with its limitation as it's getting unfeasible to use CASSCF with molecules bigger in size or with larger basis sets. As in this case, we couldn't perform a CASSCF calculation using the cc-pVTZ or cc-pVQZ basis sets.

Table 4.1. Relative energies (kcal·mol-1) of L1, L2, L3, L4 and L5 optimized at different DFT levels

LEVEL OF THEORY	SPIN STATE	L1	L2	L3	L4	L5
UB3LYP/LANL2DZ	Doublet	4.0	8.4	0.0	0.0	0.0
	Quartet	0.0	2.5	8.2	4.9	9.9
	Sextet	12.5	0.0	21.2	25.0	25.5
UM06L/LANL2DZ	Doublet	9.2	15.0	0.0	0.0	0.0
	Quartet	0.0	0.0	1.5	5.1	3.9
	Sextet	14.3	5.8	19.3	26.0	21.0
UB3LYP/cc-pVTZ	Doublet	7.3	15.1	0.6	1.7	0.0
	Quartet	0.0	0.0	0.0	0.0	4.0
	Sextet	10.9	7.6	18.1	23.0	24.7
UB3LYP/cc-pVQZ//UB3LYP/cc-pVTZ	Doublet	7.3	15.5	0.9	1.8	0.0
	Quartet	0.0	0.0	0.0	0.0	3.9
	Sextet	10.7	7.6	18.2	23.0	24.6
UM06L/cc-pVTZ	Doublet	9.9	16.4	4.6	0.5	0.0
	Quartet	0.0	0.0	0.0	0.0	0.8
	Sextet	10.5	7.7	17.7	20.9	16.1
UM06L/cc-pVQZ//UM06L/cc-pVTZ	Doublet	9.8	16.3	5.1	1.0	0.0
	Quartet	0.0	0.0	0.0	0.0	0.6
	Sextet	9.9	7.9	17.7	20.8	15.7
UωB97xD/cc-pVTZ	Doublet	5.7	12.0	0.0	0.0	*
	Quartet	0.0	0.0	2.4	4.3	0.0
	Sextet	10.5	4.4	18.3	25.3	36.5
UωB97xD/cc-pVQZ//UωB97xD/cc-pVTZ	Doublet	5.8	12.4	0.0	0.0	*
	Quartet	0.0	0.0	1.9	4.0	0.0
	Sextet	10.3	4.5	17.9	25.1	36.4
CAS(11,11)/LANL2DZ//UB3LYP/LANL2DZ	Doublet	19.7	19.7	15.9	22.7	27.3
	Quartet	0.0	0.0	0.0	0.0	0.0
	Sextet	4.8	18.4	21.4	30.8	44.6

* There was no stable complex could be optimized at this level of theory.

The quartet state being the ground state comes in agreement with expectation and also with the previous work of Dede and coworkers (Turhan et al., 2018; B. Wang et al., 2017).

The three singly occupied molecular orbitals of the quartet state of Co–O complexes are constituting an interesting fingerprint. The three SOMO's and their electrons are distributed as follows, one electron is localized Co atom as Co-d(x^2-y^2) orbital and the remaining two electrons are delocalized over the Co–O antibonding orbitals, |Co-d(xz) - O-p(x)> and |Co-d(yz) – O-p(y)>. (Figure 4.1)

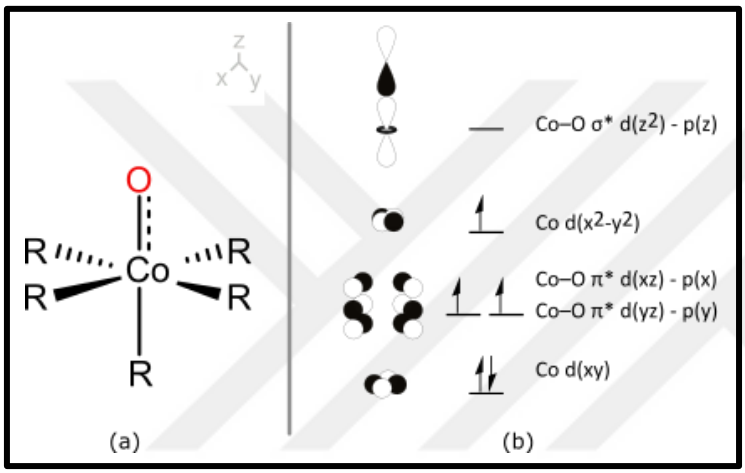

Figure 4.1. a) Drawing of a Co–O complex in C4v symmetry b) Molecular orbital representation and respective occupancies of a quartet spin complex

According to this electronic structure and in terms of frontier molecular orbitals, it could be foreseen that either the sextet or the doublet state would have one more electron occupying an antibonding MO and therefore, would conclude in a weakened Co–O bond and consequently, a higher energy complex at all. Which was viewed also in calculations.

Another point here is the length of the Co–O bond compared to other equatorial Co bonds with ligands (Table 4.1 and Table 4.2**)**. The short bond between Co and terminal oxygen exhibits an effect over ordering of orbitals; due to shorter bond on Z-axis the orbitals lay on the z-axis will have relatively higher energy compared to other orbitals on other axes. Therefore, the effect is acting as decreasing the energy of Co-d(x^2-y^2) and increasing energy of Co-d(z^2) respectively leading to unpopulated antibonding sigma orbital which helps maintain the bond order high enough.

Table 4.2. Summary of Co–O bond length R(Co–O) Å for L1, L2, L3, L4 and L5 at different levels of theory

Functional/Basis Set	2S+1	L1	L2	L3	L4	L5
UB3LYP/LANL2DZ	Sextet	1.751	2.019	1.877	1.824	1.834
	Quartet	1.744	1.644	1.646	1.693	1.637
	Doublet	1.765	1.825	1.832	1.829	1.831
UM06L/LANL2DZ	Sextet	1.735	1.799	1.796	1.778	1.777
	Quartet	1.733	1.633	1.646	1.663	1.649
	Doublet	1.734	1.802	1.816	1.820	1.822

Table 4.3. Summary of average Co-N equatorial bond lengths R(Co-N) Å for L1, L2, L3, L4, and L5 at different levels of theory

Functional/Basis Set	2S+1	L1	L2	L3	L4	L5
UB3LYP/LANL2DZ	Sextet	2.160	2.080	2.218	2.165	2.156
	Quartet	2.066	2.060	2.182	2.152	2.148
	Doublet	2.029	1.926	2.017	2.008	2.011
UM06L/LANL2DZ	Sextet	2.147	2.054	2.191	2.147	2.148
	Quartet	2.055	2.048	2.172	2.132	2.121
	Doublet	2.020	1.926	2.019	2.002	2.004

In sextet state case, the Co–O bond is longer compared to quartet state. In this manner, it will be different from the former one, that the energy of the antibonding Co-d(z^2) will be lower, which will accordingly weaken the Co–O bond.

The length of the Co–O bond is dependent on the spin state of the system, in the case of sextet and doublet states, more electrons populate the antibonding orbital which both makes the bond longer and orbitals more localized on atoms. Also, it could be said that in the case of elongated bond and localized orbitals, the weakened bond structure may suggest a formation of significant radical character on the oxygen atom. This structure may be responsible for enhanced activity in later steps of the reaction.

4.2. H_2O Attack

After identifying the Co–O center that exhibited almost identical electronic structure in all the systems studied, we carried on a detailed study of the water attack and the subsequent O–O bond formation. We have employed the CASSCF method in order to obtain qualitatively reliable results.

To elucidate the cobalt centered catalyst behavior and reaction pathway associated with it, a model system of the cobalt complexes must be chosen in order to apply the CASSCF due to computational feasibility. The model system should be small and not exceed our computational limit, and also at the same time, a good structural model of the real Co catalysts.

Luber and coworkers have used this method to study Co catalysts for WOR. They used a simple hypothetical system as in L2 to model the active species in Co WOCs (Schilling, Patzke, Hutter, and Luber, 2016). Giving the simplicity of the model, it will be more feasible to study it in a more sophisticated way. The results obtained from the simple model can be used to understand more complex systems.

The L2 complex can at least theoretically be responsible of WOR, and moreover a good model of CoOx cobalt oxides that are experimentally an active WOC.

Herein, one H_2O molecule was added to the system with fixed distances between the two oxygens of the H_2O and Co–O. the distance was varied in each scan step starting from 2.6 Å towards the full bond formation at 1.5 Å. The choice of starting 2.6 Å distance for the beginning of the interaction was rationalized by the fact that the average distance between water molecules in liquid water is ~2.6 Å (Huang et al., 2013). Thus, if the catalyst was in water and surrounded by water molecules, the average distance between Co–O and H_2O molecules is expected to be in the same range. It was assumed that interactions for larger distances are not effective in this case and not in our interest in the scope of this study.

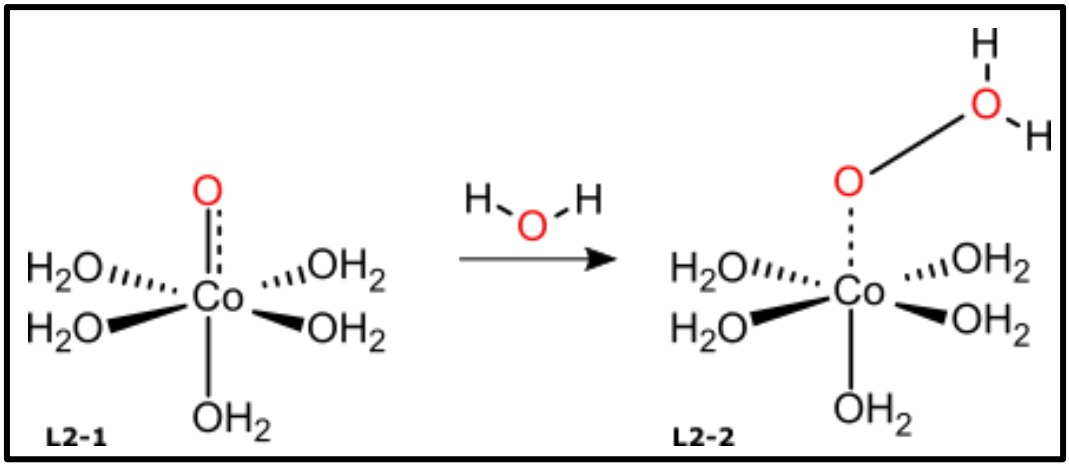

Figure 4.2. The O–O bond formation reaction coordinate

Before diving into the details of the calculations we can predict a picture of what is expected to occur based on frontier orbitals obtained in the first part of this study. A schematic representation of those orbitals is sketched in Figure 4.3 with two possible attack pathways.

The CASSCF geometry optimization of the L2-1 structure has shown that doublet structure was identical to sextet in terms of bond length, energy, and unpaired electrons count. Therefore, doublet structure was neglected in the sketch here. Consequently, the possible attack pathway to doublet would be identical to sextet as well.

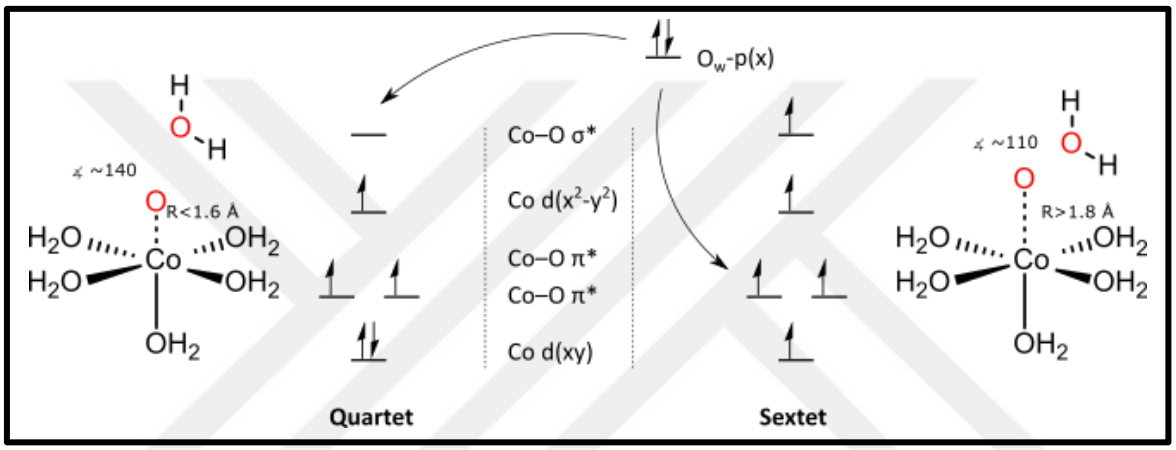

Figure 4.3. The two possible ways of attack of H2O on Co–O center and formation of O–O bond for quartet and sextet states

To make the figure clearer and easier to compare between spin states, the orbitals in Figure 4.3 were not ordered upon their energies. Nevertheless, with the effect of changing the spin state, the bond is elongated and consequently, the orbitals are reordered accordingly. Thus, in the case of the sextet state, the highest singly occupied orbitals are the degenerate O-p(x) and O-p(y) orbitals. While in case of quartet, O-p(x) and O-p(y) orbitals are lower in energy under the highest SOMO and the LUMO

The first possible pathway is the transfer of the lone pair electrons of O_w to the σ* LUMO orbital Co-d(z^2). For this transfer to occur, it is expected that the Co–O–O angle would be closer to 180º, as this position will allow for maximum overlap between the corresponding orbitals. This scenario is less expected in sextet state where the Co-d(z^2) orbital is now half filled and its energy is decreased giving rise to O-p(x) and O-p(y) orbitals, alongside with elongated bond. In this second pathway, the transfer is expected to happen toward either O-

p(x) or O-p(y) orbital. To allow for maximum overlap in this case, the attack is expected to advance with Co–O–O angle closer to 90º.

Also independent of the starting spin state, in order to form the O–O bond, the final state cannot be a sextet, because in the case of sextet state the populated antibonding orbitals result in no stable bond at all, and the final state will be either quartet or doublet. Thus, the pathway will be either over:

a) A spin forbidden reaction in case of initial sextet state that must have a crossing point in order to form the stable quartet or doublet state or

b) Quartet as spin allowed reaction.

In addition to that, the doublet spin state of the final state showed a higher energy complex with more than 40 kcal/mol (Table 4.4). Thus, independent of the path or starting state, the resulting complex is likely to be in quartet state.

Table 4.4. Relative energy of L2-2 at different spin states calculated at different levels of theory

	Level of theory	2S+1	Relative Energy (kcal/mol)	Co–O Bond Length in Å
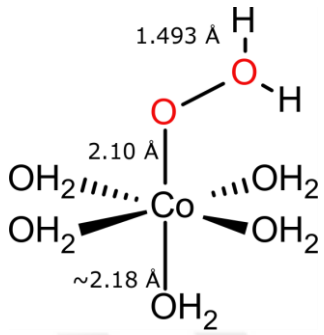	CAS(13,12) /Def2-TZVP	2	43.6	1.497
		4	0.0	1.493
		6	*	*
	NEVPT2//CAS(13,12) /Def2-TZVP	2	43.5	1.497
		4	0.0	1.493
		6	*	*

* There was no stable complex to be optimized at sextet state.

A scan was performed on the path of forming the O–O bond with intervals equal to 0.1 Å at each stop from 2.6 Å Co–O—O distance until 1.5 Å as shown in Figure 4.4 At each point of the scan, a constrained geometry optimization calculation was performed where all geometry variables were optimized except the fixed O–O distance and this was done for all the spin states.

The calculations at the initial points showed that the three spin surfaces were almost degenerate. Electronic structures, hence energies, of three states for L2-p shows similar properties at 2.6 Å O—O distance, along with the degeneracy, the three spin states showed 5 unpaired electrons similar to that of the sextet state with similar structural properties (Figure 4.4).

Importantly, previously coupled Cobalt-d and Oxygen-p orbitals are now almost localized on their atomic orbital counterparts. Significant elongation on the Co–O bond length also occurs (from 1.627 Å to 2.400 Å), approaching the value of the sextet structure of L2-1. Hence, the new MO picture is analogous to the sextet electronic structure. For L2-t we will donate quartet or doublet with five singly occupied orbitals with (5e) notation as quartet (5e) or doublet (5e) respectively, in contrast to the common three unpaired electrons quartet as quartet (3e).

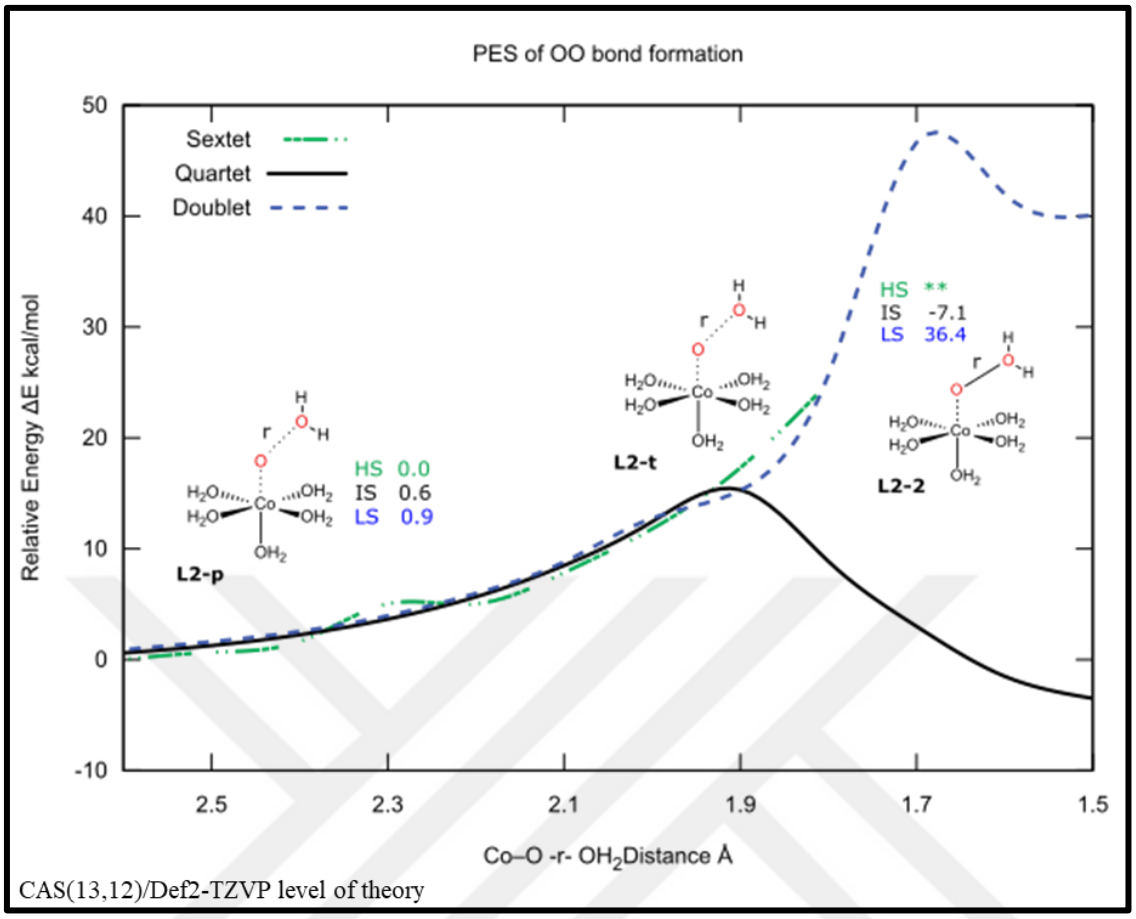

Figure 4.4. The potential energy surface (PES) of the reaction

It can be seen here that the three spin states of L2-p are almost degenerate at a distance of 2.60 Å, and sextet spin is the ground state with slightly lower energy and similar orbital occupations to quartet and doublet states. Elongation of the Co–O bond should induce a Jahn-Teller effect on the z-axis, decreasing the energy of cobalt Co-d(xz) and Co-d(yz) orbitals while increasing the energy of Co-d(xy) orbital (Figure 4.5).

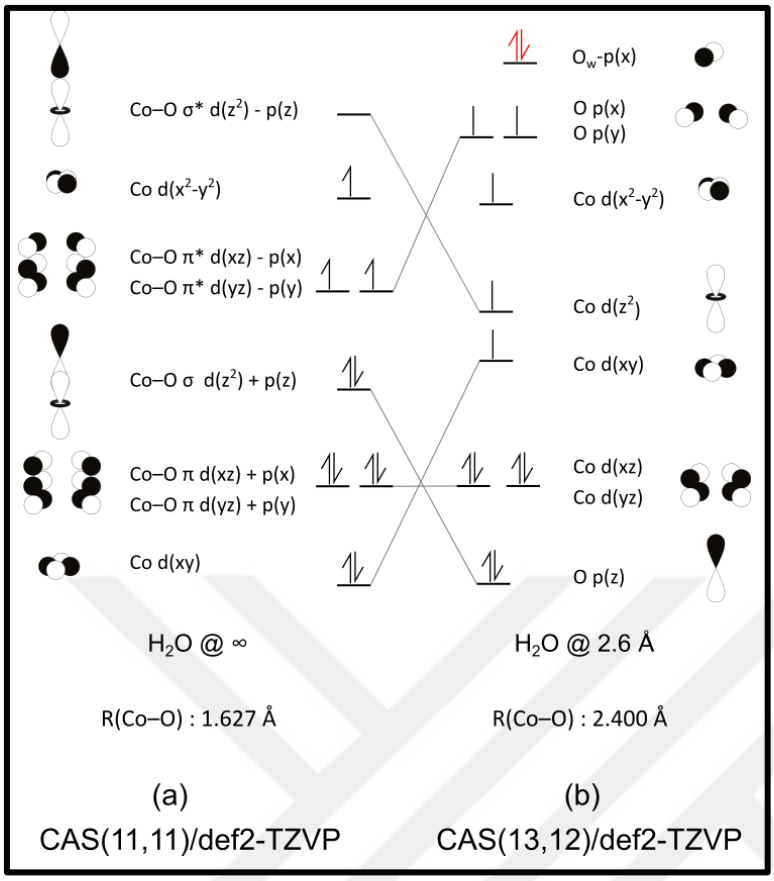

Figure 4.5. a) electronic structure of L2-1 at quartet state and b) L2-p at doublet, quartet, and sextet states

*Note that CASSCF results show five unpaired electrons for all states considered, thus alpha/beta spins are not indicated.

Another way to describe the events would be the formation of a biradicaloid Cobalt oxene [Co(II)– O·]$^{2+}$. This intensified radical character on oxygen will facilitate electron transfer. The radical character on the O atom is manifested with O-p(y) (↑), O-p(x) (↑), and O-p(z) (↑↓) electronic configuration which is consistent with the electronic structure of the highly reactive O (^{3}P).

Atomic oxygen O (^{3}P) can be found in the atmosphere in low Earth orbit (Brunsvold et al., 2007; Conforti, Braunstein, Braams, and Bowman, 2010; Filatov et al., 2000). O (^{3}P) species are highly reactive, and attacks H_2O producing H_2O_2 or H_2 and O_2 as in conventional WOR.

However, the high reactivity nature of the atomic oxygen and the loss of stability associated with it makes it hard to find or produce O (^{3}P) in normal conditions on earth. Nonetheless,

some studies have suggested it as a model to better understand the reaction (Miyagawa et al., 2021).

One of the systems that this approach is used in, is the oxygen absorption reaction of the P450 system, at some point of the reaction it is assumed that the oxygen acts as atomic oxygen. Herein, it may be a good model to assume in situ of atomic oxygen in order to study the reaction mechanism (Yamaguchi et al., 2009) (Nakamura and Sato, 2002).

The whole energy of the complex will keep rising in all of the degenerate three spin states, until the electron transfer event occurs. The first electron transfer is observed for the quartet state between 1.9 Å and 2.0 Å distance.

At this point, an electron transfer event is observed on the quartet surface and it could be seen that quartet surface is diverging from the other surfaces. The changes in the energies are also revealed in the electronic structure of the quartet state.

To examine the crossing point in more detail a more detailed scan was performed between 1.9 Å and 2.0 Å with a 0.01 Å difference at each step. Electron transfer occurs at the Co–O ---- OH_2 distance of 1.92 Å for the quartet state. This structure corresponds to an electron transfer point on the quartet (5e) spin surface (Figure 4.6**)** At this point, lone pair electrons of H_2O are transferred to previously singly occupied O-p(x) and O-p(y) orbitals.

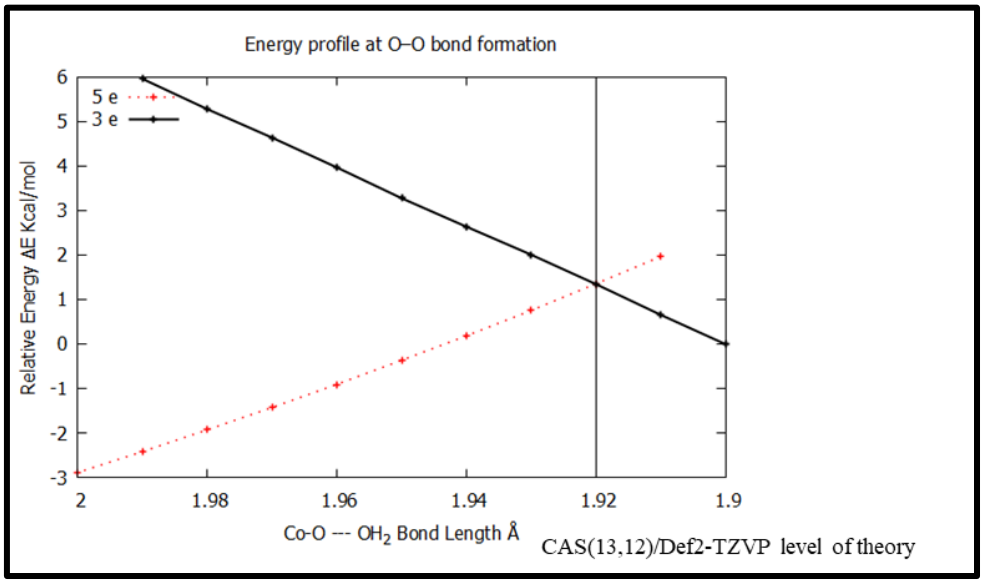

Figure 4.6. Energy profile for electron transfer point for O–O bond formation

Evidently, the entatic state of five singly occupied orbital scheme of the quartet state at the initial points gave rise to O-p(x) and O-p(y) orbitals resulting in significant radical character on the O atom. This was shown to be crucial in electron transfer events within this pathway.

H_2O approach angle from 2.6 Å until 1.92 Å, was in the middle between the axis of O-p(x) and O-p(y) orbitals. And after electron transfer, it was directed into one axis only, which is the axis of the O–O bond. This ends the degeneracy of O-p(y) and O-p(x) which is now doubly occupied bonding orbital O-(p(x)+p(x)).

After the electron transfer, the Co–O center has 13 electrons, six of which are located on the O-p(x), O-p(y), and Co-d(xy) orbitals. [Co-d(z^2) + O-p(z)] orbital is also doubly occupied. Since now the electronic structure is comprised of three singly occupied orbitals, Co–O bond length is shortened back to 2.10 A, creating a JT-compression effect. The previously singly occupied Co-d(xy) orbital has lower energy and became doubly occupied.

As O-p(x) is used for bonding with O_w, it is not available to form π bonding interactions with the Co-d(xz) orbital. O-p(y), on the other hand, can form π bonding interactions with Co-d(yz) orbitals. Therefore, two of the five remaining electrons on the Co–O center populates Co-d(xz) orbital, two populates the bonding [Co-d(yz) + O-p(y)] orbital, and the last electron is located on the antibonding orbital [Co-d(yz) - O-p(y)].

During the electron transfer event, the d electrons of the Co center does not involve in the transfer. Since the electrons and radical character are localized over the O atom, there was no change in local charge or d electron count on the Co atom.

For doublet (5e) surface the electron transfer happens later at ~1.75 Å and with a barrier of 43.5 kcal/mol higher in energy than the quartet. The fact that quartet as a product is more feasible and lower in energy can be explained by the weak ligand effect of the H_2OO. The weak ligand will favor the higher spin state of the complex (Figure 4.7). Accordingly, it's not unexpected that quartet PES has lower activation energy. Also, electron transfer occurs at ~1.92 Å earlier than that of doublet ~1.75 Å.

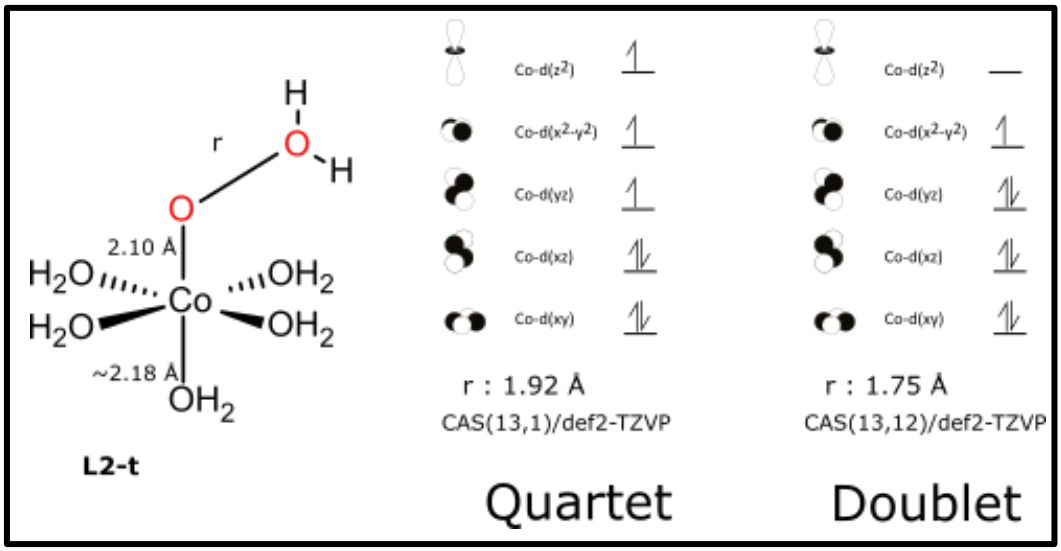

Figure 4.7. Electronic structure and orbital representation of d electrons in L2-t for doublet and quartet states after the electron transfer

Investigation of O–O bond formation pathway by scanning the approaching H_2O revealed an interesting mechanism. The H_2O disrupt the complex and form a prepared state at a long distance from the Co–O center. The disruption is manifested by an increased radical character over oxygen atom in the Co–O center. That may be the reason behind the reactivity of Co complexes.

4.3. Conclusion

The O–O bond formation is believed to be the most demanding part of water oxidation reaction, some rare earth metals (such as Ru and Ir) and first row early metals (like Mn and Fe) are found to have catalytic activity toward the WOR. Interestingly, the properties of late first row metal Co show potential toward catalytic water oxidation. Its fine-tuned bond with oxygen that can allow for an important radical character on the O center is responsible for high activity.

The CASSCF based calculations in this study showed the importance of a structure of an entatic state with five unpaired electrons on the Co–O bond prior to the attack by H_2O and forming of the O–O bond. This electronic structure will smooth the reaction and lower the energy barrier compared to usual quartet electron structure. Thus, this may be the key that describes the potential in cobalt based mono-metal catalysts.

We believe that formation of an oxene coordinated to Co center may be responsible for catalyzing the reaction without the direct involvement of the metal center in O–O bond formation step, thus the role of the metal center is to assist the in-situ formation of oxene. Nevertheless, it’s important to mention that this idea is still early to be judged as the main mechanism and needs further research and experiments.

REFERENCES

Allakhverdiev, S. I. (2011). Recent progress in the studies of structure and function of photosystem II. *Journal of Photochemistry and Photobiology B: Biology, 104*(1-2), 1-8.

Andris, E., Navrátil, R., Jašík, J., Srnec, M., Rodríguez, M., Costas, M., and Roithová, J. (2019). M−O Bonding Beyond the Oxo Wall: Spectroscopy and Reactivity of Cobalt(III)-Oxyl and Cobalt(III)-Oxo Complexes. *Angewandte Chemie - International Edition, 58*(28), 9619-9624.

Angeli, C., Cimiraglia, R., Evangelisti, S., Leininger, T., and Malrieu, J. P. (2001). Introduction of n-electron valence states for multireference perturbation theory. *The Journal of Chemical Physics,* 114(23), 10252-10252.

Angeli, C., Cimiraglia, R., and Malrieu, J.-P. (2002). n-electron valence state perturbation theory: A spinless formulation and an efficient implementation of the strongly contracted and of the partially contracted variants. *The Journal of Chemical Physics,* 117(20), 9138-9138.

Angeli, C., Pastore, M., and Cimiraglia, R. (2006). New perspectives in multireference perturbation theory: the n-electron valence state approach. *Theoretical Chemistry Accounts.* 117(5), 743-754.

Balabanov, N. B., and Peterson, K. A. (2005). Systematically convergent basis sets for transition metals. I. All-electron correlation consistent basis sets for the 3d elements Sc-Zn. *Journal of Chemical Physics,* 123(6) 4107.

Becke, A. D. (1998). Density-functional thermochemistry. III. The role of exact exchange. *The Journal of Chemical Physics, 98*(7), 5648-5648.

Bernasconi, L., Kazaryan, A., Belanzoni, P., and Baerends, E. J. (2017). Catalytic Oxidation of Water with High-Spin Iron(IV)-Oxo Species: Role of the Water Solvent. *ACS Catalysis*, 7(6), 4018-4025.

Brunsvold, A. L., Zhang, J., Upadhyaya, H. P., Minton, T. K., Camden, J. P., Paci, J. T., and Schatz, G. C. (2007). Crossed-beams and theoretical studies of the O(3P) + H 2O → HO 2 + H reaction excitation function. *Journal of Physical Chemistry A,* 111(43) 10907–10913.

Chai, J. D., and Head-Gordon, M. (2008). Systematic optimization of long-range corrected hybrid density functionals. *Journal of Chemical Physics,* 128(8) 4106.

Chen, X., Aschaffenburg, D., and Cuk, T. (2017). One-electron intermediates of water oxidation and the role of solvation in their stability. *Journal of Materials Chemistry A,* 5(23), 11410-11417.

Coehn, A., and Gläser, M. (1902). Studien über die Bildung von Metalloxyden I. Über das anodische Verhalten von Kobalt- und Nickel-Lösungen. *Zeitschrift für anorganische Chemie, 33*(1), 9-24.

Conforti, P. F., Braunstein, M., Braams, B. J., and Bowman, J. M. (2010). Global potential energy surfaces for O (3P) + H 2O(1A1) collisions. *Journal of Chemical Physics*, 133(16) 164312.

Cramer, C. J. (2004) Essentials of Computational Chemistry Theories and Models. (Second edition). New York: Wiley, 203-305.

Crandell, D. W., Ghosh, S., Berlinguette, C. P., and Baik, M. H. (2015). How a [CoIV-O]2+ Fragment Oxidizes Water: Involvement of a Biradicaloid [CoII-(·O·)]2+ Species in Forming the O-O Bond. *ChemSusChem*, 8(5), 844-852.

Daniel, Q., Ambre, R. B., Zhang, B., Philippe, B., Chen, H., Li, F., Sun, L. (2017). Re-Investigation of Cobalt Porphyrin for Electrochemical Water Oxidation on FTO Surface: Formation of CoOx as Active Species. *ACS Catalysis*, 7(2), 1143-1149.

Dau, H., Limberg, C., Reier, T., Risch, M., Roggan, S., and Strasser, P. (2010). The Mechanism of Water Oxidation: From Electrolysis via Homogeneous to Biological Catalysis. *ChemCatChem*, 2(7), 724-761.

Fan, T., Zhan, S., and Ahlquist, M. S. G. (2016). Why is there a Barrier in the coupling of two radicals in the water oxidation reaction? *ACS Catalysis*, 6(12) 8308–8312.

Filatov, M., Reckien, W., Peyerimhoff, S. D., and Shaik, S. (2000). What are the reasons for the kinetic stability of a mixture of H2 and O2? *Journal of Physical Chemistry A*, 104(51) 12014–12020.

Frisch, M. J., Trucks, G. W., Schlegel, H. B., Scuseria, G. E., Robb, M. A., Cheeseman, J. R., .Fox, D. J. (2009). Gaussian 09, Revision D.01. Wallingford CT. Retrieved from https://gaussian.com.

Fromme, P., and Grotjohann, I. (2011). Structure of Cyanobacterial Photosystems I and II. *Bioenergetic Processes of Cyanobacteria*, 285-335.

Funes-Ardoiz, I., Garrido-Barros, P., Llobet, A., and Maseras, F. (2017). Single Electron Transfer Steps in Water Oxidation Catalysis. Redefining the Mechanistic Scenario. *ACS Catalysis*, 7(3), 1712-1719.

Ga, Z., and Da, Z. (2020). Chemcraft. Retrieved from https://www.chemcraftprog.com.

Govindjee, and Krogmann, D. (2005). Discoveries in oxygenic photosynthesis (1727–2003): a perspective. *Discoveries in Photosynthesis*, 63-105.

Hay, P. J., and Wadt, W. R. (1998). Ab initio effective core potentials for molecular calculations. Potentials for K to Au including the outermost core orbitals. *The Journal of Chemical Physics*, 82(1), 299-299.

Hemmerling, J. R., Mathur, A., and Linic, S. (2021). Design Principles for Efficient and Stable Water Splitting Photoelectrocatalysts. *Accounts of Chemical Research*, 54(8), 1992-2002.

Hohenberg, P., and Kohn, W. (1964). Inhomogeneous Electron Gas. *Physical Review*, 136(3B), B864-B864.

Huang, Y., Zhang, X., Ma, Z., Li, W., Zhou, Y., Zhou, J., Sun, C. Q. (2013). Size, separation, structural order, and mass density of molecules packing in water and ice *Sci Rep* 3, 3005.

Jensen, F. (2007). Introduction to computational chemistry. (Second edition). New York: Wiley, 299-342.

Kadish, K. M. (1986). The Electrochemistry of Metalloporphyrins in Nonaqueous Media. *Progress in Inorganic Chemistry,* 34, 435-605.

Kim, S., Cho, K.-B., Lee, Y.-M., Chen, J., Fukuzumi, S., and Nam, W. (2016). Factors Controlling the Chemoselectivity in the Oxidation of Olefins by Nonheme Manganese(IV)-Oxo Complexes. *Journal of the American Chemical Society*, 138(33), 10654-10663.

Kohn, W., and Sham, L. J. (1965). Self-Consistent Equations Including Exchange and Correlation Effects. *Physical Review,* 140(4A), A1133-A1133.

Kreplin, D. A., Knowles, P. J., and Werner, H.-J. (2019). Second-order MCSCF optimization revisited. I. Improved algorithms for fast and robust second-order CASSCF convergence. *The Journal of Chemical Physics,* 150(19), 194106-194106.

Kreplin, D. A., Knowles, P. J., and Werner, H.-J. (2020). MCSCF optimization revisited. II. Combined first- and second-order orbital optimization for large molecules. *The Journal of Chemical Physics,* 152(7), 074102-074102.

Lai, W., Cao, R., Dong, G., Shaik, S., Yao, J., and Chen, H. (2012). Why Is Cobalt the Best Transition Metal in Transition-Metal Hangman Corroles for O−O Bond Formation during Water Oxidation? Scheme 1. Co Hangman Corrole Complex. *J. Phys. Chem. Lett, 3, 17, 2315–2319.*

Larson, V. A., Battistella, B., Ray, K., Lehnert, N., and Nam, W. (2020). Iron and manganese oxo complexes, oxo wall and beyond. *Nature Reviews Chemistry*, 4(8), 404–419.

Lewars, E. (2011). Computational chemistry : introduction to the theory and applications of molecular and quantum mechanics. 664-664.

Lewis, N. S. (2007). Toward cost-effective solar energy use. *Science,* 315(5813), 798-801.

Li, P., Zhao, R., Chen, H., Wang, H., Wei, P., Huang, H., Sun, X. (2019). Recent Advances in the Development of Water Oxidation Electrocatalysts at Mild pH. *Small,* 15(13), 1805103-1805103.

Matheu, R., Garrido-Barros, P., Gil-Sepulcre, M., Ertem, M. Z., Sala, X., Gimbert-Suriñach, C., and Llobet, A. (2019). The development of molecular water oxidation catalysts. *Nature Reviews Chemistry,* 3(5), 331-341.

Meunier, B., and Bernadou, J. (2002). Metal-Oxo Species in P450 Enzymes and Biomimetic Models. Oxo-Hydroxo Tautomerism with Water-Soluble Metalloporphyrins. *Topics in Catalysis* 2002 21:1, 21(1), 47-54.

Miyagawa, K., Isobe, H., Shoji, M., Kawakami, T., Yamanaka, S., and Yamaguchi, K. (2021). A three states model for hydrogen abstraction reactions with the cytochrome P450 compound I is revisited. Isolobal and isospin analogy among Fe(IV)=O, O = O and O. *Journal of Photochemistry and Photobiology A: Chemistry,* 405, 112902-112902.

Najafpour, M. M., and Govindjee. (2011). Oxygen evolving complex in Photosystem II: Better than excellent. *Dalton Transactions,* 40(36), 9076-9084.

Najafpour, M. M., Moghaddam, A. N., Allakhverdiev, S. I., and Govindjee. (2012). Biological water oxidation: Lessons from Nature. 1817.

Nakamura, R., and Sato, S. (2002). Oxygen Species Active for Photooxidation of n-Decane over TiO2 Surfaces. *Journal of Physical Chemistry B,* 106(23), 5893-5896.

Nakazono, T., Rene Parent, A., and Sakai, K. (2013). Cobalt porphyrins as homogeneous catalysts for water oxidation. *Chemical Communications,* 49(56), 6325-6327.

Oxtoby, D. W., Gillis, H. P., Campion, A., Editor, A., Lockwood, L., Walker, A. J., Hart, D. (2007). *Principles of Modern Chemistry* (6th ed.): Belmont, Calif: Thomson Brook, 350-377.

Safdari, R., Mohammadi, M. R., Hołyńska, M., Chernev, P., Dau, H., and Najafpour, M. M. (2018). A mononuclear cobalt complex for water oxidation: new controversies and puzzles. *Dalton Transactions,* 47(46), 16668-16673.

Schilling, M., and Luber, S. (2018). Computational Modeling of Cobalt-Based Water Oxidation: Current Status and Future Challenges. *Frontiers in Chemistry,* 1-21.

Schilling, M., Patzke, G. R., Hutter, J., and Luber, S. (2016). Computational Investigation and Design of Cobalt Aqua Complexes for Homogeneous Water Oxidation. *Journal of Physical Chemistry C,* 120(15), 7966-7975.

Shaffer, D. W., Xie, Y., and Concepcion, J. J. (2017). O–O bond formation in ruthenium-catalyzed water oxidation: single-site nucleophilic attack vs. O–O radical coupling. *Chemical Society Reviews,* 46(20), 6170-6193.

Skoczkowski, T., Bielecki, S., and Wojtyńska, J. (2019). Long-Term Projection of Renewable Energy Technology Diffusion. *Energies,* 12(22), 4261-4262.

Stephens, P. J., Devlin, F. J., Chabalowski, C. F., and Frisch, M. J. (2002). Ab Initio Calculation of Vibrational Absorption and Circular Dichroism Spectra Using Density Functional Force Fields. *Journal of Physical Chemistry,* 98(45), 11623-11627.

Turhan, E. A., Nune, S. V. K., Ülker, E., Şahin, U., Dede, Y., and Karadas, F. (2018). Water Oxidation Electrocatalysis with a Cobalt-Borate-Based Hybrid System under Neutral Conditions. *Chemistry - A European Journal,* 24(41), 10372-10382.

Ullman, A. M., Liu, Y., Huynh, M., Bediako, D. K., Wang, H., Anderson, B. L., Nocera, D. G. (2014). Water oxidation catalysis by Co(II) impurities in Co(III)4O4 cubanes. *Journal of the American Chemical Society,* 136(50), 17681-17688.

Wang, B., Lee, Y. M., Tcho, W. Y., Tussupbayev, S., Kim, S. T., Kim, Y., Nam, W. (2017). Synthesis and reactivity of a mononuclear non-haem cobalt(IV)-oxo complex. *Nature Communications,* 8, 1-10.

Wang, J. W., Sahoo, P., and Lu, T. B. (2016). Reinvestigation of Water Oxidation Catalyzed by a Dinuclear Cobalt Polypyridine Complex: Identification of CoOx as a Real Heterogeneous Catalyst. *ACS Catalysis,* 6(8), 5062-5068.

Wang, X., Cai, Z. F., Wang, D., and Wan, L. J. (2019). Molecular Evidence for the Catalytic Process of Cobalt Porphyrin Catalyzed Oxygen Evolution Reaction in Alkaline Solution. *Journal of the American Chemical Society,* 141(19), 7665-7669.

Wasylenko, D. J., Ganesamoorthy, C., Borau-Garcia, J., and Berlinguette, C. P. (2011). Electrochemical evidence for catalytic water oxidation mediated by a high-valent cobalt complexw ChemComm. *Chemical Communications,* 47, 2-2.

Weigend, F., and Ahlrichs, R. (2005). Balanced basis sets of split valence, triple zeta valence and quadruple zeta valence quality for H to Rn: Design and assessment of accuracy. *Physical Chemistry Chemical Physics,* 7(18), 3297-3305.

Werner, H. J., Knowles, P. J., Knizia, G., Manby, F. R., and Schütz, M. (2012). Molpro: A general-purpose quantum chemistry program package. *Wiley Interdisciplinary Reviews: Computational Molecular Science,* 2(2), 242-253.

Werner, H. J., Knowles, P. J., Knizia, G., Manby, F. R., Schütz, M., Celani, P., Welborn, M. (2020). MOLPRO, version 2020.2 , a package of ab initio programs. Retrieved from https://www.molpro.net.

Werner, H. J., Knowles, P. J., Manby, F. R., Black, J. A., Doll, K., Heßelmann, A., Sibaev, M. (2020). The Molpro quantum chemistry package. *Journal of Chemical Physics,* 152(14).

Yamaguchi, K., Shoji, M., Isobe, H., Yamanaka, S., Shimada, J., Kitagawa, Y., and Okumura, M. (2009). Theory of chemical bonds in metalloenzymes XII: Electronic and spin structures of metallo–oxo and isoelectronic species and spin crossover phenomena in oxygenation reactions. *Polyhedron, 28*(9-10), 2044-2052.

Zhao, Y., and Truhlar, D. G. (2006). A new local density functional for main-group thermochemistry, transition metal bonding, thermochemical kinetics, and noncovalent interactions. *Journal of Chemical Physics,* 125, 194101-194101.

APPENDIX

APPENDIX-1. Relative energies (kcal·mol-1) of L1, L2, L3, L4 and L5 optimized at different levels of theory

Level of theory	Spin Hali	L1	L2	L3	L4	L5
UB3LYP/LANL2DZ	Doublet	4.0	8.4	0.0	0.0	0.0
	Quartet	0.0	2.5	8.2	4.9	9.9
	Sextet	12.5	0.0	21.2	25.0	25.5
UM06L/LANL2DZ	Doublet	9.2	15.0	0.0	0.0	0.0
	Quartet	0.0	0.0	1.5	5.1	3.9
	Sextet	14.3	5.8	19.3	26.0	21.0
CAS(11,11)/LANL2DZ//UB3LYP/LANL2DZ	Doublet	19.7	19.7	15.9	22.7	27.3
	Quartet	0.0	0.0	0.0	0.0	0.0
	Sextet	4.8	18.4	21.4	30.8	44.6
UB3LYP/cc-pVTZ	Doublet	7.3	15.1	0.6	1.7	0.0
	Quartet	0.0	0.0	0.0	0.0	4.0
	Sextet	10.9	7.6	18.1	23.0	24.7
UB3LYP/cc-pVQZ//UB3LYP/cc-pVTZ	Doublet	7.3	15.5	0.9	1.8	0.0
	Quartet	0.0	0.0	0.0	0.0	3.9
	Sextet	10.7	7.6	18.2	23.0	24.6
UM06L/cc-pVTZ	Doublet	9.9	16.4	4.6	0.5	0.0
	Quartet	0.0	0.0	0.0	0.0	0.8
	Sextet	10.5	7.7	17.7	20.9	16.1
UM06L/cc-pVQZ//UM06L/cc-pVTZ	Doublet	9.8	16.3	5.1	1.0	0.0
	Quartet	0.0	0.0	0.0	0.0	0.6
	Sextet	9.9	7.9	17.7	20.8	15.7
UωB97xD/cc-pVTZ	Doublet	5.7	12.0	0.0	0.0	F
	Quartet	0.0	0.0	2.4	4.3	0.0
	Sextet	10.5	4.4	18.3	25.3	36.5
UωB97xD/cc-pVQZ//UωB97xD/cc-pVTZ	Doublet	5.8	12.4	0.0	0.0	F
	Quartet	0.0	0.0	1.9	4.0	0.0
	Sextet	10.3	4.5	17.9	25.1	36.4

APPENDIX-2. Active space orbitals of L2 calculated at CAS(11,11)/def2-TZVP level of theory for doublet, quartet, and sextet states. Natural orbital occupancy numbers (NOON) are also given for each state

MO	Doublet	NOON	Quartet	NOON	Sextet	NOON
47		0.01	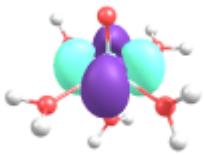	0.01	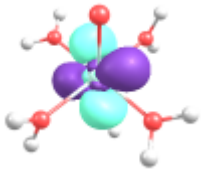	0.01
46	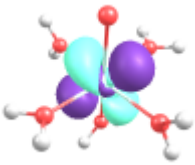	0.01	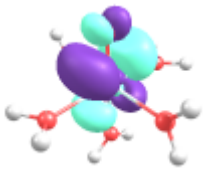	0.01	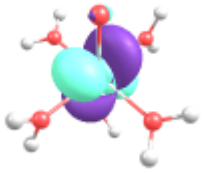	0.01
45	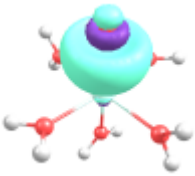	0.01	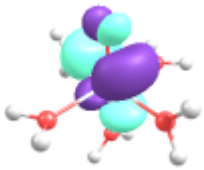	0.01		0.01
44	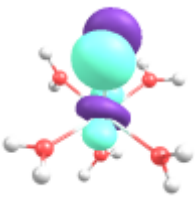	0.97	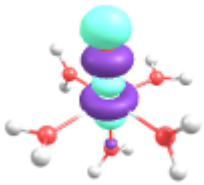	0.21	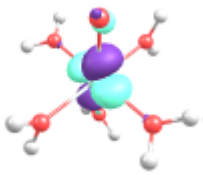	1.00
43	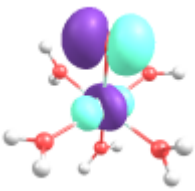	0.99	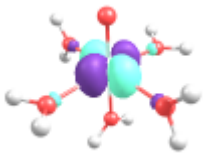	1.00	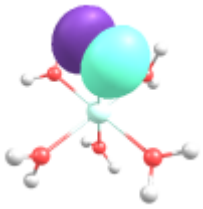	1.00
42	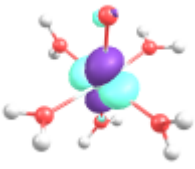	1.01	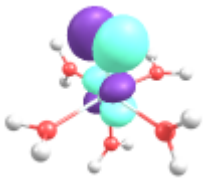	1.10	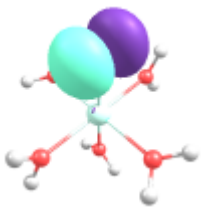	1.00

APPENDIX-2. (continued) Active space orbitals of L2 calculated at CAS(11,11)/def2-TZVP level of theory for doublet, quartet, and sextet states. Natural Orbital Occupancy Numbers (NOON) are also given for each state

MO	Doublet	NOON	Quartet	NOON	Sextet	NOON
41	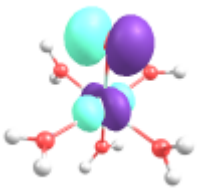	1.01	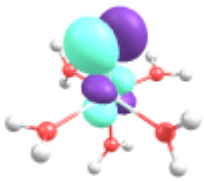	1.10	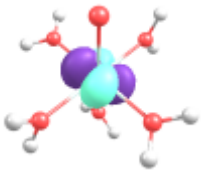	1.01
40	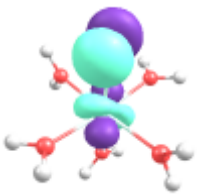	1.03	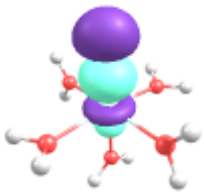	1.81	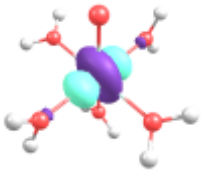	1.01
39	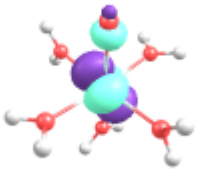	1.99	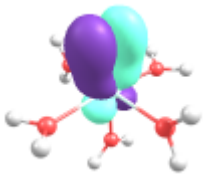	1.89	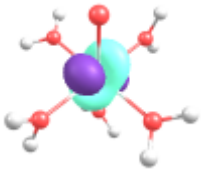	1.98
38	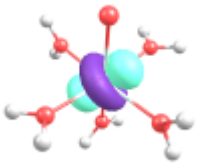	1.99	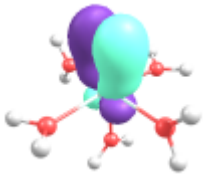	1.89	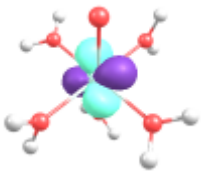	1.98
37	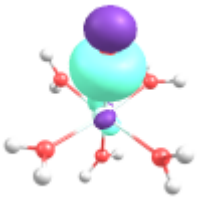	1.99		1.97	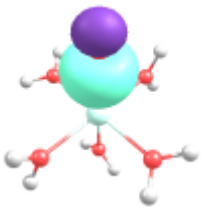	1.98

APPENDIX-3. Active space orbitals of L2-p calculated at CAS(13,12)/def2-TZVP level of theory for doublet, quartet, and sextet states. Natural orbital occupancy numbers (NOON) are also given for each state

MO	Doublet	NOON	Quartet	NOON	Sextet	NOON
52	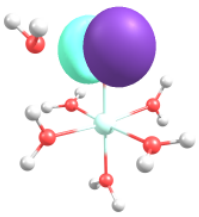	0.00	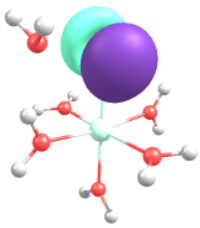	0.00	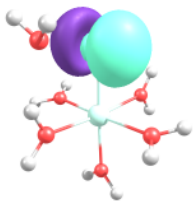	0.00
51	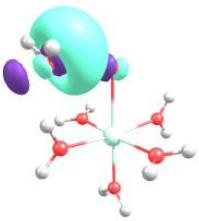	0.01	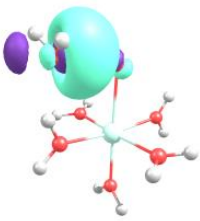	0.01	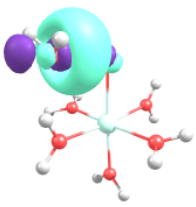	0.01
50	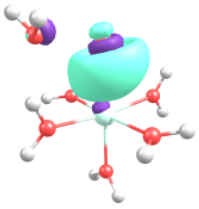	0.01	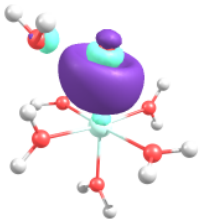	0.02	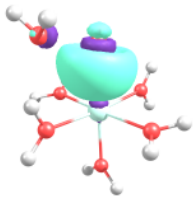	0.02
49	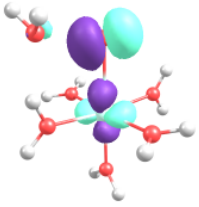	0.97	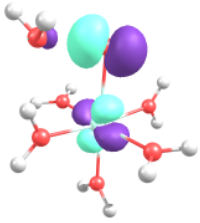	0.98	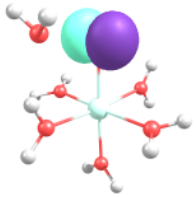	1.00

APPENDIX-3. (continued) Active space orbitals of L2-p calculated at CAS(13,12)/def2-TZVP level of theory for doublet, quartet, and sextet states. Natural Orbital Occupancy Numbers (NOON) are also given for each state

MO	Doublet	NOON	Quartet	NOON	Sextet	NOON
48	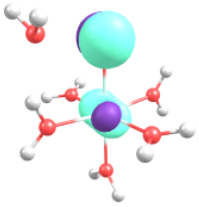	0.98	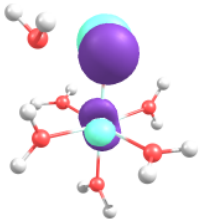	0.99	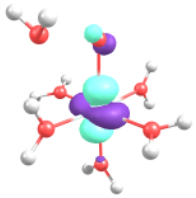	1.00
47	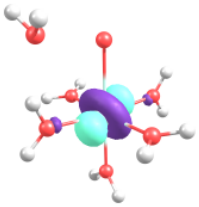	1.02	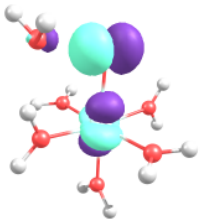	1.02	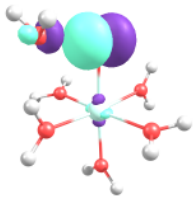	1.00
46	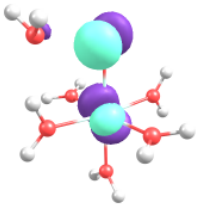	1.02	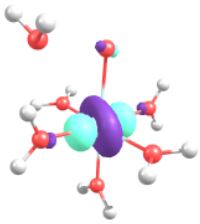	1.02	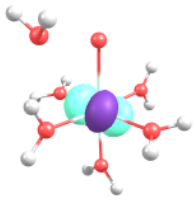	1.03
45	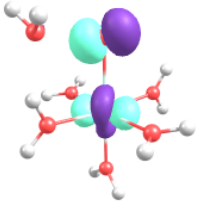	1.04	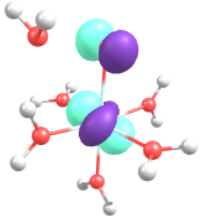	1.03	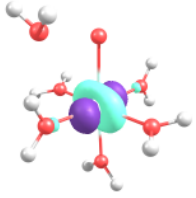	1.03

APPENDIX-3. (continued) Active space orbitals of L2-p calculated at CAS(13,12)/def2-TZVP level of theory for doublet, quartet, and sextet states. Natural Orbital Occupancy Numbers (NOON) are also given for each state

MO	Doublet	NOON	Quartet	NOON	Sextet	NOON
44	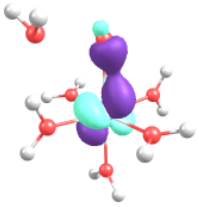	1.98	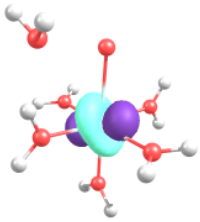	1.98	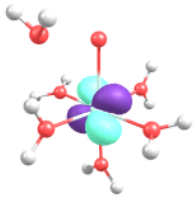	1.97
43	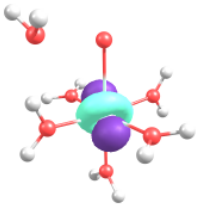	1.98	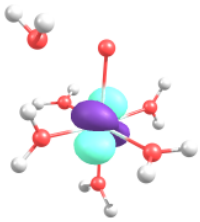	1.98	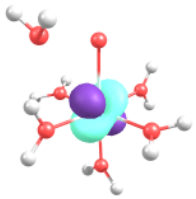	1.97
42	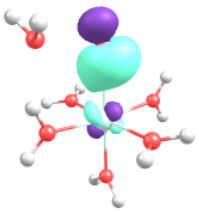	1.98		1.98	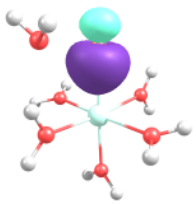	1.98
41	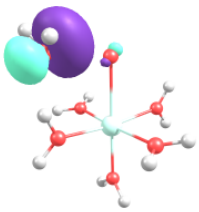	1.99	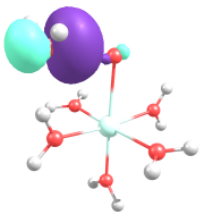	1.99	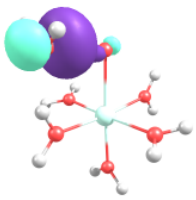	1.99

APPENDIX-4. Active space orbitals of L2-t calculated at CAS(13,12)/def2-TZVP level of theory for doublet, quartet, and sextet states. Natural orbital occupancy numbers (NOON) are also given for each state

MO	Doublet	NOON	Quartet	NOON	Sextet	NOON
52	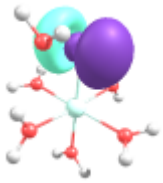	0.00	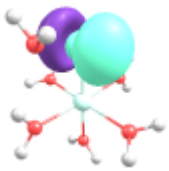	0.00	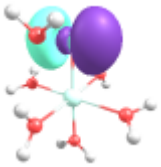	0.00
51	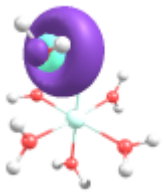	0.01	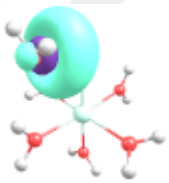	0.01	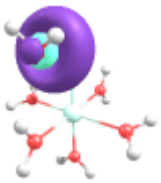	0.01
50	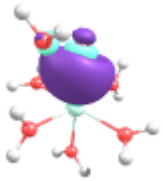	0.02		0.02		0.02
49	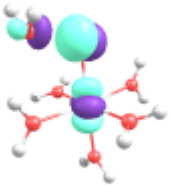	0.95	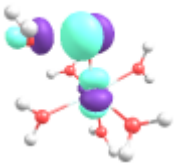	0.97	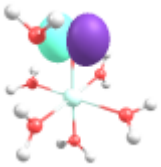	1.00

APPENDIX-4 (continued). Active space orbitals of L2-t calculated at CAS(13,12)/def2-TZVP level of theory for doublet, quartet, and sextet states. Natural Orbital Occupancy Numbers (NOON) are also given for each state, continued

MO	Doublet	NOON	Quartet	NOON	Sextet	NOON
48	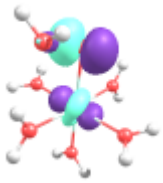	0.97	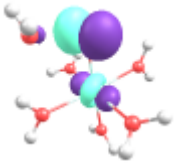	0.98		1.00
47	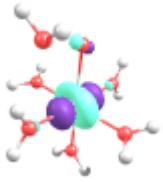	1.01	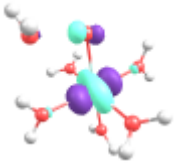	1.01	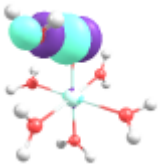	1.00
46	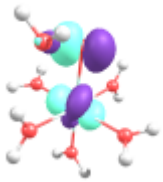	1.04	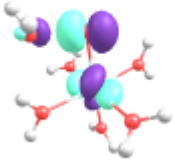	1.03		1.02
45	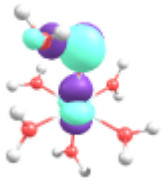	1.06	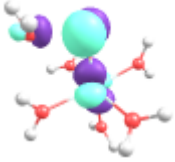	1.04		1.02

APPENDIX-4 (continued). Active space orbitals of L2-t calculated at CAS(13,12)/def2-TZVP level of theory for doublet, quartet, and sextet states. Natural Orbital Occupancy Numbers (NOON) are also given for each state, continued

MO	Doublet	NOON	Quartet	NOON	Sextet	NOON
44	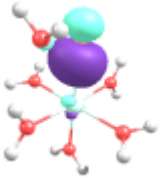	1.98	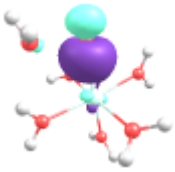	1.98		1.98
43	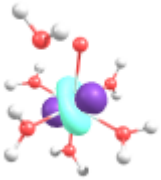	1.99	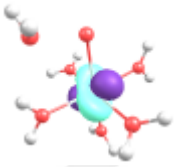	1.98	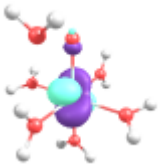	1.98
42	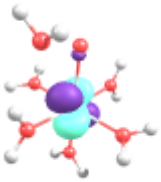	1.99	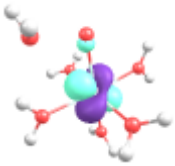	1.98	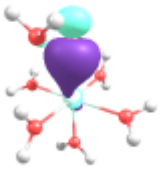	1.98
41		1.99	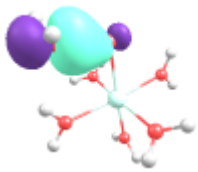	1.99	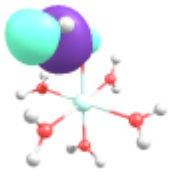	1.99

APPENDIX-5. Active space orbitals of L2-2 calculated at CAS(13,12)/def2-TZVP level of theory for doublet and quartet states. Natural orbital occupancy numbers (NOON) are also given for each state

MO	Doublet	NOON	Quartet	NOON
52	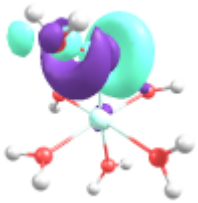	0.00	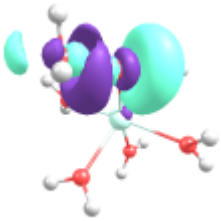	0.00
51	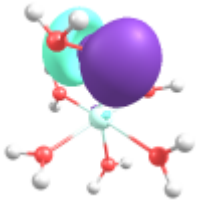	0.02	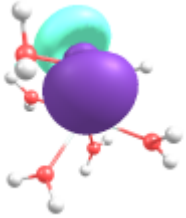	0.02
50	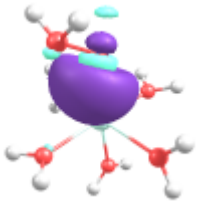	0.02	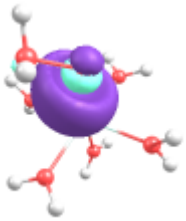	0.02
49	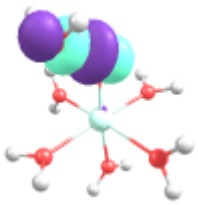	0.07	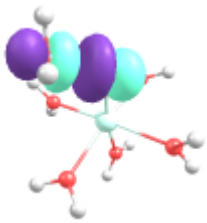	0.07

APPENDIX-5. (continued) Active space orbitals of L2-2 calculated at CAS(13,12)/def2-TZVP level of theory for doublet and quartet states. Natural Orbital Occupancy Numbers (NOON) are also given for each state, continued

MO	Doublet	NOON	Quartet	NOON
48	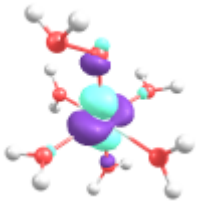	0.13	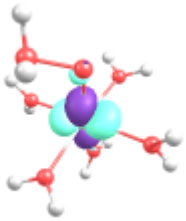	1.00
47	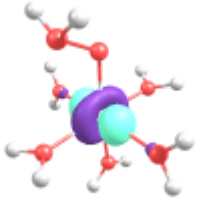	1.02	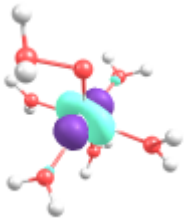	1.02
46	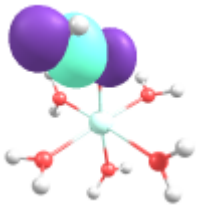	1.91	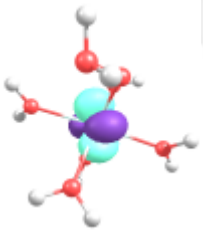	1.02
45	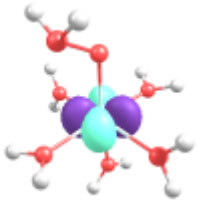	1.94	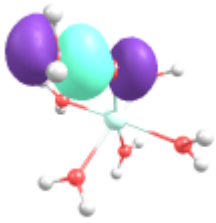	1.93

APPENDIX-5. (continued) Active space orbitals of L2-2 calculated at CAS(13,12)/def2-TZVP level of theory for doublet and quartet states. Natural Orbital Occupancy Numbers (NOON) are also given for each state, continued

MO	Doublet	NOON	Quartet	NOON
44	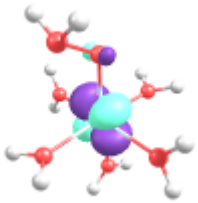	1.95	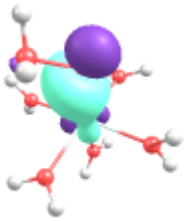	1.98
43	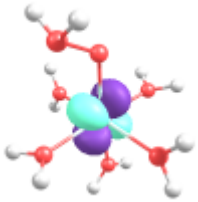	1.97	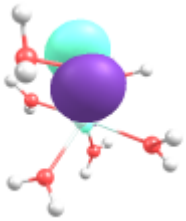	1.98
42	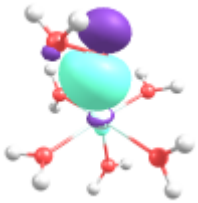	1.98	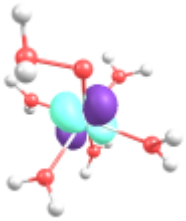	1.98
41	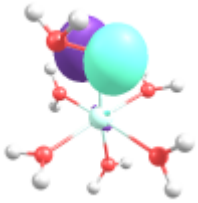	1.98	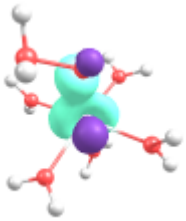	1.98

APPENDIX-6. CASSCF Configurations of L2-1 calculated at CAS(11,11)/def2-TZVP level of theory for doublet spin state. Configurations with weights less than 0.1 are not shown

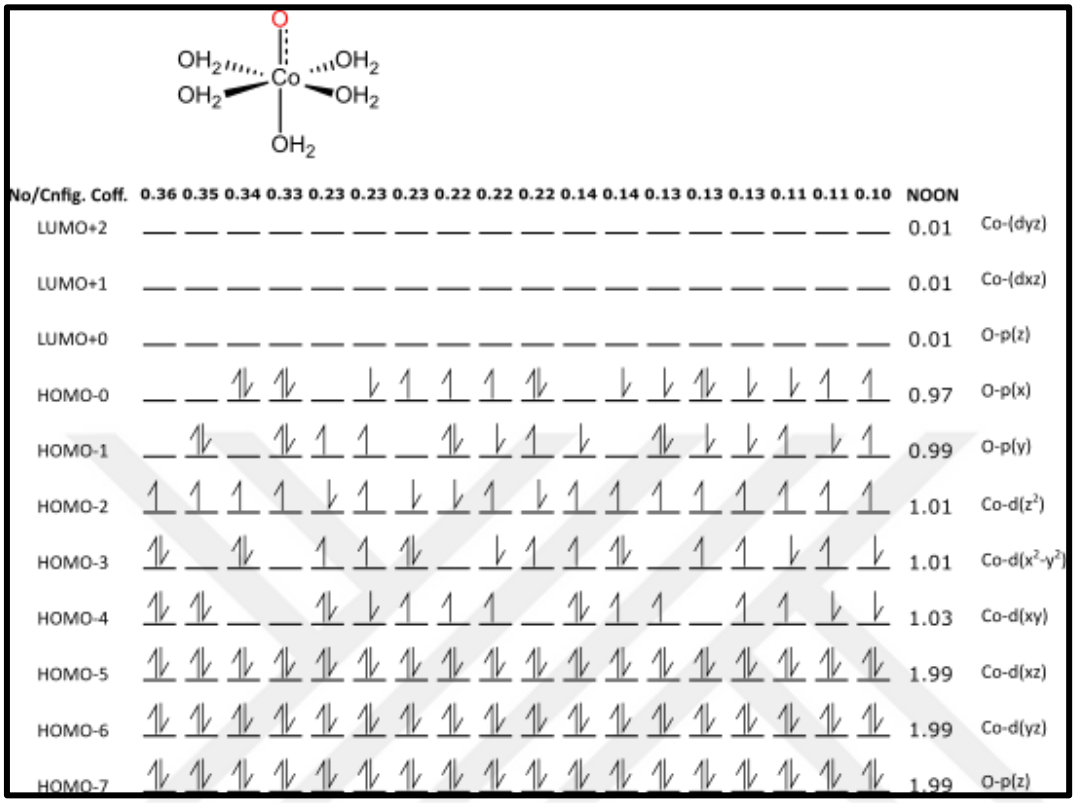

APPENDIX-7. CASSCF Configurations of L2-1 calculated at CAS(11,11)/def2-TZVP level of theory for quartet spin state. Configurations with weights less than 0.1 are not shown

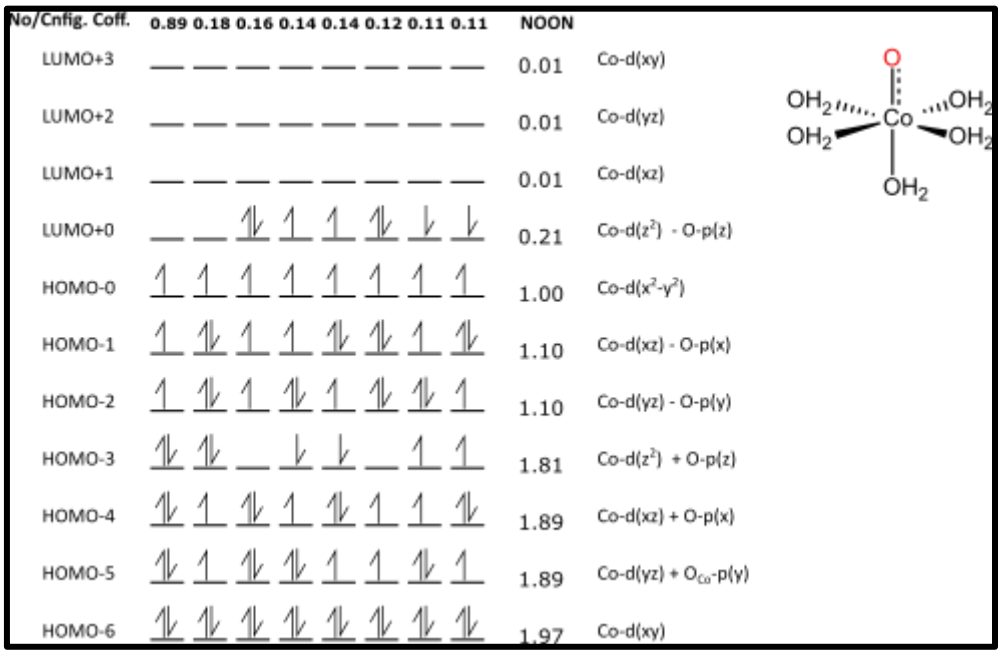

APPENDIX-8. CASSCF Configurations of L2-1 calculated at CAS(11,11)/def2-TZVP level of theory for sextet spin state. Configurations with weights less than 0.1 are not shown

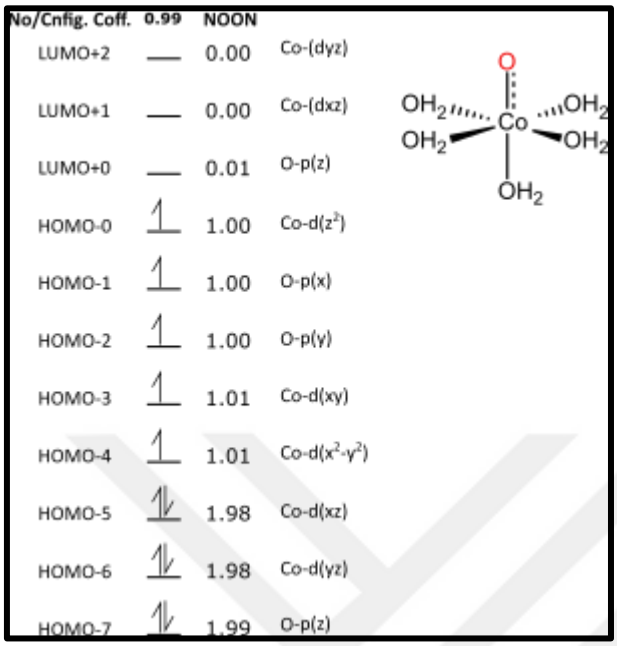

APPENDIX-9. CASSCF Configurations of L2-p calculated at CAS(13,12)/def2-TZVP level of theory for doublet spin state. Configurations with weights less than 0.1 are not shown

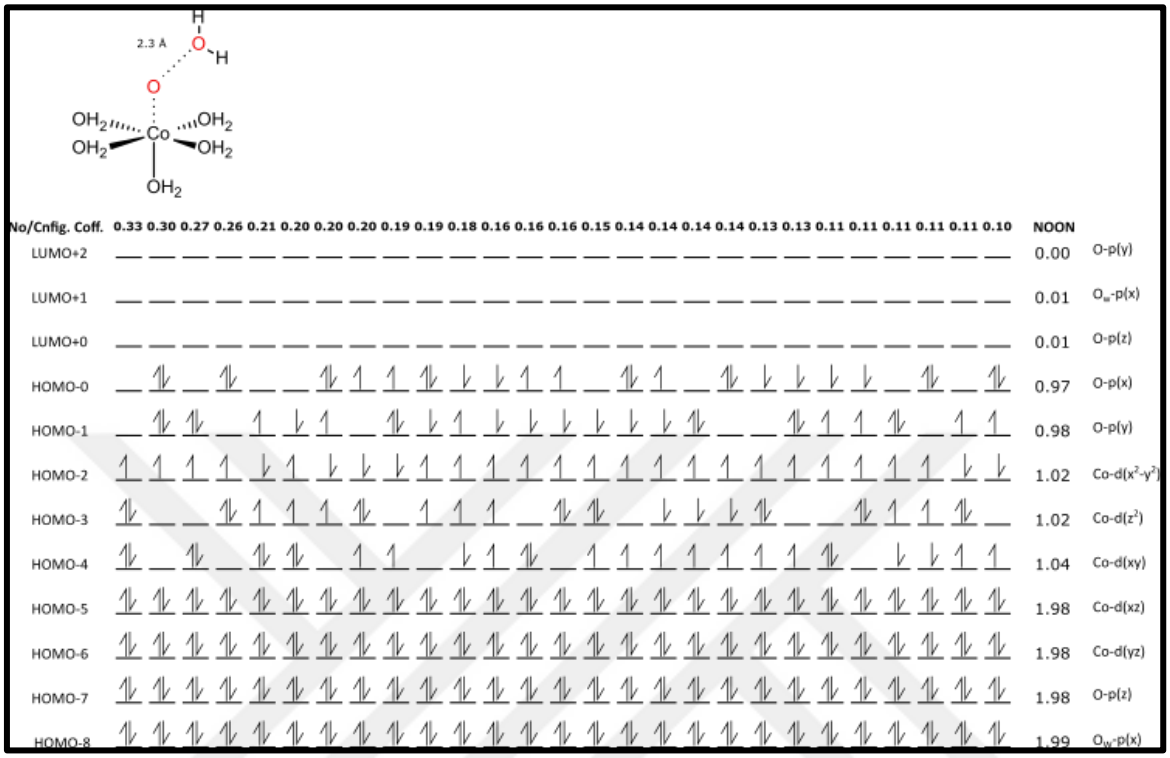

APPENDIX-10. CASSCF Configurations of L2-p calculated at CAS(13,12)/def2-TZVP level of theory for quartet spin state. Configurations with weights less than 0.1 are not shown

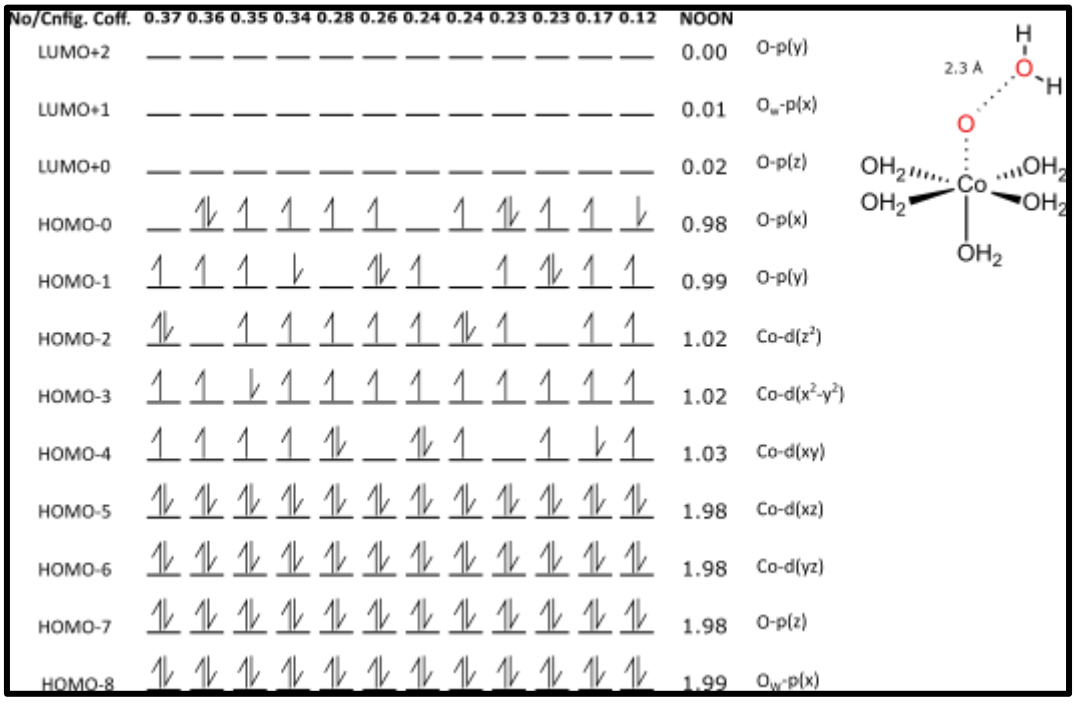

APPENDIX-11. CASSCF Configurations of L2-p calculated at CAS(13,12)/def2-TZVP level of theory for sextet spin state. Configurations with weights less than 0.1 are not shown

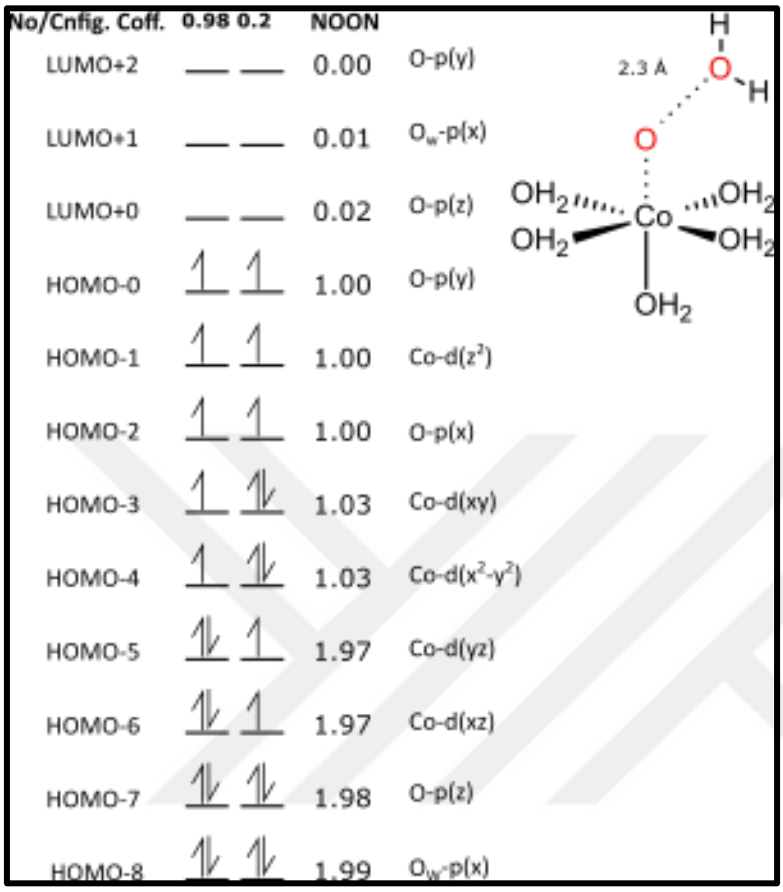

APPENDIX-12. CASSCF Configurations of L2-t calculated at CAS(13,12)/def2-TZVP level of theory for doublet spin state. Configurations with weights less than 0.1 are not shown

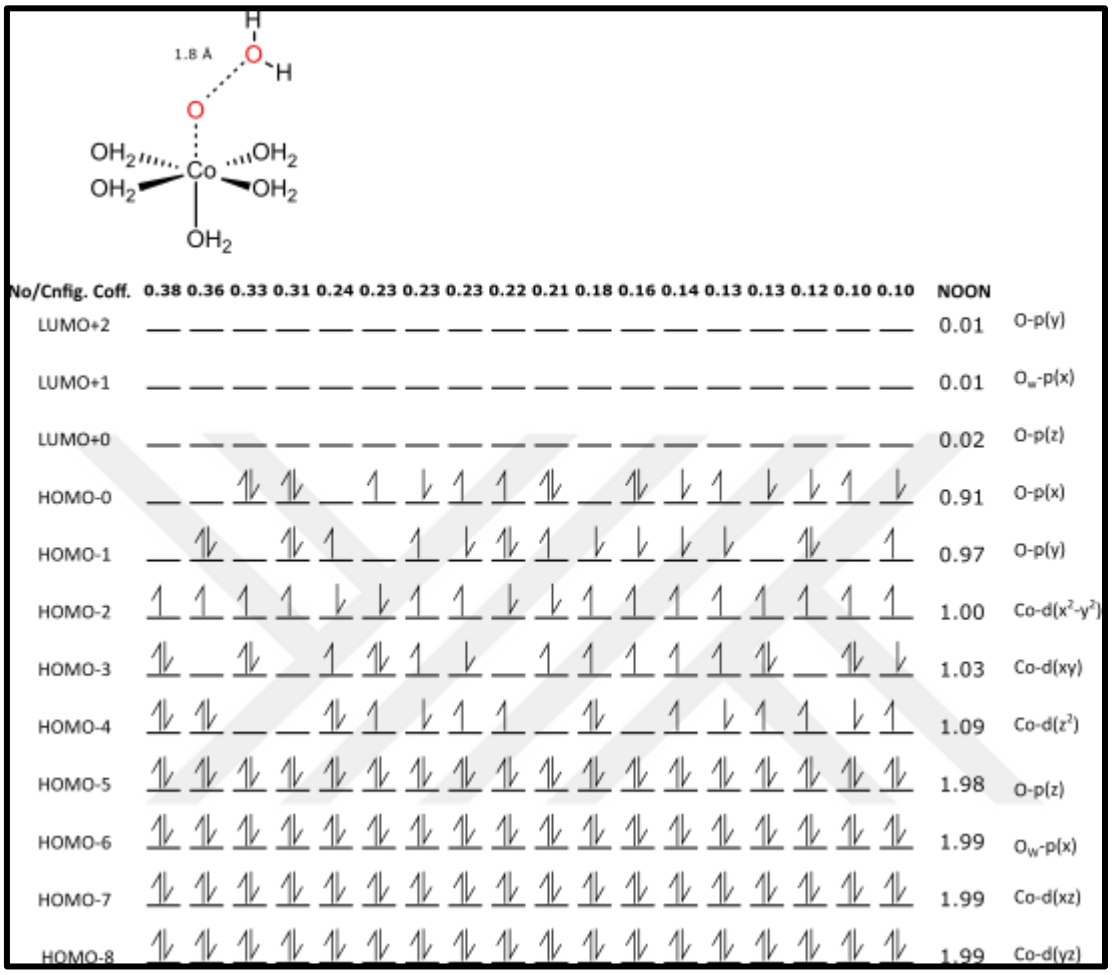

APPENDIX-13. CASSCF Configurations of L2-t calculated at CAS(13,12)/def2-TZVP level of theory for quartet spin state. Configurations with weights less than 0.1 are not shown

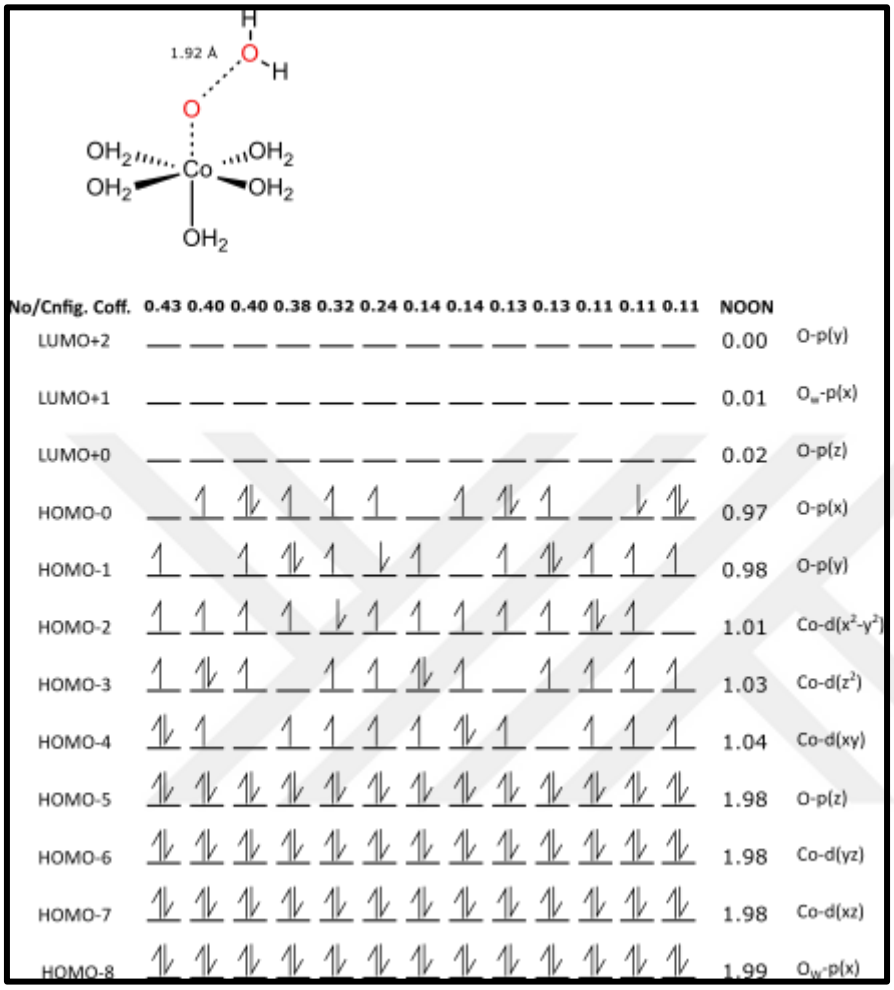

APPENDIX-14. CASSCF Configurations of L2-t calculated at CAS(13,12)/def2-TZVP level of theory for sextet spin state. Configurations with weights less than 0.1 are not shown

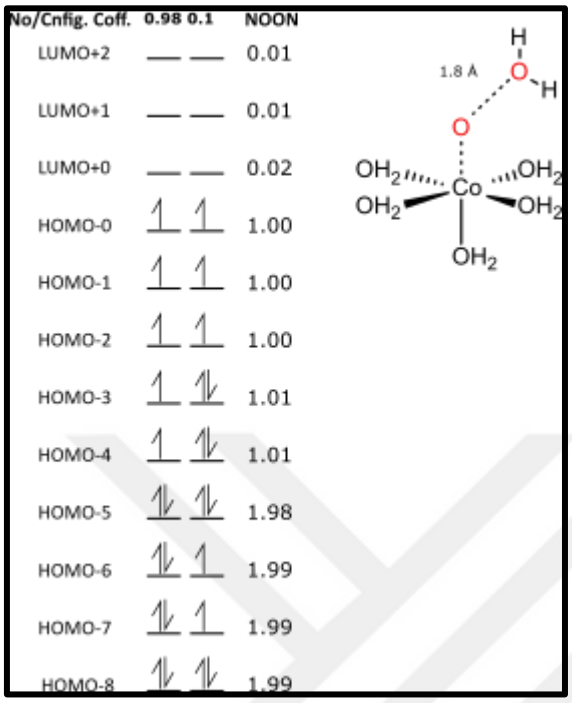

APPENDIX-15. CASSCF Configurations of L2-2 calculated at CAS(13,12)/def2-TZVP level of theory for doublet spin state. Configurations with weights less than 0.1 are not shown

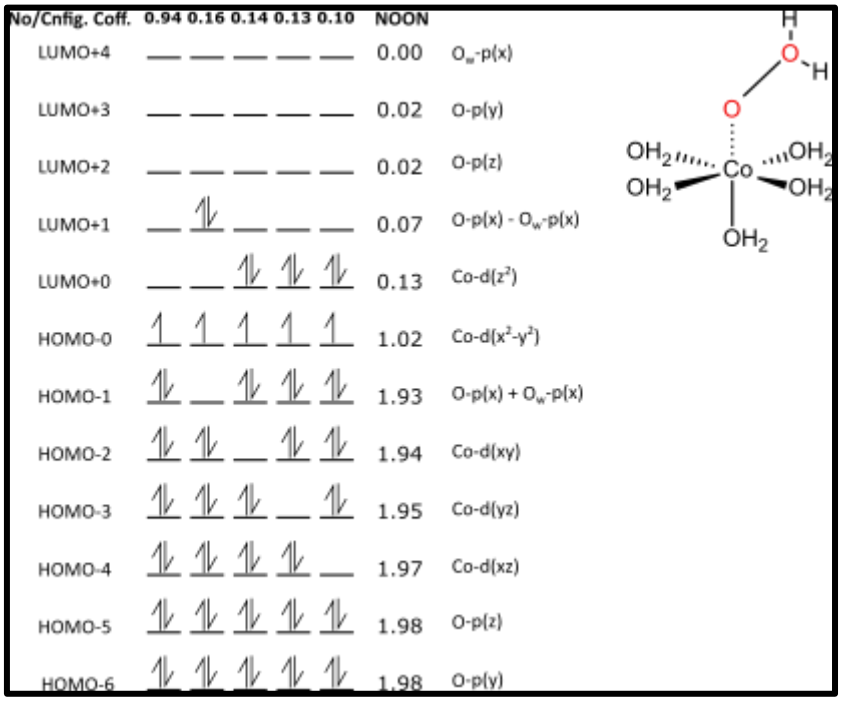

APPENDIX-16. CASSCF Configurations of L2-2 calculated at CAS(13,12)/def2-TZVP level of theory for quartet spin state. Configurations with weights less than 0.1 are not shown

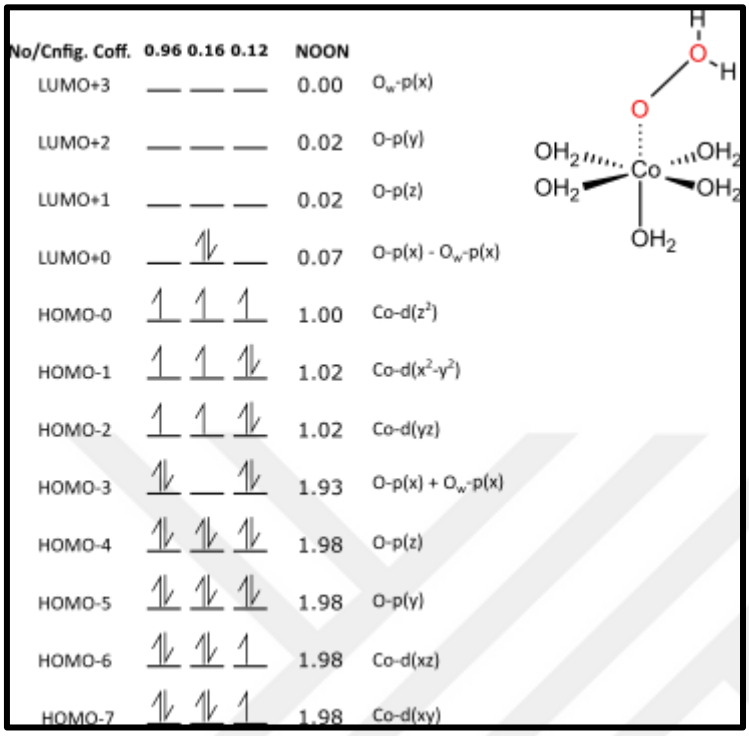

APPENDIX-17. MOs and their corresponding NOON's for L2 optimized at UB3LYP/cc-pVTZ level of theory at different states

Doublet			Quartet			Sextet		
Orbital nature	NOON		Orbital nature	NOON		Orbital nature	NOON	
dz2-pz	0	σ^*	dz2-pz	0	σ^*	dz2-pz	A	σ^*
dx2y2	0	nb	dx2y2	α	nb	dx2y2	A	nb
dyz-py	2	π^*	dyz-py	α	π^*	dyz-py	A	π^*
dxz-px	α	π^*	dxz-px	α	π^*	dxz-px	A	π^*
dz2+pz	2	σ	dz2+pz	2	σ	dz2+pz	2	σ
dyz+py	2	π	dyz+py	2	π	dyz+py	2	π
dxz+px	2	π	dxz+px	2	π	dxz+px	2	π
dxy	2	nb	dxy	2	nb	dxy	A	nb

L2-1

APPENDIX-18. Summary of Co-O–OH2 and CO–O bond lengths through quartet surface of O–O Bond formation

	3e wavefunction	5e wavefunction
CoO- -OH2 Å	Co – O Å	Co – O Å
1.91	2.105	2.279
1.92	2.100	2.284
1.93	2.101	2.289
1.94	2.101	2.292
1.95	2.096	2.296
1.96	2.097	2.299
1.97	2.099	2.303
1.98	2.093	2.308
1.99	2.095	2.312

APPENDIX-19. Active space orbitals for L1 using CAS(11,11)/LANL2DZ level of theory

MO	L1 Doublet	NOON	L1 Quartet	NOON	L1 Sextet	NOON
85	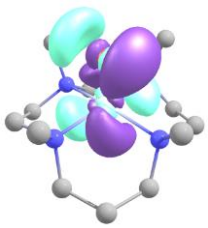	0.01	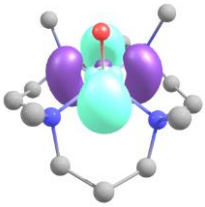	0.01	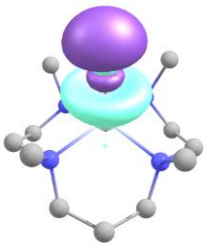	0.01
84	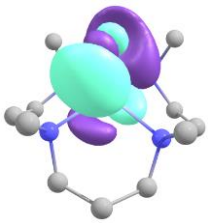	0.01	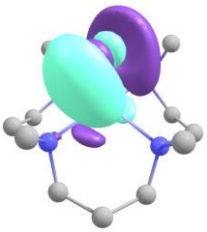	0.02	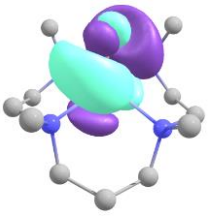	0.02
83	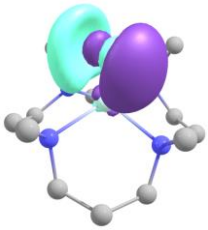	0.02	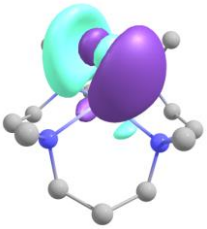	0.02	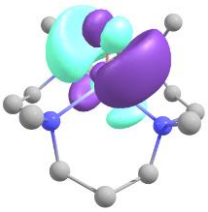	0.02
82	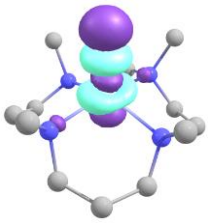	0.35	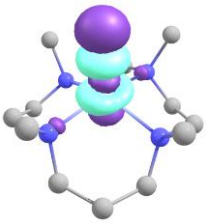	0.27	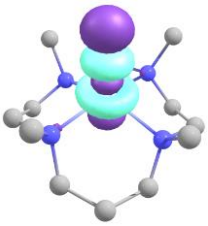	1.07
81	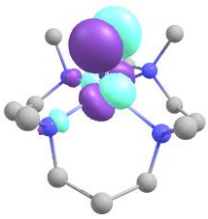	0.85	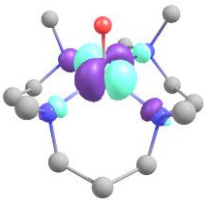	1.00	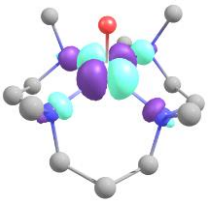	1.01
80	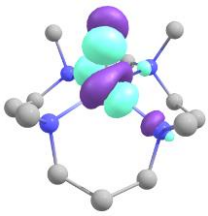	1.02	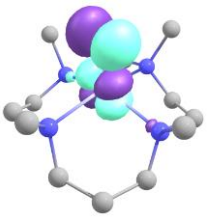	1.10	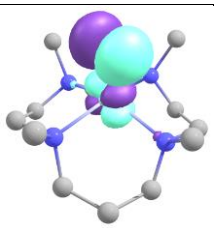	1.08
79	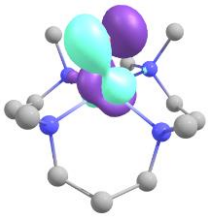	1.17	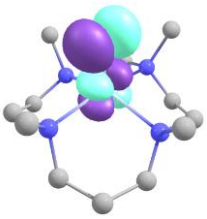	1.11	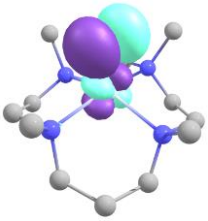	1.08

APPENDIX-19 (continued) Active space orbitals for L1 using CAS(11,11)/LANL2DZ level of theory , continued

MO	L1 Doublet	NOON	L1 Quartet	NOON	L1 Sextet	NOON
78	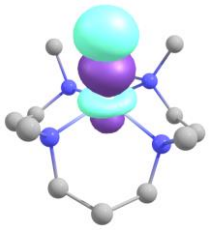	1.66	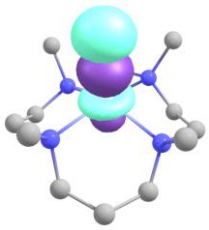	1.75	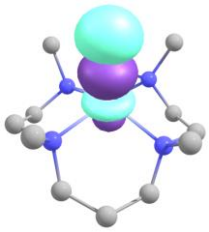	1.90
77	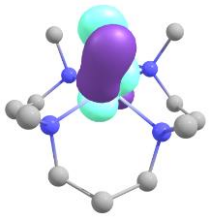	1.97	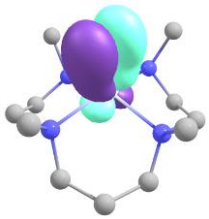	1.86	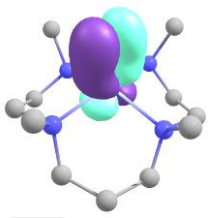	1.90
76	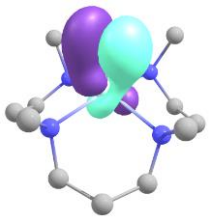	1.97	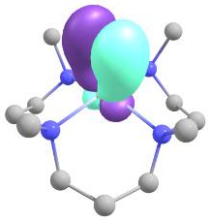	1.88	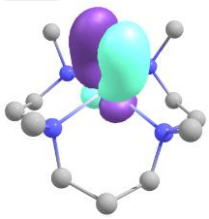	1.90
75	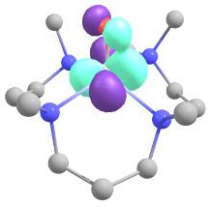	1.98	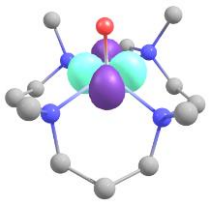	1.97	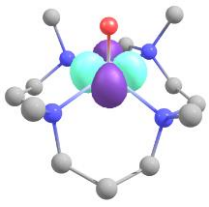	1.01

APPENDIX-20. Active space orbitals for L3 using CAS(11,11)/LANL2DZ level of theory

MO	L3 Doublet	NOON	L3 Quartet	NOON	L3 Sextet	NOON
47	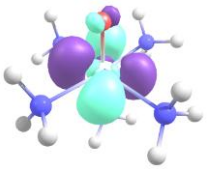	0.01	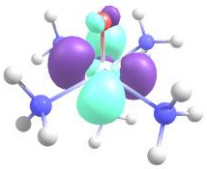	0.01	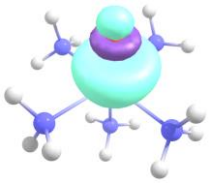	0.01
46	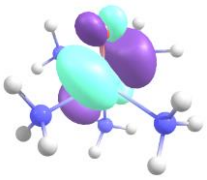	0.01	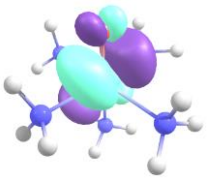	0.01	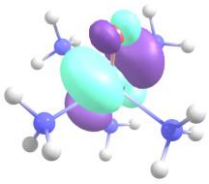	0.01
45	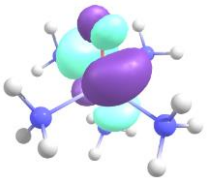	0.01	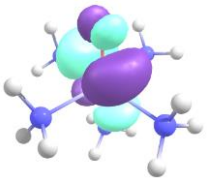	0.01	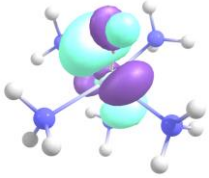	0.02
44	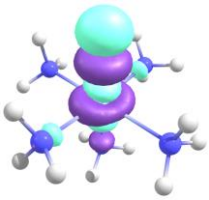	0.22	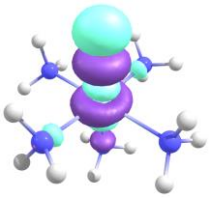	0.17	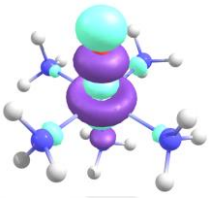	1.04
43	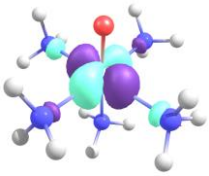	1.02	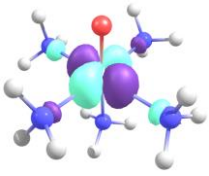	1.00	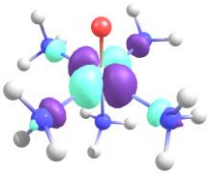	1.01
42	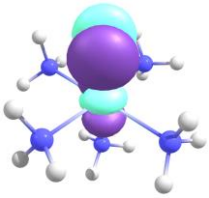	0.76	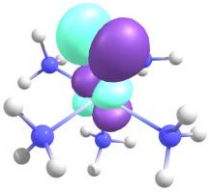	1.09	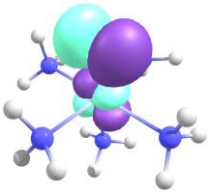	1.04
41	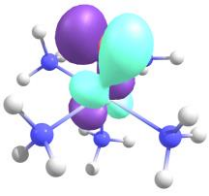	1.39	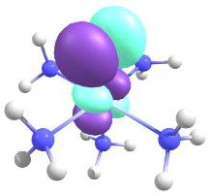	1.09	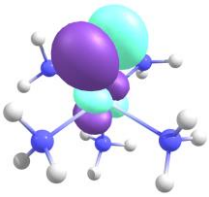	1.04

APPENDIX-20 (continued) Active space orbitals for L3 using CAS(11,11)/LANL2DZ level of theory

MO	L3 Doublet	NOON	L3 Quartet	NOON	L3 Sextet	NOON
40	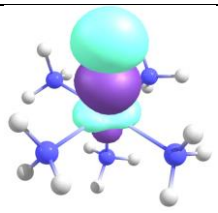	1.79	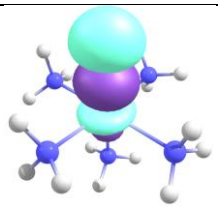	1.84	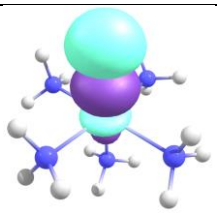	1.94
39	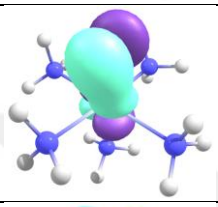	1.88	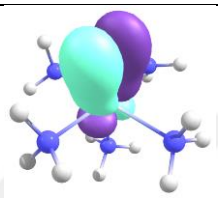	1.89	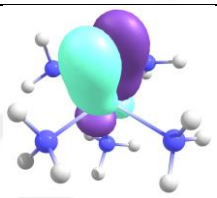	1.93
38	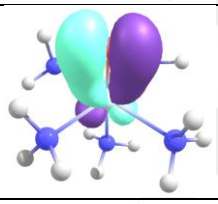	1.95	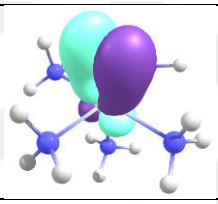	1.89	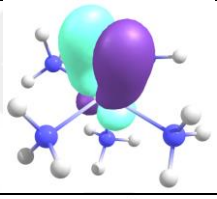	1.94
37	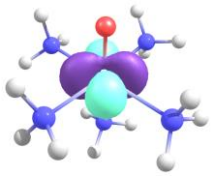	1.96	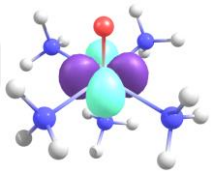	1.97	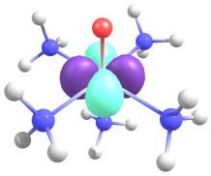	1.02

APPENDIX-21. Active space orbitals for L4 Quartet using CAS(11,11)/LANL2DZ level of theory

MO	L4 Quartet	NOON
142	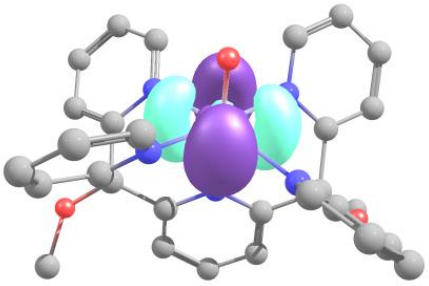	0.01
141	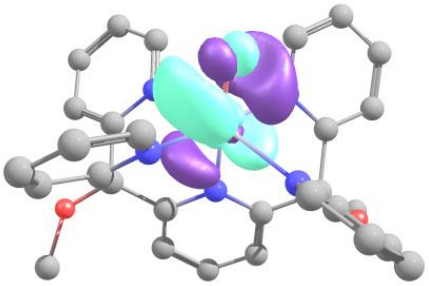	0.01
140	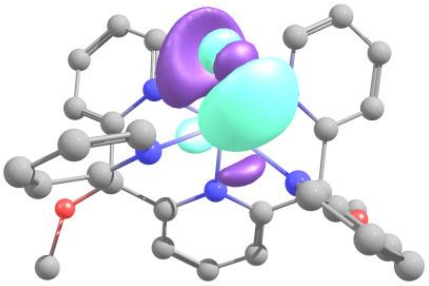	0.02
139	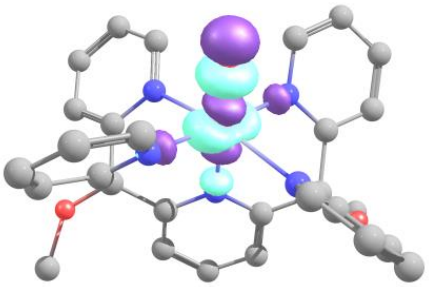	0.19
138	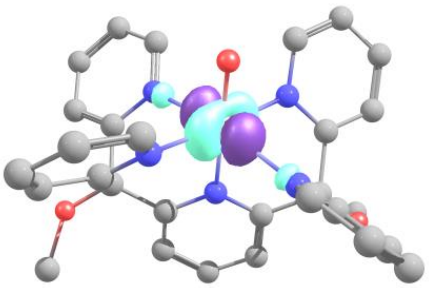	1.01

APPENDIX-21. (continued) Active space orbitals for L4 Quartet using CAS(11,11)/ LANL2DZ level of theory,

MO	L4 Quartet	NOON
137	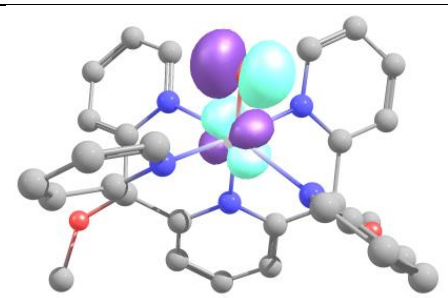	1.10
136	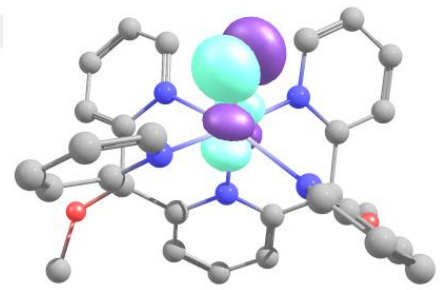	1.10
135	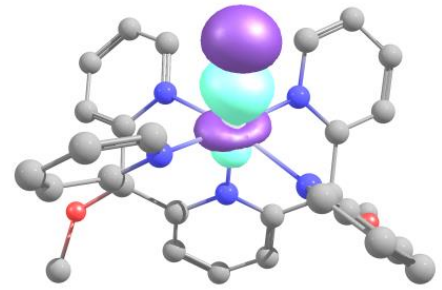	1.82

APPENDIX-21. (continued) Active space orbitals for L4 Quartet using CAS(11,11)/ LANL2DZ level of theory,

MO	L4 Quartet	NOON
134	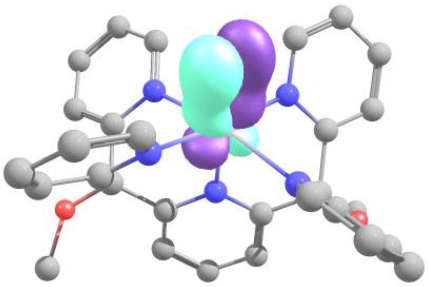	1.88
133	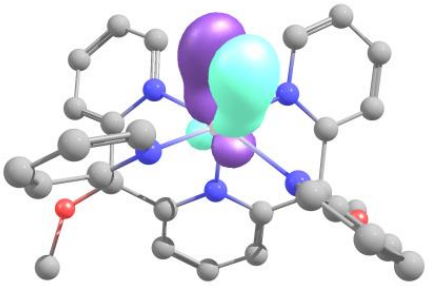	1.89
132	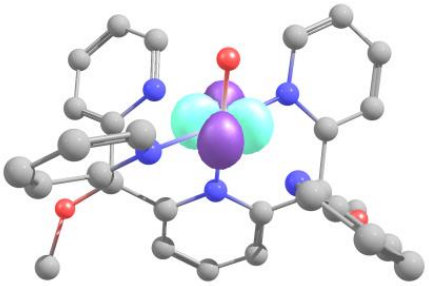	1.97

APPENDIX-22. Active space orbitals for L4 Sextet using CAS(11,11)/LANL2DZ level of theory

MO	L4 Sextet	NOON
142	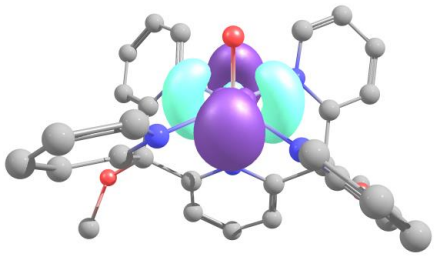	0.01
141	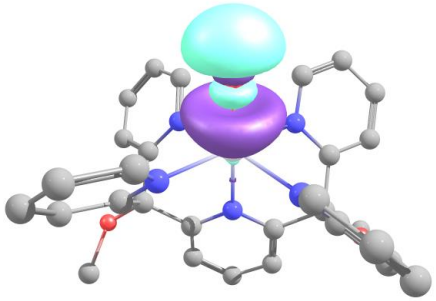	0.01
140	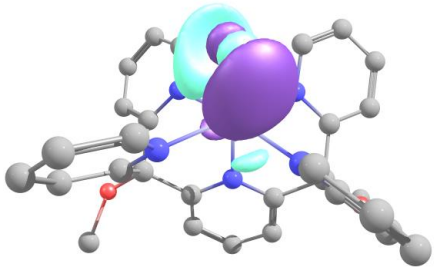	0.02
139	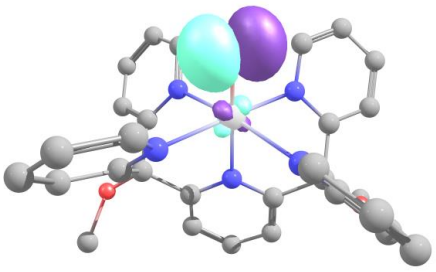	1.00
138	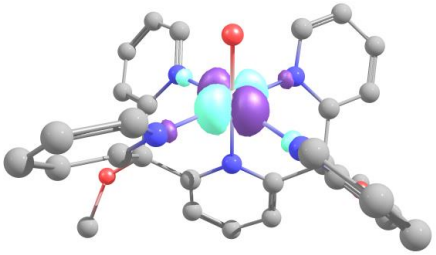	1.00
137	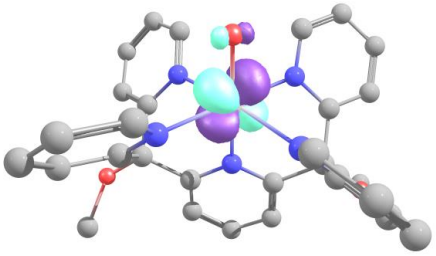	1.00

APPENDIX-22 (continued) Active space orbitals for L4 Sextet using CAS(11,11)/ LANL2DZ level of theory, continued

MO	L4 Sextet	NOON
136	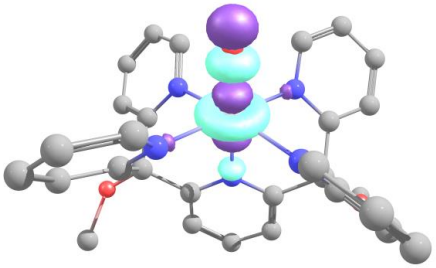	1.06
135	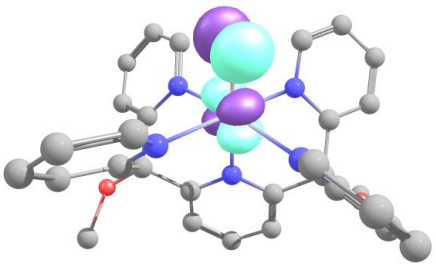	1.06
134	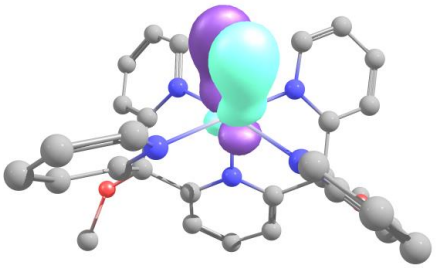	1.91
133	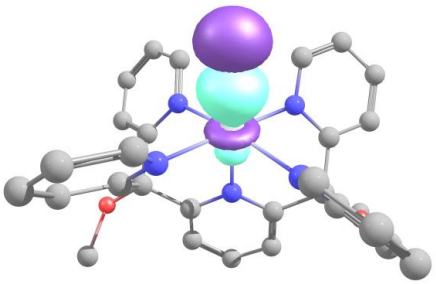	1.93
132	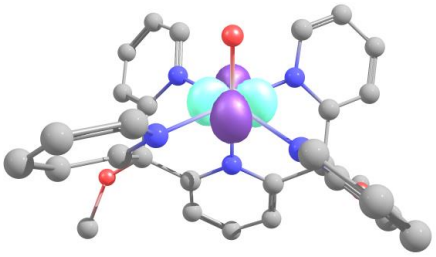	1.99

APPENDIX-23. Active space orbitals for L5 Doublet using CAS(11,11)/LANL2DZ level of theory

MO	L5 Doublet	NOON
167	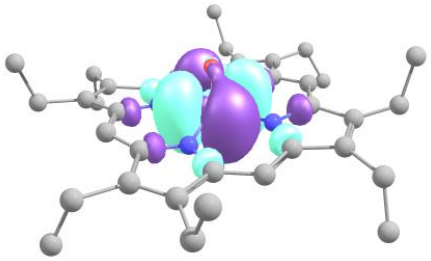	0.01
166	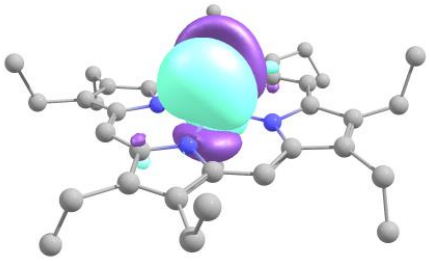	0.02
165	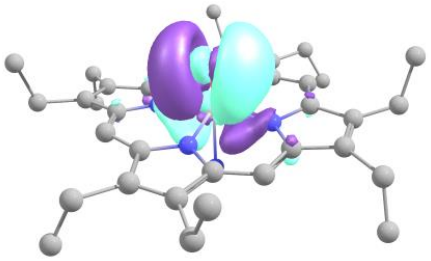	0.02
164	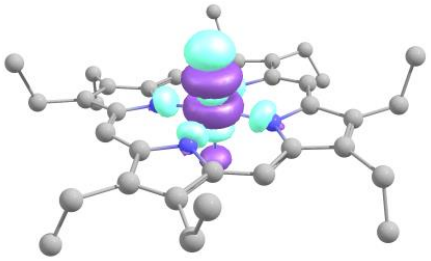	0.24
163	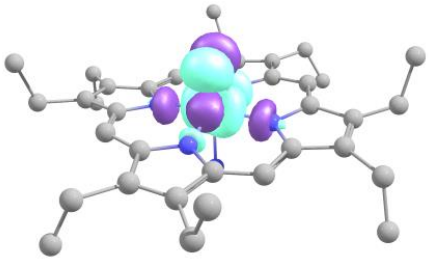	0.73
162	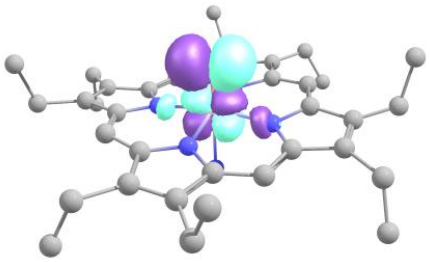	1.01

APPENDIX-23 (continued) Active space orbitals for L5 Doublet using CAS(11,11)/ LANL2DZ level of theory, continued

MO	L5 Doublet	NOON
161	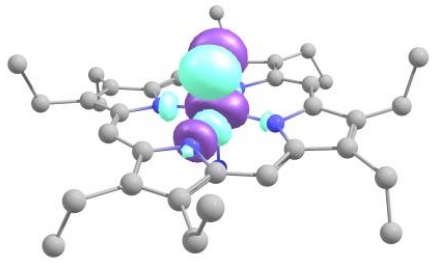	1.27
160	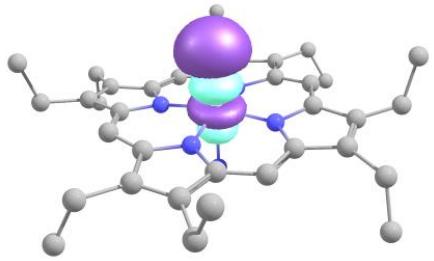	1.68
159	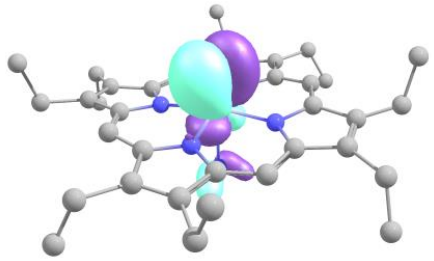	1.96
158	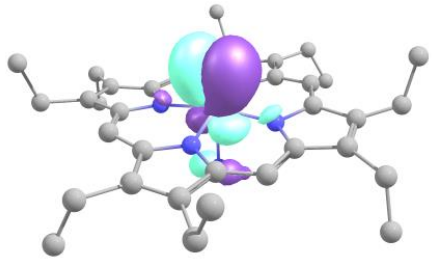	1.96
157	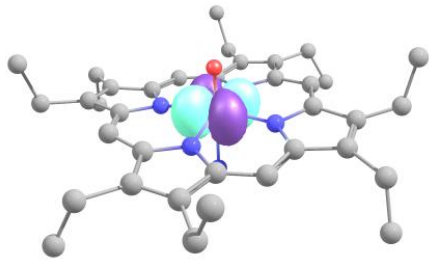	1.98

APPENDIX-24. Active space orbitals for L5 Quartet using CAS(11,11)/LANL2DZ level of theory

MO	L5 Quartet	NOON
167	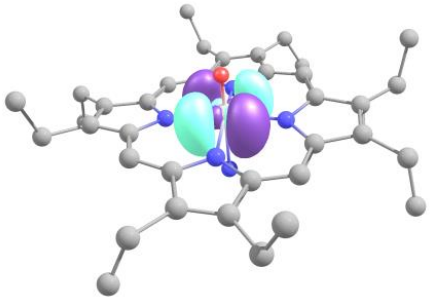	0.01
166	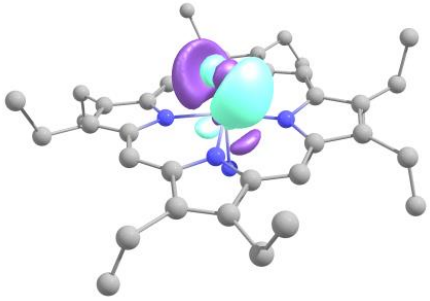	0.01
165	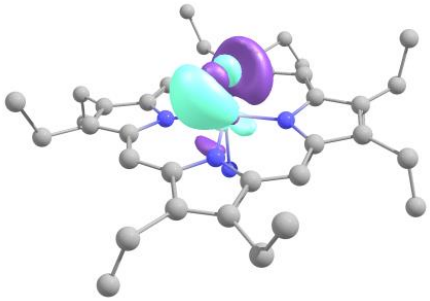	0.01
164	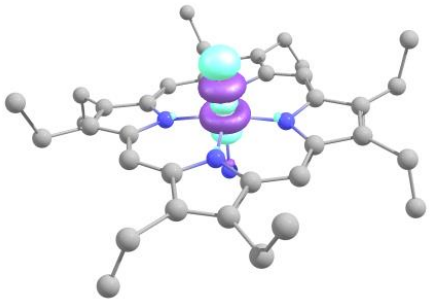	0.13
163	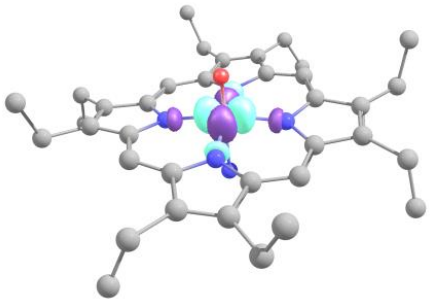	1.00

APPENDIX-24. (continued) Active space orbitals for L5 Quartet using CAS(11,11)/ LANL2DZ level of theory, continued

MO	L5 Quartet	NOON
162	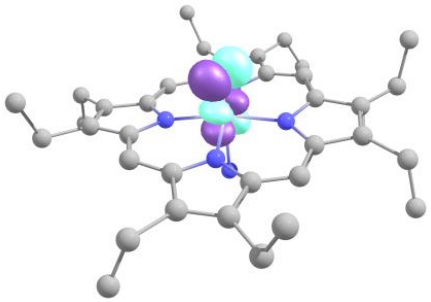	1.04
161	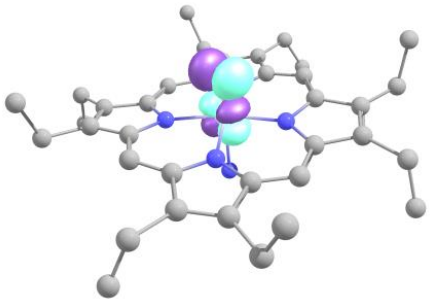	1.05
160	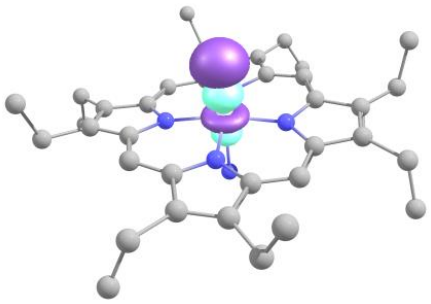	1.88

APPENDIX-24. (continued) Active space orbitals for L5 Quartet using CAS(11,11)/ LANL2DZ level of theory, continued

MO	L5 Quartet	NOON
159	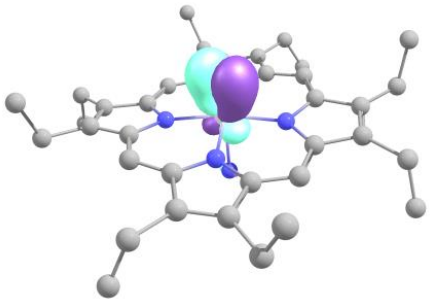	1.94
158	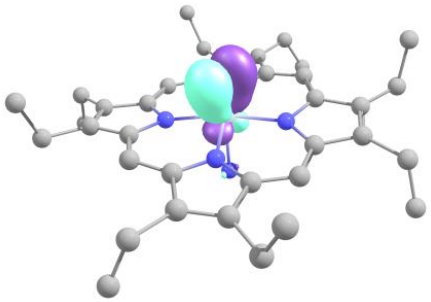	1.94
157	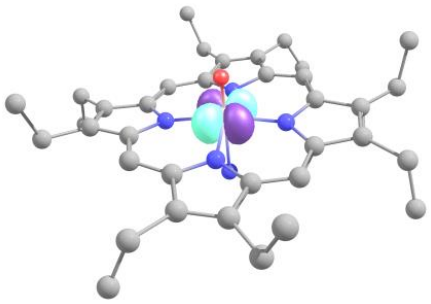	1.98

APPENDIX-25. Active space orbitals for L5 Sextet using CAS(11,11)/LANL2DZ level of theory

MO	L5 Sextet	NOON
167	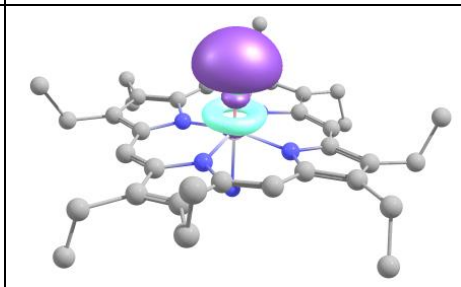	0.01
166	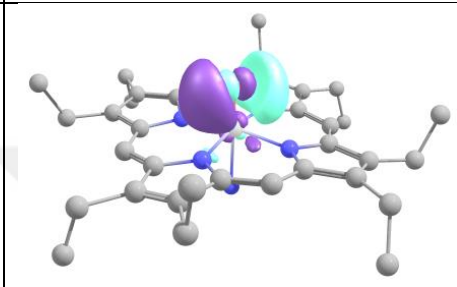	0.02
165	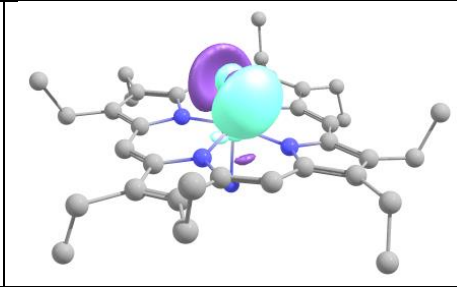	0.02
164	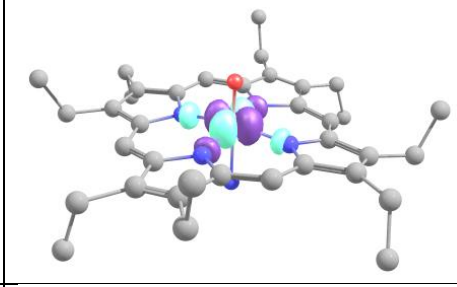	1.00
163	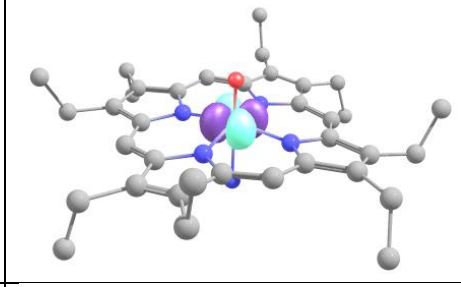	1.00
162	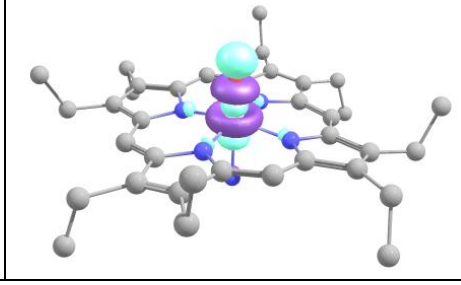	1.04

APPENDIX-25. (continued) Active space orbitals for L5 Sextet using CAS(11,11)/ LANL2DZ level of theory, continued

MO	L5 Sextet	NOON
161	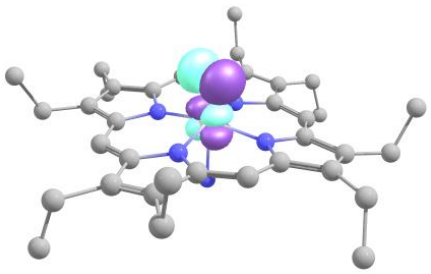	1.06
160	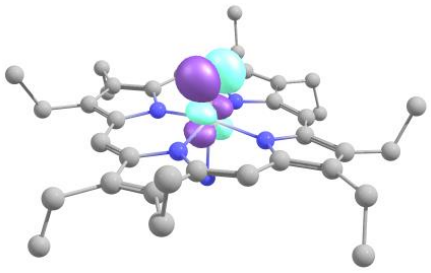	1.06
159	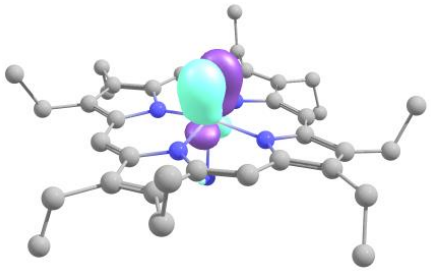	1.92
158	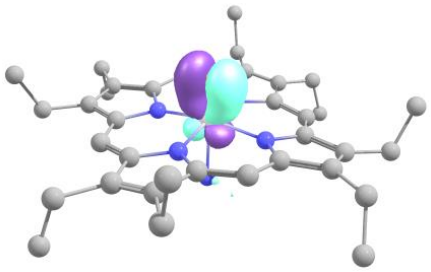	1.92
157	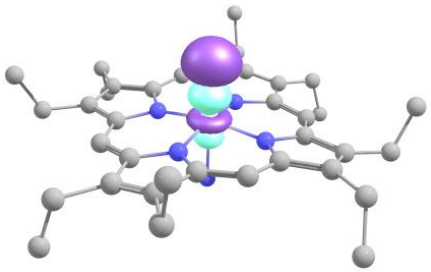	1.94

APPENDIX-26. UB3LYP/LANL2DZ optimized cartesian coordinates

L1 Doublet, -952.078629

	x	y	z
Co	0.1028310000	0.0213060000	0.1580410000
C	2.2631160000	-1.7615450000	1.2028140000
N	1.7149400000	-1.1745490000	-0.0847090000
C	2.8198830000	-0.3865620000	-0.7882820000
C	2.2404280000	0.9193960000	-1.3344930000
N	1.3456230000	1.5350450000	-0.2754020000
C	0.4795880000	2.6372940000	-0.8515010000
C	-0.7671510000	2.7442290000	0.0150240000
N	-1.4223120000	1.3697660000	0.1665020000
C	-2.2466350000	1.4294120000	1.4387440000
C	1.1620280000	-2.2658670000	-0.9803710000
C	-0.1103290000	-2.8118730000	-0.3417660000
N	-1.0601140000	-1.6635550000	0.0119570000
C	-1.8250210000	-2.0736270000	1.2524470000
C	2.1503800000	2.0643910000	0.8913670000
C	-2.0045820000	-1.4610910000	-1.1742020000
C	-2.9759000000	-0.2790610000	-1.0607050000
C	-2.3159460000	1.1059010000	-1.0407870000
H	1.0263490000	3.5882600000	-0.8662200000
H	0.2327170000	2.3886830000	-1.8894890000
H	-0.5142520000	3.1007990000	1.0160160000
H	-1.4888900000	3.4508970000	-0.4133400000
H	-3.0947220000	1.8810100000	-1.0560950000
H	-1.7098480000	1.2417670000	-1.9467130000
H	-3.6624210000	-0.4071370000	-0.2181240000
H	-3.6132150000	-0.3114370000	-1.9544200000
H	-2.5803660000	-2.3886820000	-1.2985940000
H	-1.3843300000	-1.3482960000	-2.0753110000
H	0.1196230000	-3.3589760000	0.5738110000
H	-0.6128080000	-3.5138770000	-1.0175780000
H	1.9050000000	-3.0638710000	-1.1109180000
H	0.9678540000	-1.8360890000	-1.9719260000
H	3.6171130000	-0.1917330000	-0.0688360000
H	3.2540630000	-0.9862150000	-1.5960970000
H	3.0401230000	1.6146070000	-1.6221550000
H	1.6312380000	0.7392660000	-2.2305070000
H	1.4829110000	2.4771980000	1.6470720000
H	2.7201830000	1.2653390000	1.3634270000
H	2.8384820000	2.8425640000	0.5376720000
H	-2.8725560000	0.5479290000	1.5485980000
H	-1.5759600000	1.4975740000	2.2978410000
H	-2.8970500000	2.3128960000	1.4088400000
H	-2.6335380000	-1.3778820000	1.4621780000
H	-2.2571770000	-3.0716130000	1.1059940000
H	-1.1461890000	-2.0822410000	2.1063830000
H	3.0852460000	-2.4505870000	0.9712220000
H	2.6332750000	-0.9575920000	1.8411500000
H	1.4855570000	-2.2875540000	1.7534400000
O	0.2451310000	0.0596030000	1.9171750000

L1 Quartet, -952.084989

	x	y	z
Co	0.1119270000	0.0305600000	0.3077250000
C	2.3505450000	-1.7297300000	1.2028320000
N	1.7699790000	-1.1065530000	-0.0516640000
C	2.8448820000	-0.2607710000	-0.7378430000
C	2.1983470000	0.9628700000	-1.3844180000
N	1.2724990000	1.5870730000	-0.3650140000
C	0.3403270000	2.6175340000	-0.9580630000
C	-0.8736180000	2.7139160000	-0.0402690000
N	-1.4783120000	1.3249320000	0.1874540000
C	-2.3068630000	1.3967440000	1.4552900000
C	1.2687280000	-2.1704580000	-1.0133740000
C	0.0109720000	-2.8078060000	-0.4442000000
N	-0.9986270000	-1.7243090000	-0.0696550000
C	-1.7404400000	-2.1939720000	1.1687030000
C	2.0672670000	2.2086910000	0.7700650000
C	-1.9682880000	-1.5412900000	-1.2275280000
C	-2.9783020000	-0.4030820000	-1.0438010000
C	-2.3631890000	1.0000980000	-1.0144960000
H	0.8400990000	3.5913180000	-1.0411690000
H	0.0650270000	2.3047220000	-1.9704780000
H	-0.5968370000	3.1192630000	0.9355680000
H	-1.6380640000	3.3776470000	-0.4634400000
H	-3.1703590000	1.7461230000	-1.0272640000
H	-1.7654020000	1.1550290000	-1.9206710000
H	-3.6279760000	-0.5781650000	-0.1805470000
H	-3.6471270000	-0.4302820000	-1.9143260000
H	-2.5116830000	-2.4873890000	-1.3622610000
H	-1.3756390000	-1.3737370000	-2.1366480000
H	0.2400220000	-3.3911500000	0.4498320000
H	-0.4334920000	-3.4987980000	-1.1703520000
H	2.0515240000	-2.9244790000	-1.1725780000
H	1.0707130000	-1.6923950000	-1.9804180000
H	3.5804890000	0.0332150000	0.0128180000
H	3.3712890000	-0.8680190000	-1.4836350000
H	2.9636480000	1.6794750000	-1.7120030000
H	1.6057630000	0.6880690000	-2.2653380000
H	1.3973170000	2.7059480000	1.4710870000
H	2.6134960000	1.4484610000	1.3257070000
H	2.7724070000	2.9426430000	0.3587480000
H	-2.8541170000	0.4705680000	1.6175370000
H	-1.6501520000	1.5699060000	2.3100990000
H	-3.0295050000	2.2191470000	1.3736330000
H	-2.5180880000	-1.4879790000	1.4511510000
H	-2.2077940000	-3.1675170000	0.9702240000
H	-1.0427220000	-2.2836760000	2.0023430000
H	3.2205800000	-2.3458940000	0.9415900000
H	2.6575270000	-0.9399680000	1.8910810000
H	1.6097580000	-2.3479880000	1.7090190000
O	0.2407850000	0.0770420000	2.0458600000

APPENDIX-26. (continued) UB3LYP/ LANL2DZ optimized cartesian coordinates

L1 Sextet, -952.065110

	x	y	z
Co	0.0668280000	0.0264540000	0.4113900000
C	2.7992660000	-1.2820290000	1.1196420000
N	2.0491810000	-0.7697680000	-0.0905040000
C	2.8620000000	0.3042370000	-0.7893880000
C	1.9399840000	1.3707620000	-1.3861750000
N	0.9496040000	1.8359750000	-0.3423920000
C	-0.1765970000	2.6457570000	-0.9467150000
C	-1.4197160000	2.5334530000	-0.0621840000
N	-1.8007560000	1.0768560000	0.1580930000
C	-2.6633030000	0.9872850000	1.4002580000
C	1.6910730000	-1.8940500000	-1.0372540000
C	0.5860380000	-2.7654730000	-0.4357290000
N	-0.6367360000	-1.9366910000	-0.0532480000
C	-1.3199170000	-2.5959630000	1.1289290000
C	1.6306820000	2.6206330000	0.7591340000
C	-1.5809890000	-1.8578450000	-1.2502010000
C	-2.8173060000	-0.9589330000	-1.0782620000
C	-2.5549860000	0.5562320000	-1.0575320000
H	0.1221840000	3.6980400000	-1.0424130000
H	-0.3708450000	2.2723800000	-1.9574560000
H	-1.2409430000	2.9839700000	0.9181810000
H	-2.2609800000	3.0727000000	-0.5181610000
H	-3.5181540000	1.0854550000	-1.1017720000
H	-1.9904870000	0.8395810000	-1.9538480000
H	-3.4232490000	-1.2717940000	-0.2215940000
H	-3.4521590000	-1.1457370000	-1.9548800000
H	-1.9175690000	-2.8825800000	-1.4652660000
H	-0.9936480000	-1.5240910000	-2.1162290000
H	0.9423050000	-3.2755610000	0.4618410000
H	0.2910870000	-3.5436960000	-1.1509400000
H	2.5778920000	-2.5103660000	-1.2424390000
H	1.3736350000	-1.4553710000	-1.9909800000
H	3.5445570000	0.7460090000	-0.0601270000
H	3.4829640000	-0.1415590000	-1.5771510000
H	2.5327580000	2.2180310000	-1.7590010000
H	1.3734760000	0.9708070000	-2.2361760000
H	0.8887730000	2.9845680000	1.4715110000
H	2.3345360000	1.9926970000	1.3055370000
H	2.1657130000	3.4767780000	0.3273240000
H	-2.9728220000	-0.0418090000	1.5843100000
H	-2.0989490000	1.3393740000	2.2666420000
H	-3.5633410000	1.6043870000	1.2772790000
H	-2.2127640000	-2.0434770000	1.4199140000
H	-1.6135250000	-3.6210100000	0.8668020000
H	-0.6376280000	-2.6212930000	1.9810560000
H	3.7511330000	-1.7347040000	0.8110220000
H	2.9996520000	-0.4544180000	1.8032350000
H	2.2094280000	-2.0244730000	1.6584050000
O	0.2607740000	0.1079870000	2.1496370000

L2 Doublet, -601.833919

	x	y	z
Co	0.0000010000	0.0000080000	-0.0480080000
O	-1.9206210000	0.0085770000	-0.1447100000
O	-0.0087460000	-1.9292820000	-0.0267230000
O	1.9206330000	-0.0086090000	-0.1445540000
O	0.0087470000	1.9293230000	-0.0265550000
O	0.0000740000	0.0000940000	-1.8726470000
O	-0.0000760000	-0.0000800000	1.9635310000
H	0.0035660000	0.8113320000	2.5106310000
H	-0.0037730000	-0.8115400000	2.5105590000
H	-2.3347280000	0.0103340000	-1.0349420000
H	-2.5516270000	0.0117780000	0.6030930000
H	-0.8028150000	2.4457420000	-0.2124600000
H	0.8252620000	2.4382220000	-0.2115140000
H	2.5515790000	-0.0119250000	0.6033000000
H	2.3348130000	-0.0105170000	-1.0347520000
H	0.8028380000	-2.4456770000	-0.2126030000
H	-0.8252450000	-2.4381530000	-0.2118340000

L2 Quartet, -601.843357

	x	y	z
Co	0.0000030000	0.0000040000	-0.1113260000
O	-2.0984650000	0.0019350000	-0.0969270000
O	-0.0020540000	-2.0160180000	0.0135290000
O	2.0984730000	-0.0019200000	-0.0967530000
O	0.0020580000	2.0160150000	0.0136710000
O	0.0000730000	0.0000610000	-1.7551110000
O	-0.0000790000	-0.0000700000	1.8352380000
H	0.0006680000	0.8189720000	2.3718270000
H	-0.0008710000	-0.8191550000	2.3717620000
H	-2.6429180000	0.0024780000	-0.9120580000
H	-2.6562540000	0.0026840000	0.7072900000
H	-0.8083260000	2.5394580000	-0.1596460000
H	0.8137420000	2.5376240000	-0.1590940000
H	2.6561960000	-0.0027530000	0.7075100000
H	2.6429920000	-0.0023810000	-0.9118390000
H	0.8083500000	-2.5394380000	-0.1597710000
H	-0.8137180000	-2.5376200000	-0.1593540000

L2 Sextet, -601.847374

	x	y	z
Co	-0.0258470000	-0.0002730000	-0.0547280000
O	2.0487910000	-0.0195030000	-0.3551620000
O	0.0602250000	2.0698120000	-0.1571060000
O	-2.0657540000	0.0197610000	0.3341990000
O	0.0207170000	-2.0714600000	-0.1497280000
O	-0.4669090000	0.0007750000	-2.0248870000
O	0.3502770000	0.0015360000	2.0068810000
H	0.4180990000	-0.8032960000	2.5602660000
H	0.4347190000	0.8085030000	2.5548400000
H	2.5145310000	-0.0256700000	-1.2174400000
H	2.6875960000	-0.0246250000	0.3865490000
H	0.8440060000	-2.6012760000	-0.1522690000
H	-0.7580650000	-2.6368480000	-0.3328100000
H	-2.4000700000	0.0239650000	1.2544450000
H	-2.8083830000	0.0264220000	-0.3045920000
H	-0.7075650000	2.6502670000	-0.3394260000
H	0.8942200000	2.5825670000	-0.1654720000

APPENDIX-26. (continued) UB3LYP/ LANL2DZ optimized cartesian coordinates

L3 Doublet, -502.582600

	x	y	z
Co	-0.0002040000	-0.0048360000	-0.0136230000
N	-0.1360140000	-1.9981170000	-0.2559900000
N	-2.0053920000	0.1777950000	-0.1608800000
N	-0.0222550000	-0.1621770000	2.0475030000
N	0.1384230000	2.0073650000	-0.0084570000
N	2.0122200000	-0.0975180000	-0.1425800000
O	0.0170170000	0.1056140000	-1.8425300000
H	0.6464440000	-2.5453270000	0.1196530000
H	-0.9955400000	-2.4317040000	0.0991860000
H	-2.4348120000	0.7424100000	0.5812920000
H	-2.1888090000	0.6349360000	-1.0649660000
H	0.0385380000	0.7529160000	2.5091410000
H	-0.8816080000	-0.6140830000	2.3818930000
H	-0.6565500000	2.5047980000	0.4079860000
H	2.5093200000	0.3679990000	0.6254760000
H	2.3687070000	-1.0581270000	-0.2035430000
H	2.2684830000	0.3660040000	-1.0250810000
H	0.7622310000	-0.7281600000	2.3922970000
H	-0.1289350000	-2.0665560000	-1.2849180000
H	-2.4947760000	-0.7238550000	-0.1832350000
H	0.9911850000	2.3897380000	0.4160930000
H	0.1566280000	2.2032240000	-1.0203720000
H	1.0113370000	-2.5033320000	0.6681450000
H	-2.3296070000	-1.4312360000	0.4015880000
H	-2.6886060000	0.1693760000	0.6308590000
H	-2.5875320000	-0.4493300000	-0.9119860000
H	-0.5361230000	0.7576260000	2.5417780000
H	0.1138640000	2.5503860000	-1.0136820000
H	2.3683590000	1.3882930000	0.2984370000
H	-0.2037310000	-2.7179560000	-0.4456850000
H	1.2855340000	-2.2295560000	-0.9493470000

L3 Quartet, -502.569463

	x	y	z
Co	0.0036220000	-0.0008990000	-0.0820040000
N	-0.0355390000	-2.1168090000	-0.1565720000
N	-2.2431950000	0.0002980000	-0.0050840000
N	0.0857430000	-0.0051480000	1.9624140000
N	-0.0456310000	2.1178680000	-0.1554980000
N	2.2455560000	0.0101050000	-0.0986430000
O	-0.0206960000	-0.0056670000	-1.7282730000
H	0.8790440000	-2.4732160000	-0.4555840000
H	-0.3023640000	-2.5918390000	0.7125430000
H	-2.6492030000	0.8174650000	0.4637300000
H	-2.5264560000	0.0284550000	-0.9918300000
H	0.4733630000	0.8729830000	2.3255860000
H	-0.8441880000	-0.1297270000	2.3783500000
H	-0.5095820000	2.5718690000	0.6388240000
H	2.6733880000	0.8034710000	0.3911060000
H	2.6724380000	-0.8466670000	0.2703210000
H	2.4850970000	0.0801870000	-1.0949500000
H	0.6866100000	-0.7639600000	2.3035420000
H	-0.7100010000	-2.3728420000	-0.8874310000
H	-2.6511050000	-0.8413150000	0.4167380000
H	0.8992960000	2.5074850000	-0.2450460000
H	-0.5571070000	2.3630690000	-1.0119370000

L3 Sextet, -502.548752

	x	y	z
Co	-0.0102660000	0.0031620000	-0.0609100000
N	-0.3945720000	2.1750380000	-0.2037080000
N	2.1518870000	0.4913530000	-0.1503250000
N	0.0340940000	0.0037310000	2.1410940000
N	0.5982990000	-2.1291090000	-0.1926530000
N	-2.1782220000	-0.4868810000	0.0290410000
O	-0.2459050000	-0.0799940000	-1.9209600000
H	-1.3921580000	2.3487760000	-0.3742030000
H	-0.1156000000	2.7086450000	0.6266020000
H	2.7375990000	-0.2248380000	0.2927060000
H	2.4321680000	0.5599360000	-1.1363510000
H	-0.3216670000	-0.8787250000	2.5264630000
H	0.9901730000	0.1275900000	2.4927760000

APPENDIX-26. (continued) UB3LYP/ LANL2DZ optimized cartesian coordinates

L4 Doublet, -1763.910957

	x	y	z
Co	-0.000001784	0.000445596	-0.949790124
O	-3.639444897	-0.120172626	1.894314474
O	3.639230572	0.119069307	1.894695707
O	-0.000260774	0.000973234	-2.773977259
N	-1.667602985	1.331227147	-0.910808539
N	1.667616445	-1.330351282	-0.911643703
N	-0.000074405	-0.000204659	1.148993033
N	1.583195946	1.510900460	-0.772670602
N	-1.582781296	-1.510760679	-0.773265614
C	-4.013669526	1.014977439	2.773133038
C	-2.502059241	-0.051196177	1.010287820
C	4.013165138	-1.016398533	2.773225274
C	2.501908039	0.050616833	1.010559229
C	-1.852517487	2.226545877	-1.922545957
C	-3.045988817	2.935364827	-2.092098757
C	-4.106826202	2.673093500	-1.209206176
C	-3.925246416	1.728871304	-0.184816214
C	-2.682414361	1.087692432	-0.033761279
C	1.852656786	-2.224819468	-1.924103440
C	3.045927995	-2.933963122	-2.093723660
C	4.106424900	-2.672937003	-1.210057100
C	3.924782514	-1.729449711	-0.184997907
C	2.682167567	-1.087840709	-0.034005826
C	1.182766275	0.012057479	1.824049999
C	1.207706619	0.075815424	3.226703338
C	-0.000219870	-0.000704643	3.933043239
C	-1.208070576	-0.077013979	3.226547035
C	-1.182989922	-0.012766231	1.823919169
C	1.636454103	2.597956949	-1.590597699
C	2.605103098	3.599416878	-1.443278073
C	3.557358859	3.473215804	-0.416527991
C	3.527091531	2.334227789	0.409300619
C	2.532145636	1.369586622	0.197648649
C	-1.635641762	-2.597663166	-1.591413636
C	-2.604181901	-3.599304983	-1.444589240
C	-3.556764484	-3.473467064	-0.418104169
C	-3.526856349	-2.334686270	0.408019342
C	-2.531981561	-1.369858011	0.196880279
H	-4.026603857	0.646892258	3.802182175
H	-3.326056211	1.862372200	2.683359035
H	-5.027359754	1.325353489	2.507891146
H	5.026863810	-1.326803492	2.508043128
H	3.325461539	-1.863680344	2.683079262
H	4.025990015	-0.648642661	3.802393288
H	-1.044177464	2.344271682	-2.630915312
H	-3.146441309	3.638260325	-2.911749264
H	-5.063681140	3.172076651	-1.328658264
H	-4.750660034	1.468775140	0.460096739
H	1.044636060	-2.341498026	-2.633019198
H	3.146503819	-3.636147840	-2.913967279
H	5.063113852	-3.172255104	-1.329445024
H	4.750039342	-1.470223831	0.460458242
H	2.140905952	0.187437096	3.754896827
H	-0.000279042	-0.000877132	5.018709318
H	-2.141317592	-0.188851582	3.754607625
H	0.909556415	2.653181928	-2.388832549
H	2.611433841	4.445449869	-2.121927403
H	4.318368767	4.234044872	-0.271886211
H	4.256170646	2.173774989	1.191935614
H	-0.908454759	-2.652681601	-2.389387903
H	-2.610164459	-4.445200411	-2.123414008
H	-4.317720028	-4.234426520	-0.273863927
H	-4.256143950	-2.174548184	1.190524463

L4 Quartet, -1763.903144

	x	y	z
Co	-0.0000120000	0.0003030000	-0.9254470000
O	-3.6393980000	0.1177230000	1.8405170000
O	3.6393610000	-0.1185000000	1.8404130000
O	-0.0000790000	0.0006330000	-2.6186890000
N	-1.5545650000	1.2649700000	-1.0088120000
N	1.5544610000	-1.2644150000	-1.0093370000
N	0.0000060000	-0.0000680000	1.0624300000
N	1.6320640000	1.5963320000	-0.6594310000
N	-1.6319050000	-1.5958980000	-0.6599600000
C	-3.9018980000	1.3392560000	2.6424820000
C	-2.5128640000	0.0414210000	0.9485040000
C	3.9015390000	-1.3404100000	2.6418990000
C	2.5128530000	-0.0416820000	0.9484260000
C	-1.6589310000	2.1124340000	-2.0742020000
C	-2.8097050000	2.8669290000	-2.3160470000
C	-3.9098570000	2.7080510000	-1.4561320000
C	-3.8072820000	1.8130910000	-0.3798470000
C	-2.6053060000	1.1178090000	-0.1570280000
C	1.6586870000	-2.1116280000	-2.0749450000
C	2.8093200000	-2.8663100000	-2.3169020000
C	3.9094180000	-2.7079790000	-1.4568050000
C	3.8069610000	-1.8133210000	-0.3802570000
C	2.6051660000	-1.1177350000	-0.1574320000
C	1.1844800000	-0.0385760000	1.7401340000
C	1.2080220000	0.0192510000	3.1416360000
C	0.0000800000	-0.0006690000	3.8504790000
C	-1.2078970000	-0.0202830000	3.1416710000
C	-1.1844470000	0.0381970000	1.7401910000
C	1.6872820000	2.7619000000	-1.3552730000
C	2.7225460000	3.6928940000	-1.1790420000
C	3.7379500000	3.4112010000	-0.2483000000
C	3.6906630000	2.2015860000	0.4706840000
C	2.6244620000	1.3245820000	0.2310260000
C	-1.6869280000	-2.7612540000	-1.3561650000
C	-2.7220140000	-3.6924910000	-1.1801780000
C	-3.7374240000	-3.4112740000	-0.2492930000
C	-3.6903220000	-2.2018830000	0.4700810000
C	-2.6242910000	-1.3246110000	0.2306520000
H	-3.9490550000	1.0396100000	3.6924210000
H	-3.1326810000	2.1063790000	2.5034650000
H	-4.8789050000	1.7319420000	2.3508120000
H	4.8785310000	-1.7330970000	2.3501740000
H	3.1322170000	-2.1073450000	2.5024130000
H	3.9485710000	-1.0412420000	3.6919800000
H	-0.8288570000	2.1332280000	-2.7666850000
H	-2.8481530000	3.5276640000	-3.1750470000
H	-4.8352980000	3.2472630000	-1.6335890000
H	-4.6600720000	1.6248780000	0.2556810000
H	0.8285790000	-2.1321700000	-2.7674070000
H	2.8476650000	-3.5268630000	-3.1760450000
H	4.8347040000	-3.2474580000	-1.6342580000
H	4.6596880000	-1.6256060000	0.2555100000
H	2.1508920000	0.0848320000	3.6621640000
H	0.0001020000	-0.0009460000	4.9361030000
H	-2.1507180000	-0.0862160000	3.6622280000
H	0.8990180000	2.9531280000	-2.0696560000
H	2.7270640000	4.6084980000	-1.7606450000
H	4.5513300000	4.1123260000	-0.0881220000
H	4.4495320000	1.9314770000	1.1928790000
H	-0.8986340000	-2.9520960000	-2.0706320000
H	-2.7263860000	-4.6079160000	-1.7620630000
H	-4.5506630000	-4.1126030000	-0.0892870000
H	-4.4491960000	-1.9321480000	1.1924120000

APPENDIX-26. (continued) UB3LYP/ LANL2DZ optimized cartesian coordinates

L4 Sextet, -1763.871184

	x	y	z
Co	-0.0000040000	0.0004670000	-0.9763100000
O	-3.6380380000	-0.1572060000	1.8677840000
O	3.6378260000	0.1560810000	1.8681860000
O	-0.0002640000	0.0010120000	-2.8004970000
N	-1.6810590000	1.3142120000	-0.9373180000
N	1.6810680000	-1.3132940000	-0.9381740000
N	-0.0000750000	-0.0002070000	1.1224730000
N	1.5677430000	1.5269500000	-0.7991700000
N	-1.5673260000	-1.5267670000	-0.7998060000
C	-4.0237950000	0.9740680000	2.7466140000
C	-2.5014110000	-0.0766510000	0.9837610000
C	4.0232920000	-0.9755330000	2.7467040000
C	2.5012610000	0.0760700000	0.9840460000
C	-1.8750710000	2.2076140000	-1.9490460000
C	-3.0756920000	2.9042550000	-2.1185940000
C	-4.1338080000	2.6311940000	-1.2357070000
C	-3.9426330000	1.6888570000	-0.2113270000
C	-2.6933420000	1.0603550000	-0.0602760000
C	1.8752020000	-2.2058220000	-1.9506430000
C	3.0756270000	-2.9027860000	-2.1202680000
C	4.1334110000	-2.6309930000	-1.2365960000
C	3.9421760000	-1.6894140000	-0.2115270000
C	2.6930970000	-1.0604830000	-0.0605310000
C	1.1825780000	0.0240820000	1.7975330000
C	1.2068650000	0.0880750000	3.2001870000
C	-0.0002220000	-0.0007390000	3.9065230000
C	-1.2072320000	-0.0893260000	3.2000230000
C	-1.1828030000	-0.0248110000	1.7973960000
C	1.6099400000	2.6145010000	-1.6170850000
C	2.5683490000	3.6257630000	-1.4697520000
C	3.5218370000	3.5092460000	-0.4430010000
C	3.5031580000	2.3700000000	0.3828150000
C	2.5180790000	1.3952880000	0.1711500000
C	-1.6091230000	-2.6141420000	-1.6179660000
C	-2.5674220000	-3.6255880000	-1.4711550000
C	-3.5212380000	-3.5094600000	-0.4446710000
C	-3.5029200000	-2.3704430000	0.3814650000
C	-2.5179130000	-1.3955400000	0.1703390000
H	-4.0329860000	0.6058590000	3.7756590000
H	-3.3448390000	1.8284160000	2.6568510000
H	-5.0405900000	1.2741170000	2.4813730000
H	5.0400970000	-1.2756050000	2.4815210000
H	3.3442450000	-1.8297670000	2.6565470000
H	4.0323720000	-0.6076770000	3.7758760000
H	-1.0679690000	2.3335660000	-2.6574120000
H	-3.1832890000	3.6061010000	-2.9382370000
H	-5.0956900000	3.1204170000	-1.3551560000
H	-4.7653590000	1.4203690000	0.4335810000
H	1.0684120000	-2.3307080000	-2.6595620000
H	3.1833440000	-3.6039020000	-2.9405190000
H	5.0951310000	-3.1205500000	-1.3559870000
H	4.7647510000	-1.4218120000	0.4339340000
H	2.1388790000	0.2091800000	3.7283840000
H	-0.0002820000	-0.0009240000	4.9921890000
H	-2.1392940000	-0.2106590000	3.7280800000
H	0.8825200000	2.6623360000	-2.4153210000
H	2.5660730000	4.4718240000	-2.1483920000
H	4.2750660000	4.2777770000	-0.2983490000
H	4.2338300000	2.2169650000	1.1654500000
H	-0.8814120000	-2.6617500000	-2.4159390000
H	-2.5647960000	-4.4714930000	-2.1499890000
H	-4.2744120000	-4.2781240000	-0.3004410000
H	-4.2338010000	-2.2177420000	1.1639700000

APPENDIX-26. (continued) UB3LYP/ LANL2DZ optimized cartesian coordinates

L5 Doublet, -1894.033223

	x	y	z
Co	0.0001320000	-0.0014670000	0.0445430000
N	0.5099480000	1.9454600000	0.0648390000
C	-0.3503260000	3.0389290000	0.0310620000
C	-1.7407160000	2.9722870000	0.0360780000
C	-2.4837560000	1.7956270000	0.0486210000
C	-3.9452110000	1.7475160000	-0.0027690000
C	-4.2957350000	0.4127070000	0.0002340000
C	-3.0460710000	-0.3466590000	0.0470080000
C	-2.9743370000	-1.7362670000	0.0216320000
C	-1.7945340000	-2.4752960000	0.0112110000
C	-1.7446360000	-3.9354400000	-0.0383200000
C	-0.4094140000	-4.2860510000	-0.0266820000
C	0.3504820000	-3.0382290000	0.0226610000
C	1.7410760000	-2.9719990000	0.0289630000
C	2.4844740000	-1.7954010000	0.0429800000
C	3.9461790000	-1.7470750000	-0.0057130000
C	4.2959190000	-0.4122440000	0.0015230000
C	3.0454850000	0.3465330000	0.0488970000
C	2.9749490000	1.7363060000	0.0268610000
C	1.7958940000	2.4762200000	0.0189760000
C	1.7451810000	3.9356740000	-0.0358300000
C	0.4095740000	4.2860410000	-0.0238620000
C	-0.1874850000	5.6726620000	-0.0415160000
C	-0.5905030000	6.1859350000	1.3680650000
C	2.9446710000	4.8462080000	-0.1418130000
C	3.4716460000	4.9860710000	-1.5966180000
N	1.9546080000	-0.5120910000	0.0900520000
C	5.6814170000	0.1872060000	-0.0175620000
C	6.1847630000	0.6157570000	1.3881090000
C	4.8552760000	-2.9480220000	-0.1062900000
C	5.0064050000	-3.4734900000	-1.5605200000
N	-0.5094170000	-1.9451490000	0.0512670000
C	0.1877870000	-5.6727260000	-0.0392020000
C	0.5936100000	-6.1797670000	1.3718100000
C	-2.9447530000	-4.8460300000	-0.1365650000
C	-3.4803450000	-4.9881870000	-1.5879490000
N	-1.9541860000	0.5120820000	0.0938280000
C	-5.6814950000	-0.1860170000	-0.0224930000
C	-6.1865030000	-0.6200680000	1.3809160000
C	-4.8541990000	2.9487330000	-0.1014030000
C	-5.0046090000	3.4768490000	-1.5547490000
H	-2.2861200000	3.9087670000	0.0010990000
H	-3.9085880000	-2.2852410000	-0.0159780000
H	2.2862000000	-3.9086540000	-0.0046260000
H	3.9095730000	2.2846110000	-0.0115290000
H	-1.0695950000	5.6964650000	-0.6964800000
H	0.5333710000	6.3751980000	-0.4794980000
H	0.2816180000	6.2190140000	2.0333980000
H	-1.3371510000	5.5279090000	1.8297180000
H	-1.0147830000	7.1971340000	1.3083650000
H	3.7588430000	4.4797980000	0.4992280000
H	2.6846380000	5.8431510000	0.2376310000
H	2.6947750000	5.3980370000	-2.2526320000
H	3.7650890000	4.0115980000	-2.0052770000
H	4.3432450000	5.6533160000	-1.6335630000
H	5.7077240000	1.0580570000	-0.6874900000
H	6.3882670000	-0.5395280000	-0.4385260000
H	6.2138230000	-0.2444620000	2.0688880000
H	5.5230160000	1.3697790000	1.8321340000
H	7.1959900000	1.0399400000	1.3278000000
H	4.4820040000	-3.7623630000	0.5306800000
H	5.8495660000	-2.6903730000	0.2818050000
H	5.4256610000	-2.6966210000	-2.2118590000
H	4.0347650000	-3.7639320000	-1.9779950000
H	5.6718900000	-4.3466550000	-1.5929330000
H	1.0685630000	-5.6995770000	-0.6958380000
H	-0.5339630000	-6.3771870000	-0.4725610000
H	-0.2770770000	-6.2091620000	2.0391630000
H	1.3416930000	-5.5201550000	1.8288560000
H	1.0172330000	-7.1914610000	1.3158360000
H	-3.7550830000	-4.4788580000	0.5089160000
H	-2.6823800000	-5.8424370000	0.2427010000
H	-2.7075150000	-5.4017440000	-2.2477210000
H	-3.7757860000	-4.0143800000	-1.9967760000
H	-4.3524510000	-5.6550980000	-1.6185330000
H	-5.7074730000	-1.0540700000	-0.6960410000
H	-6.3876320000	0.5427890000	-0.4410370000
H	-6.2156610000	0.2373470000	2.0652470000
H	-5.5259780000	-1.3766420000	1.8224740000
H	-7.1980020000	-1.0431760000	1.3178710000
H	-4.4811430000	3.7617850000	0.5372790000
H	-5.8487240000	2.6904790000	0.2857230000
H	-5.4234010000	2.7011460000	-2.2077800000
H	-4.0327720000	3.7681540000	-1.9711610000
H	-5.6701900000	4.3499830000	-1.5859190000
O	-0.0011450000	0.0070850000	-1.7860210000
N	0.0017520000	-0.0107750000	2.0977350000
H	0.5619820000	-0.8016680000	2.4156320000
H	-0.9718040000	-0.0847680000	2.3933630000
H	0.4094350000	0.8802290000	2.3849060000

APPENDIX-26. (continued) UB3LYP/ LANL2DZ optimized cartesian coordinates

L5 Quartet, -1894.017437

	x	y	z
Co	0.0020490000	-0.0014260000	0.0482910000
N	-2.0824830000	0.0003540000	-0.1232630000
C	-2.9018100000	1.1173250000	-0.0722990000
C	-2.4495170000	2.4453090000	-0.0563500000
C	-1.1171120000	2.8856020000	-0.0537810000
C	-0.6917750000	4.2889670000	0.0167660000
C	0.6924280000	4.2898830000	0.0128080000
C	1.1185690000	2.8869180000	-0.0548820000
C	2.4503590000	2.4447620000	-0.0474370000
C	2.9008840000	1.1157480000	-0.0574590000
C	4.3055980000	0.6915020000	0.0033190000
C	4.3060560000	-0.6930610000	-0.0061380000
C	2.9011950000	-1.1169370000	-0.0658990000
C	2.4490510000	-2.4453430000	-0.0512030000
C	1.1165660000	-2.8863830000	-0.0497120000
C	0.6907120000	-4.2895500000	0.0185690000
C	-0.6935150000	-4.2893720000	0.0120740000
C	-1.1186750000	-2.8859610000	-0.0554970000
C	-2.4510190000	-2.4445410000	-0.0496540000
C	-2.9023130000	-1.1163060000	-0.0617800000
C	-4.3063160000	-0.6912700000	0.0024830000
C	-4.3062130000	0.6934470000	-0.0081820000
C	-5.4968840000	1.6217350000	0.0180950000
C	-5.8822870000	2.1636080000	-1.3858970000
C	-5.4921250000	-1.6190600000	0.1182450000
C	-5.7556590000	-2.0863300000	1.5762650000
N	-0.0011220000	-2.0669700000	-0.1068470000
C	-1.6193010000	-5.4817240000	0.0451950000
C	-2.1454650000	-5.8886320000	-1.3584570000
C	1.6166410000	-5.4763180000	0.1355520000
C	2.0777260000	-5.7411490000	1.5953310000
N	2.0820820000	-0.0001130000	-0.1131700000
C	5.4969940000	-1.6211900000	0.0180880000
C	5.8823940000	-2.1608360000	-1.3867240000
C	5.4912930000	1.6201070000	0.1140780000
C	5.7556960000	2.0948120000	1.5695210000
N	0.0004660000	2.0667990000	-0.1104640000
C	1.6176230000	5.4826390000	0.0483940000
C	2.1435800000	5.8926560000	-1.3544530000
C	-1.6184580000	5.4753070000	0.1324380000
C	-2.0860710000	5.7366630000	1.5907710000
H	-3.2126410000	3.2168750000	-0.0112960000
H	3.2145640000	3.2152150000	-0.0015420000
H	3.2123600000	-3.2167720000	-0.0076930000
H	-3.2145820000	-3.2156090000	-0.0027910000
H	-5.2968380000	2.4720510000	0.6854070000
H	-6.3629870000	1.0987620000	0.4441700000
H	-6.1413890000	1.3394100000	-2.0624620000
H	-5.0493720000	2.7162930000	-1.8379600000
H	-6.7461970000	2.8385820000	-1.3201890000
H	-5.3441660000	-2.5031950000	-0.5180160000
H	-6.3927230000	-1.1181600000	-0.2610360000
H	-5.9626910000	-1.2277370000	2.2270510000
H	-4.8824370000	-2.6082850000	1.9860890000
H	-6.6166140000	-2.7669420000	1.6188660000
H	-2.4767180000	-5.2751470000	0.7011010000
H	-1.0981050000	-6.3400210000	0.4888860000
H	-1.3135260000	-6.1532160000	-2.0233040000
H	-2.6974530000	-5.0646500000	-1.8274170000
H	-2.8170250000	-6.7548110000	-1.2873440000
H	2.5032030000	-5.3297790000	-0.4974580000
H	1.1154290000	-6.3757040000	-0.2461160000
H	1.2158270000	-5.9459810000	2.2424820000
H	2.5999380000	-4.8690110000	2.0072520000
H	2.7560020000	-6.6037640000	1.6408030000
H	5.2974890000	-2.4725030000	0.6842830000
H	6.3630240000	-1.0984940000	0.4447200000
H	6.1401300000	-1.3354780000	-2.0623980000
H	5.0499970000	-2.7140860000	-1.8391490000
H	6.7471480000	-2.8348500000	-1.3222660000
H	5.3429290000	2.5009650000	-0.5266670000
H	6.3917460000	1.1173960000	-0.2631510000
H	5.9633980000	1.2395700000	2.2244890000
H	4.8826410000	2.6185860000	1.9774370000
H	6.6164590000	2.7758910000	1.6080940000
H	2.4751270000	5.2750640000	0.7038450000
H	1.0960160000	6.3397790000	0.4938230000
H	1.3114490000	6.1572560000	-2.0190500000
H	2.6969870000	5.0702660000	-1.8246440000
H	2.8139760000	6.7595860000	-1.2817550000
H	-2.5021050000	5.3299830000	-0.5048870000
H	-1.1157380000	6.3757070000	-0.2448170000
H	-1.2270980000	5.9398420000	2.2423030000
H	-2.6102530000	4.8636380000	1.9982830000
H	-2.7644490000	6.5992400000	1.6351810000
O	-0.0058290000	0.0014720000	1.6852680000
N	0.0176720000	-0.0091800000	-2.0123490000
H	0.6293800000	-0.7692530000	-2.3067810000
H	0.3641990000	0.9055930000	-2.3002660000
H	-0.9524280000	-0.1597590000	-2.2906000000

APPENDIX-26. (continued) UB3LYP/ LANL2DZ optimized cartesian coordinates

L5 Sextet, -1893.992526

	x	y	z
Co	-0.0040530000	0.0028330000	-0.1416770000
N	-1.8643360000	-0.9287060000	-0.0026620000
C	-2.0952370000	-2.2952160000	-0.0013190000
C	-1.0986900000	-3.2851060000	0.0006190000
C	0.2927290000	-3.0928040000	0.0034850000
C	1.3024160000	-4.1597580000	-0.0028260000
C	2.5413330000	-3.5409730000	0.0035590000
C	2.2946250000	-2.0928310000	0.0079000000
C	3.2840800000	-1.0956430000	-0.0002640000
C	3.0913500000	0.2959050000	-0.0081770000
C	4.1589710000	1.3050110000	-0.0079620000
C	3.5408040000	2.5441720000	-0.0030850000
C	2.0927750000	2.2976050000	-0.0052290000
C	1.0952170000	3.2868070000	-0.0084430000
C	-0.2960620000	3.0926510000	-0.0124370000
C	-1.3054350000	4.1595370000	-0.0117620000
C	-2.5441830000	3.5407960000	-0.0042080000
C	-2.2975320000	2.0929770000	-0.0056770000
C	-3.2884750000	1.0974610000	-0.0070060000
C	-3.0963160000	-0.2939700000	-0.0088700000
C	-4.1625290000	-1.3037390000	-0.0095730000
C	-3.5429350000	-2.5423860000	-0.0008020000
C	-4.1941850000	-3.9042820000	0.0352120000
C	-4.2625700000	-4.5126930000	1.4628930000
C	-5.6423750000	-1.0073230000	-0.0571010000
C	-6.1585630000	-0.7145630000	-1.4928570000
N	-0.9315770000	1.8606710000	-0.0082050000
C	-3.9059020000	4.1925470000	0.0310220000
C	-4.5162200000	4.2580130000	1.4580380000
C	-1.0083000000	5.6393120000	-0.0574690000
C	-0.7149330000	6.1571780000	-1.4924830000
N	1.8609690000	0.9321570000	-0.0055120000
C	4.1926480000	3.9058720000	0.0304530000
C	4.2570790000	4.5189170000	1.4563170000
C	5.6386750000	1.0070250000	-0.0503540000
C	6.1584000000	0.7088380000	-1.4837180000
N	0.9284720000	-1.8624180000	0.0163240000
C	3.9033280000	-4.1924190000	0.0309500000
C	4.5222290000	-4.2584540000	1.4542070000
C	1.0050210000	-5.6392480000	-0.0549650000
C	0.7127580000	-6.1505500000	-1.4925910000
H	-1.4432410000	-4.3152480000	-0.0047760000
H	4.3142720000	-1.4399520000	-0.0052910000
H	1.4386080000	4.3172850000	-0.0107400000
H	-4.3183790000	1.4426220000	-0.0091830000
H	-3.6518510000	-4.5984150000	-0.6222240000
H	-5.2124920000	-3.8362780000	-0.3691960000
H	-4.8443060000	-3.8670200000	2.1328870000
H	-3.2594170000	-4.6214740000	1.8935670000
H	-4.7368920000	-5.5030550000	1.4430640000
H	-5.8765580000	-0.1479660000	0.5873540000
H	-6.2033650000	-1.8571780000	0.3536430000
H	-5.9889890000	-1.5767020000	-2.1498650000
H	-5.6360790000	0.1438280000	-1.9324390000
H	-7.2347330000	-0.4952960000	-1.4833780000
H	-4.5993060000	3.6520460000	-0.6286760000
H	-3.8368700000	5.2117540000	-0.3709100000
H	-3.8722260000	4.8398000000	2.1295840000
H	-4.6238520000	3.2541300000	1.8872710000
H	-5.5073140000	4.7307910000	1.4376810000
H	-0.1491580000	5.8724970000	0.5876260000
H	-1.8581280000	6.2000400000	0.3536790000
H	-1.5775030000	5.9900270000	-2.1495560000
H	0.1424890000	5.6339560000	-1.9330580000
H	-0.4939080000	7.2329720000	-1.4814280000
H	3.6526800000	4.5980540000	-0.6309960000
H	5.2121690000	3.8360310000	-0.3705340000
H	4.8361830000	3.8748810000	2.1301320000
H	3.2527180000	4.6299470000	1.8836360000
H	4.7322260000	5.5088520000	1.4347840000
H	5.8702190000	0.1497510000	0.5977670000
H	6.1993620000	1.8577590000	0.3589990000
H	5.9917590000	1.5690480000	-2.1439970000
H	5.6359240000	-0.1502170000	-1.9220170000
H	7.2342460000	0.4881550000	-1.4705970000
H	4.5926680000	-3.6514340000	-0.6326470000
H	3.8320850000	-5.2114470000	-0.3710170000
H	3.8828350000	-4.8414050000	2.1291390000
H	4.6317880000	-3.2548150000	1.8835910000
H	5.5135890000	-4.7303480000	1.4274930000
H	0.1451620000	-5.8747880000	0.5882720000
H	1.8542370000	-6.2021180000	0.3545690000
H	1.5760530000	-5.9810930000	-2.1481090000
H	-0.1437550000	-5.6245590000	-1.9316270000
H	0.4908600000	-7.2262120000	-1.4865790000
O	0.0571830000	-0.0657710000	-1.9738630000
N	0.0019300000	0.0291050000	2.1263520000
H	0.2318400000	0.9819030000	2.4011010000
H	0.7048660000	-0.6465600000	2.4210680000
H	-0.9407400000	-0.2405410000	2.4011590000

GAZİ GELECEKTİR...